CoA Note No. 57

CONFIDENTIAL

THE COLLEGE OF AERONAUTICS

CRANFIELD

AERODYNAMIC CHARACTERISTICS OF A SWEPT WING WITH SPANWISE BLOWING

by

R. F. AYERS and M. R. WILDE

CONFIDENTIAL

NOTE No. 57

SEPTEMBER, 1956

THE COLLEGE OF AERONAUTICS

CRANFIELD

An Experimental Investigation of the Aerodynamic Characteristics of a Low Aspect Ratio Swept Wing with Blowing in a Spanwise Direction * From the Tips

-by-

R.F. Ayers, B.Sc., D.C.Ae.

and

M.R. Wilde, B.Sc., D.C.Ae

of the

Department of Aerodynamics

SUMMARY

This report is the first of a series of studies to investigate the effectiveness of spanwise blowing on the aerodynamic characteristics of low aspect ratio wings and bodies. The model used in this investigation was an untapered half-wing of aspect ratio 1.39, 50° sweep back, and mounted on a reflection plate.

The test was conducted at a Reynolds number of 1.39×10^6 based on the streamwise chord.

---

* The work described in this report was conducted as a partial requirement for the Diploma of the College of Aeronautics.

Broadly speaking the main effects of spanwise blowing are to increase the wing effective aspect ratio and to increase the loading towards the wing tips.

It is found that with $C_{\mu} = 0.138$ (the momentum discharge rate coefficient) the maximum lift coefficient is increased by 36 per cent. Other effects of tip blowing are (i) the lift coefficient is increased at all incidences, (ii) the drag coefficient is reduced at a given lift coefficient, and (iii) the aerodynamic centre is moved aft and varies little with incidence up to $C_L = 0.7$. In addition the stalling angle is increased as well as the angle of incidence at which leading edge separation first occurs.

It is concluded that tip blowing has an application to aircraft with low aspect ratio wings for the purpose of improving stability and control, particularly at low flying speeds.

CONTENTS

LIST OF SYMBOLS

c	wing chord in streamwise direction
C_D	drag coefficient $\frac{D}{\frac{1}{2}\rho_\infty U_\infty^2 S}$
C_L	lift coefficient $\frac{L}{\frac{1}{2}\rho_\infty U_\infty^2 S}$
C_{L_L}	local lift coefficient
C_M	pitching moment coefficient measured about quarter-chord point of M.A.C. $\frac{M}{\frac{1}{2}\rho_\infty U_\infty^2 Sc}$
C_p	static pressure coefficient $\frac{p - p}{\frac{1}{2}\rho_\infty U_\infty^2}$
C_Q	mass discharge rate coefficient $\frac{M'}{\rho_\infty U_\infty S}$
C_μ	momentum discharge rate coefficient $\frac{M'V}{\frac{1}{2}\rho_\infty U_\infty^2 S}$
D	drag
$h_o C$	distance of aerodynamic centre measured from the leading edge of the M.A.C.
L	lift
M	pitching moment measured about quarter-chord point of M.A.C.
M'	total blowing mass rate, slugs/sec.
p	static pressure
s	semi-span of wing
S	gross wing area
U	velocity
V	blowing jet velocity assuming isentropic expansion of the jet flow to free stream pressure

x	distance downstream from local leading edge
y	spanwise distance from wing root
α_G	geometric measured angle of attack (i.e. not corrected for wind tunnel interference and working section flow datum direction).
η	y/s
Λ	sweep angle of wing quarter chord line, degrees.
ρ	air density
	Suffix
∞	free stream conditions

-----

1. Introduction

Recent studies on the aerodynamic characteristics of low aspect ratio swept and unswept wings have shown the relatively large importance of the tip vortices, especially when leading edge separation of the boundary layer occurs. This is contrary to their effect on wings of large aspect ratio where the presence of the tip vortex plays only a minor role in the determination of such qualities as the wing loading and aerodynamic centre position. If, then, large changes in the size and position of the tip vortices, shed from a low aspect ratio wing, could be made by some external control, it follows that large changes in the aerodynamic characteristics of such wings would result.

The present investigation is concerned with one such type of external control of the tip vortices, in the form of air ejection from the wing tip in a spanwise direction. The work reported below is of an exploratory nature to understand this type of flow and to determine the order of magnitude of the effects involved. How far this method is successful in modifying such aerodynamic characteristics as the effective aspect ratio, the wing loading, the maximum lift coefficient, and the aerodynamic centre position will be discussed below.

It should be noted that this form of air ejection is essentially different from that investigated in the jet flap or wing trailing edge blowing (2), and air ejection over flaps (1). In the latter cases their overall effects can be related to increases in the wing effective camber and chord. When applied to wings of finite aspect ratio they represent reductions in the wing effective aspect ratio. The gains resulting from trailing edge blowing or air ejection over flaps are of great practical value for wings of large aspect ratio, but their effectiveness decreases with reduction in wing aspect ratio. In the case of air ejection in a spanwise direction it is crudely the wing span which is artificially increased which thus leads to an effective increase in aspect ratio, and may therefore be attractive for wings of low, rather than high, aspect ratio. Since it is reasonable to expect that the effects of all three methods of air ejection will prove complementary it is possible that practical cases will arise where all three methods will be utilised.

Attention is drawn to the fact that although air ejection in a spanwise direction is not primarily one of boundary layer control, its influence on the size and position of the tip vortex results in large changes in the boundary layer flow. Thus a large part of this exploratory study is concerned with the changes in the boundary layer flow.

The model used for this preliminary investigation is an untapered swept wing ($\Lambda = 50^{\circ}$) of aspect ratio 1.39 with streamwise tips. Air was ejected in a spanwise direction from a slot of length 45 per cent of the tip chord. Only the low speed characteristics of the wing were studied and the

Reynolds number, based on the streamwise chord, was 1.39 x 10^6.

2. Description of apparatus

2.1. Wind tunnel

The wind tunnel used was the College of Aeronautics No. 2 tunnel. This is an open jet closed return tunnel with a circular working section of 3.5 ft. diameter.

2.2. Model

The model tested was a half-wing mounted on a reflection plate. The wing was untapered, and had a sweepback angle of 50°. The aspect ratio (including the reflected half) was 1.39. The aerofoil section, in a direction normal to the leading edge, was 12 per cent thick, elliptic nosed, with a maximum thickness at 30 per cent chord and smoothly faired to the trailing-edge. The model was suspended from a 'Warden' type 6-component balance which was used to measure the aerodynamic forces and moments.

Photographs and dimensioned diagrams of the model are given in figs. 1 to 4. The blowing slot (shown in fig. 2) is 0.005in. wide and 10.5in. long, extending from 11.7 per cent to 56.4 per cent of the tip chord. Compressed air was supplied to the model by flexible pipes, and was ducted through the reflection plate and then inside the wing in a spanwise direction. A pressure tapping between the two supply pipes enabled the static pressure (jet stagnation pressure) in the slot settling chamber to be measured.

Small diameter pressure tubes were let into one surface of the model at 15 spanwise stations. These tubes were led away from the wing through the reflection plate to prevent them from interfering with the flow near the model. The tubes were connected to a bank of manometers. The free stream static pressure in the wind tunnel working section was, for all practical purposes, atmospheric. The wind speed in the working section was set with the aid of a vertical type Chattock gauge connected to a static hole in the wind tunnel settling chamber.

2.3. The 'cone'

In order to determine qualitatively local flow directions, a paper cone (1/4in. diameter x 1/4in. long) was attached to a piece of cotton, and suspended from a traversing rod. The free length of cotton was variable. For convenience the paper cone will be referred to in this report as the 'cone'.

3. Test procedure

The wind speed used for all tests was 110.9 ft/sec., corresponding to a Reynolds number, based on wing streamwise chord, of 1.39×10^6.

3.1. Balance measurements

The lift, drag and pitching moment were first measured for the wing with no tip-blowing (i.e. $C_\mu = 0$). These force and moment measurements were then repeated with $C_\mu = 0.138$*, the investigation ranging from an incidence of -6° to beyond the positive stall in each case. The initial investigation was conducted with 3° increments of incidence, but subsequent measurements were taken at smaller increments

---

* For the definition of C_μ, the momentum discharge rate coefficient, used throughout this report see Appendix I and figure 5.

over certain ranges in order to establish the precise variation of C_L, C_M and C_D with incidence.

In this preliminary investigation the variation of the aerodynamic forces with C_μ was not fully studied. However, in order to gain some idea of the effects of C_μ, balance readings were taken for a wide range of C_μ for certain selected values of incidence.

It was necessary to determine the contribution of the pressure in the supply pipes to the overall forces and moments measured by the balance. For this purpose, the air supply was shut off by means of valves attached to the supply pipes close to the reflection plate, and wind-off tests were conducted with pressure in the supply pipes but with no mass flow. When the results of these tests were compared with wind-off results with no pressure in the supply pipes, it was found that the effects of the pressure reaction on the measured forces and moments were negligible.

3.2. Pressure distributions

The layout of the pressure tubes enabled the measurement of the static pressure on the model surface to be taken at any spanwise station between the root and 0.922 s, for each of the following chordwise positions: 0.0 c, 0.025 c, 0.05 c, 0.075 c, 0.10 c, 0.15 c, 0.20 c, 0.25 c, 0.30 c, 0.40 c, 0.50 c, 0.60 c, 0.70 c, 0.80 c and 0.90 c.

Chordwise pressure distributions were obtained at 0.125 s, 0.250 s, 0.375 s, 0.500 s, 0.625 s, 0.750 s, 0.813 s, 0.875 s and 0.922 s for a wide range of incidence, for the cases $C_\mu = 0$ and $C_\mu = 0.138$.

3.3. Surface flow visualisation

Flow visualisation close to the wing surface was obtained using the titanium dioxide technique (5). The technique consists of spraying the surface with a suspension of finely divided titanium dioxide in paraffin. The wind tunnel was quickly set to the required speed, and the liquid film moved over the surface leaving traces of the white titanium dioxide along the streamlines in the boundary layer close to the surface. When the paraffin had evaporated, the tunnel was stopped and the pattern established on the wing surface was photographed.

3.4. General flow visualisation

The 'cone' described in §2.3 was used to determine qualitatively the flow direction near the wing surface and in the wake. When placed in a vortex the cone rotated, and could be used to locate the position of the core, the direction of rotation, and the approximate size and shape of the vortex.

4. Results

4.1. Balance measurements

The force and moment coefficients are plotted in figs. 6 to 12. No attempt has been made to correct these results for wind tunnel interference, and therefore the angle of attack quoted is the geometric angle of attack, α_G, as measured on the wind tunnel balance. Also, the drag of the rig has not been subtracted from the total measured drag since the tare drag was large and therefore accurate values of absolute drag could not be obtained. However the drag data can be used to obtain the increments in drag caused by tip blowing. The effects of the rig on C_L and C_M were found to be relatively small.

In addition to wind tunnel interference corrections to the measured angle of attack there were corrections for a balance datum error as well as for stream malalignment. Application of these latter corrections gave $C_L = 0$ at $\alpha = 0$

for the case of zero blow, but not for the case with blow. In view of this unexplained change in no-lift angle with tip blowing, the incidences quoted throughout this report are not corrected and are those actually recorded on the wind tunnel balance.

4.2 Pressure distributions

The chordwise pressure distributions are plotted for some of the angles of attack, and spanwise stations investigated (figs.13 to 30) and recorded in tables 1 to 36. The upper surface isobars are plotted for some angles of attack (figs.31 to 43)

The lift, pitching moment and spanwise loading obtained from integrations of the pressure distributions are plotted in figs. 44 to. 47.

4.3 Flow visualisation

Photographs of the wing surface flow using the titanium dioxide method are shown in figs.48 to 57. The flow directions near the wing surface obtained from the 'cone' tests are given in figs. 58 to 64.

4.4 Principal results (Balance measurements)

		$C\mu = 0$	$C\mu = 0.138$
Maximum lift coefficient	C_{Lmax}	0.94	1.28
Lift slope curve	$\left(\frac{\partial C_L}{\partial \alpha_G}\right) C_L = 0.1$	1.78rad^{-1}	2.12rad^{-1} *
	$\left(\frac{\partial C_L}{\partial \alpha_G}\right) C_L = 0.7$	2.29rad^{-1}	2.60rad^{-1}
Incidence at C_{Lmax}	$(\alpha_G)_{C_{Lmax}}$	30.3°	36.0°
Aerodynamic centre position behind leading edge of M.A.C.	$(h_o)C_L = 0$	.136	.328
	$(h_o)C_L = 0.7$	.314	.319
Measured drag coefficient (including tare)	C_{D_o}	.190	.180

*The gradients of the lift curves are quoted at $C_L = 0.1$ instead of $C_L = 0$ since the lift curve slope for $C_\mu = .138$ changes rapidly between $C_L = 0$ and $C_L = 0.1$

4.5. Accuracy of results

The accuracies stated below are only approximate.

4.5.1. Balance measurements

The balance was sensitive to small changes of load, and could be read with sufficient accuracy to enable C_L, C_M, and C_D to be measured to within 0.001. However, small errors were introduced by the distortion of the semi-flexible pipes (described in §2.2) when the balance turntable was rotated. Care was taken to re-adjust the pipes every time the turntable was moved, to reduce these loads to a minimum. A rough assessment of the errors introduced showed that the final results were accurate within the following limits

$\pm$ .005 for C_L
$\pm$ .005 for C_D
$\pm$ .010 for C_M.

At large angles of attack, violent buffetting of the model was experienced, making accurate readings impossible. This buffetting occurred at angles of attack greater than 25° for $C_\mu = 0$, and greater than 30° for $C_\mu = 0.138$. It was found that in this 'buffet region' the above tolerances should be increased to

$\pm$ .010 for C_L
$\pm$ .010 for C_D
$\pm$ .020 for C_M.

The incidence of the model could be set to $\pm 0.1^\circ$.

4.5.2. Pressure distributions

The manometer could be read with sufficient accuracy to enable the pressure coefficient, C_p, to be calculated to within .005.

However, for large suctions ($-C_p$ greater than about 1.5) the pressures were unsteady, and could only be obtained to an accuracy of about 5 per cent of their total value.

The lift distributions were obtained by integrating the component of force normal to the wing chord, and multiplying the result by $\cos \alpha_G$. The chordwise component of force was neglected. It was estimated that this omission would lead to errors in the integrated values of C_L of not more than 3 per cent.

C_M was calculated about the quarter chord point of the M.A.C. in order to be consistent with the balance measurements. The pitching moment obtained from integrating the moment of the chordwise component of force was neglected.

4.5.3. Flow visualisation

In making assessments of the results obtained using the titanium dioxide technique it should be noted that the model was mounted with the wing pointing vertically downwards, so that gravitational effects probably cannot be ignored.*

When the surface flow photographs were taken for the upper surface of the wing at $\alpha_G = 12^\circ$ (both for $C_\mu = 0$ and $C_\mu = 0.138$) the wing surface was not smooth and the surface irregularities may have interfered with the flow, affecting boundary layer transition and/or separation. This fact should be considered when comparisons are made between the results at this and other incidences for which the model surface had been suitably modified.

In using the titanium dioxide technique the interpretation of the flow patterns was considerably aided by watching the actual movement of the liquid while the pattern was forming.

---

* In ref. 5 it is shown that the changes in surface flow patterns arising from differences in wing attitude (i.e. horizontal or tip downwards) are small.

5. Discussion

5.1. Balance measurements

5.1.1. Lift

The $C_L \sim \alpha_G$ curve (fig. 6) for the wing with $C_\mu = 0$ is characteristic of that for a swept-back wing of low aspect ratio. $dC_L/d\alpha_G$ is small at low C_L, and increases suddenly with the formation of the leading edge vortex. The stalling angle of 30° is also typical for this type of planform, but the C_{Lmax} of 0.94 is on the low side and can only be accounted for by the relatively low Reynolds number of these tests.

By using the tip jet at $C_\mu = .138$, C_{Lmax} is increased to 1.28, an improvement of 36 per cent on the no-blowing case. The stalling incidence is increased to 36°.

The use of blowing also increases $dC_L/d\alpha_G$ (per radian) from 1.78 to 2.12 at $C_L = 0.1$, and from 2.29 to 2.60 at $C_L = 0.7$. These increases in lift curve slope with tip blowing can be interpreted as an increase in wing effective aspect ratio. The 'kink' at which the change of gradient occurs is delayed from 15° to 18°, indicating that a delay in the leading edge separation has occurred.

The value of $dC_L/d\alpha_G$ for the wing without blowing is very close* to that given by the formula of Pohlhamus (ref. 4)

$$\frac{dC_L}{d\alpha} = \frac{2\pi A}{2 + \cos\Lambda \cdot \sqrt{\frac{A^2}{\cos^4\Lambda} + 4}}$$

For $\Lambda = 50^\circ$ and $A = 1.39$, this gives a value of $dC_L/d\alpha = 1.93$ per radian.

---

* The measured result of $dC_L/d\alpha_G = 1.78$ is not corrected for wind tunnel interference. It is probable that when these effects are allowed for the experimental value will exceed that given by Pohlhamus.

Fig. 6 also shows that, with blowing, there is a marked increase of $dC_L/d\alpha_G$ in the region of $\alpha_G = 0$. This region has been investigated more closely (fig. 7), and shows that $dC_L/d\alpha_G$ reaches a value of about 7.0 per radian.*

Fig. 8 shows the variation of C_L with C_μ at $\alpha_G = 10^\circ$, 20°, and 30°. The curves for $\alpha_G = 10^\circ$ and 20° are very similar in shape and indicate that dC_L/dC_μ is approximately constant for values of C_μ less than about 0.1. The characteristics for $\alpha_G = 30^\circ$ are slightly different. It was found that at small values of C_μ (less than about .04) the wing was nearly stalled, whilst larger values of C_μ delayed the stall. This would account for the relatively large values of dC_L/dC_μ at small values of C_μ.

The variation of C_{Lmax} with C_μ has not been investigated.

5.1.2. Drag

As stated above the values of C_D have not been corrected for tare drag. Fig. 9 shows that, at a given angle of attack, C_D is slightly larger for $C_\mu = .138$ than for $C_\mu = 0$. This increment is partly due to the induced drag resulting from the increase in C_L.

Fig. 10** indicates that for a given C_L, the drag is appreciably less at $C_\mu = .138$ than it is at $C_\mu = 0$. The reduction in drag is particularly large at large angles of attack. These data can be explained in terms of an increase in effective aspect ratio and a reduction in profile drag as a result of tip blowing.

---

* These values of C_L were obtained by increasing incidence from negative values. Tests were not made under conditions of decreasing incidence. No simple explanation for the change in no-lift angle could be found.

** The non-linear relationship between C_D and C_L^2 at small incidences is partly the result of a variation in tare drag with incidence.

5.1.3. Pitching moment

Fig. 11 shows that for $C_\mu = 0$, the aerodynamic centre of the wing is well forward ($h_o = .136$) of the quarter M.A.C. point. For values of C_L greater than 0.3, the aerodynamic centre moves aft, and at $C_L = 0.7$, $h_o = 0.314$. This shape of the $C_M \sim C_L$ curve is characteristic of that for a low aspect ratio, highly swept type of planform.

It is seen from fig. 11 that at $C_\mu = .138$ the movement of the aerodynamic centre with increase in incidence is much smaller than for the basic wing. The centre of pressure of the wing with blowing is also further aft than for the basic wing for most of the C_L range. The aft movement of the aerodynamic centre with tip blowing at small incidences arises from the increase in loading at the tips. Although a similar effect takes place at larger angles of incidence, there is in this range of incidence an increase in loading towards the leading edge. Thus the two effects tend to cancel each other and although the centre of pressure moves aft the aerodynamic centre remains approximately stationary. The unusual shape of the $C_M \sim C_L$ curve for $C_\mu = 0.138$ near $\alpha_G = 0$ is associated with the non-linear lift characteristics in this region.

The variation of C_M with C_μ at constant angles of incidence is given in fig. 12.

The scatter of points about the curves in fig. 11 are within the limits of accuracy stated in §4.5.1.

5.2. Pressure distributions

Most of the comments in this section refer to the pressure distribution on the upper surface of the wing. The pressure distribution on the lower surface is only slightly affected by the tip blowing.

The $C_L \sim \alpha_G$ (fig. 44) and $C_M \sim C_L$ (fig. 45) curves, integrated from the pressure distributions, agree quite closely with the curves obtained by force measurements. There is some 'scatter' of the integrated values but in general the accuracy of the results is within the limits suggested in §4.5.2.

5.2.1. Basic wing, $C_\mu = 0$

At low angles of attack the highest suction peak occurs near the leading edge of the tip. This is shown most clearly in the isobar diagram for $\alpha_G = 6^\circ$ (fig. 31). Fig. 32 shows that, at 12°, the tip vortex increases the suction all along the upper surface of the tip. Fig. 33 shows that at 15° a leading edge boundary layer separation commences about midspan and extends to the wing tip. The separated vortex sheet rolls up and increases in size and intensity towards the wing tip, since it is being fed continuously by the separation of the outboard flow at the leading edge. The rolled up vortex sheet has the form of an expanding 'bubble' and boundary layer reattachment occurs downstream of it. The extent of the 'bubble' is indicated roughly from the portion of those isobars lying approximately normal to the wing leading edge, or from the extent of the nearly constant pressure distribution at each chordwise station. The centre, or core of the rolled up vortex sheet arising from the leading edge separation forms the core of the trailing vortex. The rolled up vortex sheet and its degeneration into the trailing vortex is referred to by Black (ref. 5) as a vortex of ram's horn type. Fig. 33 shows that at $\alpha_G = 15^\circ$ the part span leading edge boundary layer separation has just commenced. This is in agreement with the balance measurements which also indicate the formation of the part span vortex at an incidence of about 15°. The increase in the lift loading, arising from the presence of the part span vortex, is due mainly to the attainment of a region of high negative pressure over the area covered by the vortex.

As the angle of attack is increased (figs. 34 and 35) the extent of the vortex is increased and it gradually moves inboard. At 30° incidence (fig. 36) the 'bubble' is spreading out rapidly, and is affecting most of the upper surface. Figs. 63 and 64 show that after the stall, an almost uniform distribution of pressure exists on the upper surface at $\alpha_G = 36°$.

The spanwise lift distribution (fig. 46) obtained by integrating the pressures on the surface at $\alpha_G = 6°$ and $\alpha_G = 12°$, are approximately of the form predicted by linear theory, except near the wing tip. At $\alpha_G = 15°$ and $\alpha_G = 18°$, the leading edge separation increases the proportion of the lift on the outboard parts of the wing. As the angle of attack is increased further and the vortex moves inboard, the maximum local lift coefficient C_{L_L} also moves inboard, so that at $\alpha_G = 27°$, the peak value of C_{L_L} occurs at about 0.35s. The stall occurs first at the tip and then moves inboard towards the root. At $\alpha_G = 33°$ (i.e. beyond the stall) there is a considerable loss of lift over the whole wing except at the root, which has not yet stalled.

5.2.2. Wing with blowing, $C_\mu = .138$

The effect of blowing from the tip is to produce numerically larger values of pressure coefficient on both the upper wing surface and the lower wing surface at all angles of attack. In general the isobars in the 'with blowing' case tend to be slightly straighter and more nearly parallel to the wing leading edge than in the 'no blowing' case.

Fig. 39 shows that at 18° the leading edge separation is only just commencing. This again is in agreement with the balance measurements, which indicate that the separation begins at a higher angle of attack for $C_\mu = .138$ than for $C_\mu = 0$. The rolled up vortex, when formed, lies nearer the leading edge of the wing , and only extends aft to about 0.3c at the tip.

This indicates that the vortex is entrained by the tip-jet. At angles of attack approaching the stall, boundary layer separation exists over most of the surface and at $\alpha_G = 37.5^\circ$ (fig. 30), the pressure distribution over the upper surface of the wing is almost uniform.

The spanwise lift distributions (fig. 47) show that for $\alpha_G \leqslant 12^\circ$, C_{L_L} is almost constant across the span. This 'rectangular' distribution indicates that a pressure difference is maintained across the tip jet. At larger angles of attack (from $\alpha_G = 18^\circ$ to $\alpha_G = 24^\circ$) the formation of the part-span vortex causes the peak values of C_{L_L} to occur near the tip, as in the 'no-blowing' case. For angles of attack greater than 30°, the lift at the tip diminishes, and the peak C_{L_L} is at the wing root, whilst the wing tip loses considerable lift.

It is clear that the tip-jet not only delays the tip-stall by entraining the leading edge vortex but increases the lift across the whole span and in particular, large increments occur near the tip. It is interesting to note that the increase of lift due to tip-blowing is maintained even after the wing has stalled.

5.3. Flow visualisation

As the titanium dioxide flow visualisation technique and the cone technique yield similar information, the two methods are discussed concurrently in this section.

Both techniques give reliable and repeatable information, and both methods clearly indicate the position of the leading edge separation and the vortex of ram's horn type. The cone technique also shows the positions of the trailing vortex outboard and downstream of the wing (figs. 58 to 64).

5.3.1. Basic wing, $C_\mu = 0$

Fig. 48 shows that there is a small spanwise movement of the boundary layer surface flow on the wing upper surface. This movement outwards is more noticeable near the trailing edge of the wing, and increases as α_G is increased (see fig. 50). This figure also shows that the boundary layer is being swept off the wing upper surface at the tip. The cone technique (fig. 59) shows that the boundary layer only flows from the lower to the upper surface near the leading edge of the tip. Further aft, the tip vortex grows and induces flow off both the upper and lower surfaces.

Figs. 60 and 52 show the presence of the leading edge separation and the part span vortex at $\alpha_G = 18^\circ$. The vortex is represented on the photograph as small, fine streaks on the wing surface approximately perpendicular to the free stream direction. The surface flow is seen to sweep forward near the leading edge of the tip, a phenomenon which is more obvious in figs. 54 and 56. This type of flow, discussed in detail by Black (ref. 5), exists in regions near the tip when the centre of the vortex is well clear of the wing surface.

A characteristic of the flow pattern for $\alpha_G = 21^\circ$ (fig. 54) is a diagonal, dark streak starting forward of mid chord and curving down towards the trailing tip. This is associated with the reattachment of the boundary layer downstream of the separation bubble. This reattached flow is trapped between the 'bubble' and the boundary layer flow inboard and results in a region of relatively high shear stress.

Figs. 61 and 56 show that the 'bubble' extends over a large portion of the wing upper surface. At angles of attack beyond the stall, the boundary layer separation diffuses over the whole surface.

On the lower surface, the flow patterns at all angles of attack are substantially the same as shown in fig. 58. The flow near the leading edge (particularly near the stagnation point) has a noticeable spanwise component, while near the trailing edge the flow takes up a roughly streamwise direction. A small region of boundary layer separation close to the leading edge was also detected on the lower surface at the junction between the wing and the reflection plate. It is assumed that this region only influences the pressure distribution near the root leading edge, and probably does not affect the overall forces or pressure distributions further outboard.

5.3.2. Wing with blowing, C_μ = .138

At small angles of attack (before the part span vortex forms) there is a greater spanwise component of flow in the boundary layer than for $C_\mu = 0$. This can be seen by comparing fig. 48 with fig. 49, and fig. 50 with fig. 51. The cone technique indicates that the blowing has very little effect outside the boundary layer (figs. 59 and 62) except near the tip. It is clear that the trailing vortex is entrained by the tip-jet and moved in a spanwise direction away from the wing.

The photograph of boundary layer surface flow for $\alpha_G = 18^\circ$ (fig. 53) shows that the 'bubble' only extends aft to about 0.3c at the tip. The rest of the pattern indicates a large spanwise component of velocity near the surface.

The remaining flow visualisation diagrams and photographs show that the 'bubble' moves slowly inboard as the angle of attack is increased further. Fig. 64 shows that when the wing is at stalling angle (36°) the trailing vortex is still entrained by the tip jet. As α_G is increased beyond the stall, it is impossible for the cone to define the extent of vortex the ram's horn type due to the general unsteadiness of the entire flow.

The titanium dioxide flow pattern for $C_\mu = 0$, $\alpha_G = 6^\circ$ (fig. 48) shows that near the leading edge a marked change occurs at about mid span, between the flow over the inboard half of the wing and that further outboard. It is probable that this indicates the type of boundary layer instability which at higher incidences produces the leading edge separation. Fig. 49 shows that at $\alpha_G = 6^\circ$, with tip blowing, this change in flow near the leading edge outboard of mid span does not occur. The significance of these flow changes must be left for further investigation.

The 'cone' technique has been used to study the development of the tip vortex with tip blowing at small angles of incidence. At zero angle of attack vortices of opposite sign are formed above and below the jet. At a small angle of attack the upper vortex increases rapidly in size and intensity whereas the lower vortex gets smaller and eventually, at a still larger incidence, disappears completely. The upper vortex, at these small angles of incidence, is notably stronger than the trailing vortex at the same incidence without blowing. The rapid growth of these vortices at small incidences, their induced downwash and consequent lift increments, may account for the large values of lift curve slope at small incidences.

5.4. Summary of experimental results

5.4.1. Lift

At small angles of incidence tip blowing results in an increase in the lift curve slope due to an increase in the wing effective aspect ratio. The loading is increased towards the wing tip. Tip blowing delays the incidence at which leading edge separation occurs and also delays the wing stall. The maximum lift coefficient is increased.

5.4.2. Drag

At a given C_L the drag is reduced by tip blowing partly as a result of the increased effective aspect ratio, thereby reducing the induced drag, and partly by a reduction in profile drag.

5.4.3. Pitching moment

At small angles of incidence tip blowing produces an aft movement in the position of the aerodynamic centre as a result of the increased loading towards the tips. At higher incidences the effect of increased tip loading is cancelled approximately by increased loading towards the leading edge, but the resulting movement of the aerodynamic centre due to change of incidence is less than for the unblown wing.

5.5. Effects of changes of parameters

Tentative suggestions are made as to the effect of the variation of certain parameters on the lift, drag and moment characteristics.

5.5.1. C_μ

Although below the stall C_L varies roughly linearly with C_μ there is an indication that $\left(\frac{dC_L}{dC_\mu}\right)_{\alpha_G = \text{const.}}$ decreases for values of C_μ in excess of 0.1. This is consistent with experiments on blowing over flaps (ref. 1) which indicate that there is a value of C_μ above which no further improvement is obtained. A further result is that, with tip blowing, the aerodynamic centre moves aft with increasing C_μ.

5.5.2. Slot length, slot position, and shape of wing tip

As C_μ is proportional to the length of the blowing slot, it may be expected that the slot length will affect the wing characteristics in roughly the same way as does C_μ. However, this ignores the effect of slot position. It might be conjectured that over certain parts of the incidence range a more forward or a more rearward slot would give more favourable aerodynamic characteristics than those obtained from the slot used in these tests. In addition a change in the tip geometry, slot shape, jet directivity, and placing the blowing slot close to the wing upper surface might all show greater gains than those obtained so far. However all these suggestions must be the subject for further investigation.

5.5.3. Sweepback

Since with increase in leading edge sweepback the leading edge separation will occur further inboard and at lower angles of incidence, and the aerodynamic characteristics become more dependent on the trailing vortex, it appears that spanwise blowing may well prove more effective for such wings than for wings of relatively small sweepback. Although the form of spanwise blowing used in these experiments has been performed by blowing from the streamwise tip it is assumed that equal or more powerful effects will be experienced on wings of large leading edge sweepback by blowing from the leading edge.

5.5.4. Aspect ratio

Since, apart from modifications to the flow over the wing, the main effect of tip blowing is one of increasing the wing effective aspect ratio, it is reasonable to expect that tip blowing is more effective for wings of small, rather than large, aspect ratio. However, since stabilisation of the flow over the tips results from tip blowing it follows that this method might have application in the improvement of the stalling characteristics of swept or unswept wings of any aspect ratio.

5.5.5. Reynolds number and Mach number

Kuchemann (ref. 3) states that Reynolds number cannot affect the general character of the vortex patterns described, although it will greatly affect the change-over from one type of flow to another and the shape and stability of the rolled up vortex sheet. It should be noted that the Reynolds number of this experiment (1.39×10^6) is very low compared with that of full scale aircraft and it must be expected that the results obtained so far may be the subject of large Reynolds number effects.

Reference 3 also suggests that the principal features of the vortex pattern over the wing will exist for all Mach numbers up to the critical speed. In the present experiments it should be noted that the tip blowing causes greater velocities near the wing than at $C_\mu = 0$. This suggests that the critical Mach number will become smaller as C_μ is increased.

The effectiveness of tip blowing at high subsonic and supersonic speeds must remain the subject of future detailed investigations.

5.6. Possible uses of tip blowing

5.6.1. Anti-stall device

An obvious use of tip-blowing is to reduce landing speeds. The increase of $C_{L_{max}}$ obtained by tip blowing in this experiment is 36 per cent, which could no doubt be improved upon by using higher blowing coefficients. This gain in $C_{L_{max}}$ is the more important since it is not accompanied by a large nose down pitching moment, experienced with conventional blown or unblown flaps. One disadvantage of tip blowing, as indeed with all other forms of blowing, is that power must be supplied to maintain the lift.

5.6.2. Drag reduction

Fig. 21 shows that, for a given C_L the drag will be reduced by means of tip blowing. However this gain is small except at large values of C_L. In making assessments of the overall effectiveness of tip blowing the power required for blowing must be considered.

5.6.3. Lateral control

Aircraft with wings of very low aspect ratio are extremely difficult to control at low speeds (i.e. at high C_L). It appears possible that a substitute for aileron control may be obtained by blowing differentially from the tips. For an aircraft with low aspect ratio wings travelling at low E.A.S. the power requirements should not be excessive. At higher speeds and with larger aspect ratio, the lateral control problem is less likely to arise.

5.6.4. Longitudinal control

On a highly swept wing, the application of tip blowing causes both the wing centre of pressure and the wing aerodynamic centre to move further aft. These effects respectively cause a nose down pitching moment and an increase of static longitudinal stability. This may be particularly useful when applied to a delta winged aircraft with no horizontal tailplane. However, the aft movement of the aerodynamic centre with incidence is less for the blown than for the unblown wing. Thus in the case of an aircraft with a horizontal tailplane less trimming will be required.

6. Conclusions

An experimental investigation of the aerodynamic characteristics of a low aspect ratio 50° sweptback wing when air, in the form of a thin sheet, is blown out from the wing tips in a spanwise direction has shown that at a momentum discharge rate coefficient, $C_\mu = 0.138$,

(a) $C_{L_{max}}$ is increased by 36 per cent.

(b) The stalling angle is increased.

(c) The incidence at which leading edge separation over part of the span commences is increased.

(d) C_L is increased at all angles of attack.

(e) C_D is reduced for a given value of C_L.

(f) At small angles of attack the aerodynamic centre is moved aft, and varies little with incidence up to $C_L = 0.7$.

These results can be explained approximately in terms of an increase in the wing effective aspect ratio and an increase in the loading towards the wing tips. Applications of tip blowing to improve $C_{L_{max}}$, the longitudinal and lateral stability, and the control characteristics of an aircraft having wings of low aspect ratio are briefly discussed.

Acknowledgements

The authors wish to express their thanks to Mr. G.M. Lilley for suggesting this problem and for his comments and criticism during the preparation of the final report.

The authors also wish to acknowledge the help of Mr. J. Spillman in formulating the research programme, to Mr. K.D. Harris for his advice throughout the course of the investigation and to Mr. S. Lilley and his wind tunnel staff for their assistance.

References

1. Williams, J. An analysis of aerodynamic data on blowing over trailing edge flaps to increase lift. A.R.C. C.P. 209.

2. Davidson, I.M. The jet flap. J.R.Ae.S. Vol. 60, No. 541, January, 1956.

3. Küchemann, D. Types of flow on swept wings with special reference to free boundaries and vortex sheets. J.R.Ae.S. Vol. 57, No. 515, November, 1953.

4. Pohlhamus, E.C. A simple method of estimating the subsonic lift and damping in roll of sweptback wings. N.A.C.A. T.N. 1862.

5. Black, J. Flow studies of the leading edge stall on a swept-back wing at high incidence. J.R.Ae.S. Vol. 60, No. 541, January, 1956.

APPENDIX I

Blowing coefficients for compressible slot flows

When defining a blowing coefficient, it is necessary to define a standard reference area. For work involving a spanwise slot, the reference area is taken as the area corresponding to the spanwise extent of the slot. Clearly, for a chordwise slot, this assumption is unsuitable. No attempt is made in this paper to define a suitable area which would enable C_μ to be representative for all planform shapes. For the sake of expediency, the standard reference area is taken as the gross wing area of the model S.

Thus, the momentum discharge rate coefficient

$$\bar{C}_\mu = \frac{M' V}{\frac{1}{2}\rho_\infty U_\infty^2 S} \qquad \text{.............(i)}$$

and mass discharge rate coefficient

$$C_Q = \frac{M'}{\rho_\infty U_\infty S} \qquad \text{.............(ii)}$$

where V is the velocity obtained in an isentropic expansion from the stagnation pressure p_D to the freestream pressure p_∞. It is possible to express C_μ and C_Q in terms of the pressure ratio p_D/p_∞. C_Q and C_μ are plotted against p_D/p_∞ in fig. 10.

TABLE 1

UPPER SURFACE PRESSURE COEFFICIENTS

$C_\mu = 0, \quad \eta = .921$

y/c \ α°	0	6	12	15	18	24	27	30	33	36
90	+.044	-.285	-.279	-.168	-.160	-.146	-.168	-.204	-.300	-.198
80	+.015	-.131	-.360	-.387	-.300	-.270	-.263	-.262	-.292	-.308
70	-.007	-.300	-.668	-.460	-.438	-.372	-.373	-.258	-.401	-.412
60	-.029	-.168	-.588	-.490	-.548	-.497	-.467	-.453	-.467	-.470
50	-.066	-.146	-.550	-.438	-.511	-.519	-.504	-.504	-.511	-.506
40	-.080	-.153	-.375	-.474	-.504	-.541	-.548	-.555	-.576	-.530
30	-.103	-.131	-.235	-.285	-.504	-.511	-.511	-.510	-.534	-.448
25	-.250	-.321	-.515	-.563	-.621	-.642	-.650	-.679	-.715	-.544
20	-.199	-.300	-.500	-.578	-.644	-.724	-.737	-.766	-.825	-.566
15	-.066	-.058	-.059	-.058	-.534	-.051	-.022	-.022	-.022	+.015
10	-.155	-.314	-.588	-.678	-.760	-.840	-.840	-.840	-.810	-.500
7.5	-.221	-.307	-.735	-.790	-.847	-.927	-.914	-.890	-.818	-.493
5	-.566	-.875	-1.09	-.912	-.941	-1.015	-.985	-.950	-.847	-.515
2.5	+.021	-.431	-.945	-1.298	-.989	-1.044	-1.042	-1.010	-.945	-.649
0	-.221	-.700	-1.351	-.986	-.965	-1.015	-.994	-.964	-.883	-.545

Note in tables 1 to 36 the third decimal place is not accurate.

TABLE 2

LOWER SURFACE PRESSURE COEFFICIENTS

$C_\mu = 0, \quad \eta = .921$

x/c \ α°	0	6	12	15	18	24	27	30	33	36
90	+.044	0	-.036	-.044	-.036	-.032	-.036	-.051	-.073	-.073
80	+.015	-.051	-.080	-.080	-.066	-.076	-.073	-.080	-.095	-.102
70	-.007	-.066	-.124	-.109	-.102	-.099	-.094	-.095	-.102	-.109
60	-.029	-.109	-.175	-.182	-.168	-.171	-.153	-.153	-.153	-.168
50	-.066	-.102	-.277	-.139	-.139	-.113	-.094	-.109	-.080	-.095
40	-.080	-.095	-.262	-.109	-.117	-.083	-.058	-.058	-.036	-.043
30	-.103	-.080	-.219	-.066	-.066	-.068	-.051	-.044	-.036	-.007
25	-.250	-.168	-.175	-.168	-.175	-.157	-.139	-.139	-.095	-.095
20	-.199	-.146	-.153	-.131	-.131	-.113	-.087	-.073	-.058	-.058
15	-.066	-.022	-.029	-.021	-.036	+.085	-.058	-.066	-.073	-.036
10	-.155	-.058	0	+.036	+.044	+.092	+.094	+.117	+.117	+.139
7.5	-.221	-.066	+.029	+.051	+.066	+.099	+.094	+.117	+.124	+.156
5	-.566	-.248	-.124	-.080	-.058	-.051	-.007	+.007	+.022	+.051
2.5	+.021	+.161	+.269	+.268	+.254	+.226	+.204	+.176	+.162	+.198
0	-.221	+.087	+.233	+.233	+.248	+.209	+.168	+.146	+.117	+.160

TABLE 3

UPPER SURFACE PRESSURE COEFFICIENTS

$C_\mu = 0, \ \eta = .875$

x/c \ α^o	0	6	12	15	18	24	27	30	33	36
90	+.063	-.071	-.275	-.275	-.282	-.289	-.319	-.338	-.345	-.254
80	+.042	0	-.352	-.395	-.416	-.395	-.405	-.395	-.395	-.346
70	+.021	0	-.324	-.465	-.543	-.515	-.511	-.472	-.480	-.424
60	-.028	-.057	-.360	-.529	-.720	-.655	-.625	-.564	-.542	-.486
50	-.042	-.064	-.247	-.515	-.726	-.720	-.675	-.628	-.600	-.529
40	-.085	-.114	-.240	-.592	-.740	-.705	-.666	-.642	-.635	-.508
30	-.134	-.114	-.296	-.600	-.726	-.733	-.716	-.705	-.720	-.600
25	-.155	-.227	-.352	-.621	-.734	-.790	-.780	-.775	-.796	-.621
20	-.184	-.270	-.409	-.664	-.761	-.854	-.859	-.854	-.831	-.571
15	-.191	-.298	-.471	-.726	-.825	-.930	-.945	-.915	-.831	-.529
10	-.211	-.418	-.521	-.868	-.910	-.995	-.986	-.945	-.825	-.508
7.5	-.197	-.440	-.775	-.916	-.945	-1.030	-1.010	-.966	-.825	-.508
5	-.197	-.582	-1.080	-1.010	-1.000	-1.070	-1.036	-.980	-.846	-.500
2.5	-.148	-.710	-1.630	-1.080	-1.042	-1.108	-1.070	-1.008	-.852	-.515
0	+.360	-.319	-1.761	-1.290	-1.215	-1.140	-1.085	-1.016	-.860	-.515

TABLE 4

LOWER SURFACE PRESSURE COEFFICIENTS

$C_\mu = 0, \quad \eta = .875$

s/c \ α°	0	6	12	15	18	24	27	30	33	36
90	+.063	0	0	-.014	-.014	-.028	-.028	-.056	-.056	-.021
80	+.042	-.014	-.014	-.014	-.014	0	0	-.014	0	+.007
70	+.021	-.021	-.028	-.021	-.014	0	+.007	+.014	+.028	+.021
60	-.028	-.056	-.056	-.056	-.042	-.028	-.007	0	+.021	+.007
50	-.042	-.113	-.063	-.063	-.050	-.014	+.007	+.021	+.056	+.049
40	-.085	-.098	-.070	-.063	-.042	+.007	+.028	+.056	+.085	+.077
30	-.134	-.113	-.070	-.056	-.035	+.028	+.056	+.084	+.113	+.119
25	-.155	-.113	-.049	-.028	-.014	+.056	+.091	+.120	+.155	+.161
20	-.184	-.113	-.028	0	+.028	+.099	+.014	+.169	+.197	+.210
15	-.191	-.084	+.021	+.070	+.099	+.176	+.219	+.246	+.275	+.287
10	-.211	-.063	+.084	+.141	+.177	+.254	+.282	+.317	+.338	+.343
7.5	-.197	-.028	+.155	+.219	+.256	+.324	+.352	+.388	+.388	+.400
5	-.197	+.063	+.254	+.303	+.340	+.374	+.388	+.402	+.388	+.392
2.5	-.148	+.070	+.352	+.360	+.369	+.324	+.296	+.268	+.240	+.273
0	+.360	-.070	-1.155	-1.808	-1.32	-1.325	-1.20	-.109	-1.018	-.624

TABLE 5

UPPER SURFACE PRESSURE COEFFICIENTS

$C_\mu = 0, \quad \eta = .812$

x/c \ α°	0	6	12	15	18	24	27	30	33	36
90	+.063	+.042	-.071	-.247	-.296	-.381	-.451	-.494	-.437	-.296
80	+.021	+.014	-.064	-.332	-.443	-.515	-.574	-.564	-.508	-.402
70	+.007	0	-.056	-.346	-.522	-.620	-.656	-.620	-.550	-.465
60	-.035	-.050	-.084	-.416	-.684	-.790	-.781	-.720	-.614	-.515
50	-.042	-.078	-.113	-.370	-.720	-.860	-.832	-.775	-.690	-.564
40	-.113	-.142	-.204	-.480	-.910	-.945	-.866	-.803	-.734	-.564
30	-.156	-.206	-.289	-.606	-.950	-1.000	-.930	-.881	-.818	-.600
25	-.184	-.262	-.352	-.726	-.965	-1.021	-.960	-.930	-.818	-.578
20	-.198	-.305	-.430	-.876	-.974	-1.042	-1.000	-.971	-.825	-.557
15	-.213	-.354	-.529	-1.010	-1.000	-1.063	-1.036	-1.010	-.845	-.503
10	-.213	-.440	-.710	-1.164	-1.070	-1.130	-1.080	-1.035	-.860	-.536
7.5	-.191	-.482	-.825	-1.179	-1.108	-1.140	-1.100	-1.056	-.873	-.557
5	-.177	-.589	-.995	-1.280	-1.140	-1.188	-1.130	-1.071	-.873	-.529
2.5	-.106	-.760	-1.410	-1.354	-1.200	-1.212	-1.150	-1.090	-.889	-.543
0	+.341	-.270	-1.560	-1.332	-1.331	-1.250	-1.160	-1.086	-.889	-.543

TABLE 6

LOWER SURFACE PRESSURE COEFFICIENTS

$C_\mu = 0 \quad \eta = .812$

x/c \ a°	0	6	12	15	18	24	27	30	33	36
90	+.063	+.028	+.014	0	-.007	-.014	-.028	-.049	-.084	-.042
80	+.021	-.007	-.007	-.014	-.007	0	+.007	0	-.014	0
70	+.007	-.021	-.021	-.014	-.007	+.028	+.028	+.042	+.028	+.028
60	-.035	-.049	-.035	-.035	-.014	+.021	+.035	+.049	+.063	+.056
50	-.042	-.084	-.042	-.042	-.014	+.035	+.056	+.084	+.098	+.098
40	-.113	-.091	-.049	-.042	-.007	+.049	+.077	+.113	+.134	+.134
30	-.156	-.098	-.035	-.014	+.021	+.098	+.134	+.176	+.197	+.211
25	-.184	-.105	-.021	+.007	+.049	+.134	+.169	+.211	+.239	+.253
20	-.198	-.091	+.014	+.056	+.098	+.190	+.239	+.268	+.296	+.310
15	-.213	-.063	+.077	+.134	+.190	+.282	+.324	+.366	+.388	+.394
10	-.213	-.007	+.162	+.226	+.289	+.373	+.408	+.436	+.450	+.450
7.5	-.177	+.021	+.211	+.282	+.345	+.415	+.444	+.458	+.465	+.472
5	-.177	+.113	+.303	+.352	+.401	+.444	+.451	+.451	+.444	+.458
2.5	-.106	+.240	+.387	+.366	+.408	+.380	+.352	+.317	+.282	+.324
0	+.341	+.056	-1.185	-1.970	-1.705	-1.370	-1.285	-1.156	-1.056	-.676

TABLE 7

UPPER SURFACE PRESSURE COEFFICIENTS

$C_\mu = 0, \quad \eta = .750$

x/c \ α°	0	6	12	15	18	24	27	30	33	36
90	+.056	+.091	-.014	-.134	-.169	-.360	-.465	-.530	-.458	-.353
80	+.014	+.056	-.035	-.191	-.247	-.480	-.593	-.614	-.544	-.445
70	+.014	+.035	-.042	-.191	-.254	-.556	-.676	-.685	-.614	-.508
60	-.028	-.021	-.084	-.254	-.247	-.734	-.825	-.796	-.677	-.544
50	-.056	-.056	-.120	-.296	-.515	-.874	-.945	-.875	-.761	-.606
40	-.140	-.120	-.189	-.388	-.755	-1.056	-1.036	-.930	-.819	-.600
30	-.182	-.217	-.315	-.564	-1.042	-1.200	-1.108	-1.015	-.875	-.600
25	-.196	-.259	-.378	-.662	-1.120	-1.220	-1.140	-1.043	-.889	-.585
20	-.217	-.308	-.469	-.810	-1.208	-1.250	-1.158	-1.071	-.895	-.571
15	-.210	-.357	-.574	-.945	-1.212	-1.255	-1.162	-1.092	-.904	-.564
10	-.210	-.441	-.735	-1.100	-1.254	-1.275	-1.200	-1.114	-.904	-.557
7.5	-.182	-.406	-.805	-1.150	-1.261	-1.290	-1.220	-1.130	-.904	-.571
5	-.175	-.567	-.966	-1.304	-1.332	-1.340	-1.249	-1.150	-.916	-.564
2.5	-.133	-.630	-1.234	-1.540	-1.390	-1.375	-1.278	-1.162	-.924	-.571
0	+.350	-.301	-1.886	-1.635	-1.664	-1.410	-1.282	-1.158	-.924	-.564

TABLE 8

LOWER SURFACE PRESSURE COEFFICIENTS

$C_\mu = 0, \quad \eta = .750$

y/c \ α°	0	6	12	15	18	24	27	30	33	36
90	+.056	+.042	+.028	+.021	+.021	0	-.007	-.042	-.077	-.042
80	+.014	+.014	0	+.007	+.007	+.014	+.021	-.007	0	0
70	+.014	-.014	0	+.021	+.028	+.042	+.056	+.056	+.056	+.049
60	-.028	-.035	-.021	-.007	+.007	+.042	+.070	+.077	+.091	+.077
50	-.056	-.056	-.035	-.014	0	+.056	+.084	+.098	+.129	+.129
40	-.140	-.085	-.035	-.007	+.028	+.098	+.134	+.155	+.183	+.183
30	-.182	-.098	-.021	+.021	+.056	+.148	+.190	+.218	+.254	+.261
25	-.196	-.091	+.007	+.056	+.098	+.198	+.240	+.275	+.310	+.324
20	-.217	-.070	+.049	+.105	+.162	+.261	+.310	+.346	+.381	+.381
15	-.210	-.049	+.113	+.190	+.240	+.353	+.395	+.416	+.451	+.441
10	-.210	+.028	+.205	+.282	+.338	+.438	+.472	+.486	+.515	+.522
7.5	-.182	+.063	+.261	+.338	+.395	+.472	+.494	+.501	+.522	+.529
5	-.175	+.134	+.332	+3.950	+.437	+.480	+.487	+.486	+.480	+.494
2.5	-.133	+.240	+.388	+.402	+.416	+.370	+.324	+.300	+.260	+.303
0	+.350	+.049	-1.228	-1.995	-1.550	-1.601	-1.462	-1.291	-1.158	-.734

TABLE 9

UPPER SURFACE PRESSURE COEFFICIENTS

$C_\mu = 0, \quad \eta = .625$

x/c \ α°	0	6	12	15	18	24	27	30	33	36
90	+.049	+.042	0	-.015	-.028	-.042	-.374	-.543	-.536	-.395
80	+.021	+.007	-.035	-.084	-.092	-.155	-.529	-.684	-.649	-.480
70	-.035	-.007	-.071	-.120	-.113	-.226	-.642	-.783	-.713	-.522
60	-.056	-.049	-.106	-.147	-.142	-.331	-.761	-.866	-.790	-.564
50	-.092	-.085	-.147	-.190	-.226	-.544	-.960	-1.016	-.895	-.579
40	-.147	-.169	-.261	-.332	-.494	-.945	-1.198	-1.134	-.945	-.592
30	-.169	-.226	-.353	-.480	-.867	-1.226	-1.305	-1.190	-.966	-.585
25	-.183	-.268	-.416	-.642	-1.205	-1.405	-1.390	-1.240	-1.000	-.585
20	-.197	-.296	-.487	-.868	-1.481	-1.439	-1.398	-1.240	-1.016	-.579
15	-.212	-.402	-.635	-1.262	-1.784	-1.502	-1.426	-1.278	-1.030	-.579
10	-.218	-.480	-.819	-1.670	-1.934	-1.530	-1.452	-1.304	-1.058	-.585
7.5	-.204	-.494	-.910	-1.741	-1.890	-1.524	-1.474	-1.320	-1.058	-.579
5	-.240	-.649	-1.205	-1.861	-1.954	-1.573	-1.490	-1.334	-1.058	-.600
2.5	+.014	-.726	-1.729	-1.850	-1.905	-1.589	-1.510	-1.348	-1.064	-.600
0	+.325	-.620	-2.66	-2.28	-2.06	-1.638	-1.530	-1.354	-1.058	-.592

TABLE 10

LOWER SURFACE PRESSURE COEFFICIENTS

$C_\mu = 0, \quad \eta = .625$

y/c \ a^o	0	6	12	15	18	24	27	30	33	36
90	+.049	+.028	+.028	+.028	+.028	+.014	0	-.014	-.063	-.084
80	+.021	-.042	-.028	-.014	-.014	0	+.021	+.014	+.021	-.021
70	-.035	-.056	-.028	-.007	-.007	+.028	+.049	+.063	+.078	+.035
60	-.056	-.063	-.021	0	+.014	+.063	+.084	+.098	+.134	+.091
50	-.092	-.091	-.028	+.014	+.028	+.091	+.127	+.155	+.183	+.169
40	-.147	-.091	-.014	+.021	+.056	+.134	+.183	-.212	+.254	+.240
30	-.169	-.084	-.021	+.071	+.113	+.212	+.268	+.310	+.346	+.346
25	-.183	-.078	+.014	+.063	+.113	+.212	+.247	+.282	+.303	+.303
20	-.197	-.056	+.098	+.176	+.226	+.346	+.402	+.437	+.472	+.465
15	-.212	-.028	+.148	+.226	+.289	+.409	+.451	+.494	+.529	+.522
10	-.218	+.028	+.226	+.310	+.373	+.480	+.515	+.543	+.564	+.557
7.5	-.204	+.071	+.282	+.360	+.423	+.508	+.529	+.550	+.564	+.557
5	-.240	+.071	+.319	+.366	+.423	+.466	+.465	+.459	+.459	+.465
2.5	+.014	+.226	+.381	+.381	+.395	+.331	+.282	+.254	+.232	+.275
0	+.325	+.091	-1.184	-2.10	-1.970	-2.075	+1.960	-1.680	-1.420	-.819

TABLE 11

UPPER SURFACE PRESSURE COEFFICIENTS

$C_{\mu} = 0, \quad \eta = .500$

% c \ α°	0	6	12	15	18	24	27	30	33	36
90	+.014	+.028	+.042	+.014	-.028	-.056	-.070	-.427	-.54	-.483
80	0	0	-.014	-.021	-.056	-.084	-.270	-.526	-.654	-.555
70	-.042	-.056	-.056	-.084	-.112	-.168	-.412	-.710	-.767	-.583
60	-.070	-.099	-.113	-.140	-.192	-.277	-.626	-.910	-.876	-.611
50	-.128	-.156	-.185	-.220	-.277	-.455	-.924	-1.080	-.936	-.625
40	-.140	-.199	-.256	-.284	-.355	-.754	-1.206	-1.220	-.995	-.625
30	-.185	-.270	-.362	-.384	-.455	-1.365	-1.550	-1.380	-1.010	-.640
25	-.185	-.299	-.426	-.448	-.526	-1.678	-1.690	-1.436	-1.010	-.640
20	-.199	-.327	-.505	-.511	-.725	-1.975	-1.790	-1.463	-1.024	-.640
15	-.192	-.390	-.611	-.654	-1.536	-2.22	-1.835	-1.492	-1.024	-.640
10	-.230	-.455	-.782	-1.392	-2.23	-2.375	-1.850	-1.535	-1.038	-.640
7.5	-.185	-.497	-.853	-1.920	-2.345	-2.32	-1.850	-1.535	-1.038	-.640
5	-.230	-.654	-1.164	-2.36	-2.36	-2.32	-1.890	-1.550	-1.038	-.640
2.5	-.156	-.753	-1.560	-2.33	-2.33	-2.376	-1.950	-1.590	-1.038	-.640
0	+.355	-.483	-2.53	-2.84	-2.585	-2.43	-1.975	-1.609	-1.038	-.625

TABLE 12

LOWER SURFACE PRESSURE COEFFICIENTS

$C_{\mu} = 0, \quad \eta = .500$

x/c \ α°	0	6	12	15	18	24	27	30	33	36
90	+.014	+.014	+.014	+.028	+.014	+.028	+.028	+.007	-.028	-.078
80	0	0	+.014	+.028	+.028	+.056	+.056	+.064	+.056	+.021
70	-.042	-.042	-.028	0	+.007	+.084	+.071	+.085	+.099	+.071
60	-.070	-.056	-.014	+.014	+.028	+.084	+.112	+.142	+.156	+.156
50	-.128	-.078	-.014	+.028	+.056	+.142	+.170	+.199	+.228	+.242
40	-.140	-.078	0	+.056	+.099	+.199	+.242	+.284	+.313	+.327
30	-.185	-.071	+.042	+.112	+.156	+.284	+.327	+.370	+.412	+.441
25	-.185	-.057	+.084	+.149	+.213	+.341	+.365	+.362	+.384	+.426
20	-.199	-.050	+.112	+.199	+.256	+.398	+.447	+.483	+.526	+.547
15	-.192	-.036	+.168	+.256	+.327	+.455	+.511	+.547	+.583	+.611
10	-.230	+.028	+.242	+.327	+.398	+.519	+.569	+.590	+.596	+.625
7.5	-.185	+.074	+.313	+.384	+.455	+.547	+.569	+.590	+.596	+.625
5	-.230	+.114	+.327	+.398	+.448	+.498	+.505	+.511	+.497	+.540
2.5	-.156	+.220	+.384	+.405	+.398	+.313	+.277	+.256	+.235	+.341
0	+.355	+.106	-1.190	-2.18	-2.39	-3.02	-2.73	-2.09	-1.605	-.810

TABLE 13

UPPER SURFACE PRESSURE COEFFICIENTS

$C_\mu = 0, \quad \eta = .375$

x/c \ α°	0	6	12	15	18	24	27	30	33	36
90	+.014	+.021	+.035	-.007	-.035	-.070	-.120	-.282	-.564	-.529
80	-.014	-.007	-.007	-.049	-.084	-.127	-.183	-.395	-.676	-.571
70	-.035	-.049	-.063	-.091	-.134	-.197	-.268	-.550	-.790	-.600
60	-.070	-.098	-.134	-.162	-.204	-.303	-.444	-.790	-.901	-.614
50	-.125	-.148	-.190	-.233	-.268	-.402	-.655	-1.014	-.985	-.628
40	-.148	-.197	-.268	-.317	-.369	-.521	-.958	-1.254	-1.030	-.642
30	-.176	-.247	-.359	-.416	-.444	-.641	-1.410	-1.471	-1.070	-.663
25	-.190	-.296	-.429	-.500	-.564	-.825	-1.733	-1.608	-1.085	-.663
20	-.204	-.338	-.515	-.600	-.705	-1.112	-2.014	-1.708	-1.112	-.663
15	-.197	-.402	-.614	-.705	-.980	-2.05	-2.312	-1.790	-1.130	-.663
10	-.197	-.471	-.783	-.895	-1.658	-3.25	-2.54	-1.832	-1.150	-.663
7.5	-.169	-.485	-.810	-1.009	-2.095	-3.43	-2.54	-1.832	-1.155	-.663
5	-.162	-.591	-.993	-1.630	-2.940	-3.815	-2.564	-1.860	-1.155	-.663
2.5	-.141	-.711	-1.463	-2.46	-3.050	-3.785	-2.60	-1.875	-1.155	-.670
0	+.388	-.338	-2.131	-3.110	-3.71	-3.985	-2.79	-1.930	-1.155	-.670

TABLE 14

LOWER SURFACE PRESSURE COEFFICIENTS

$C_\mu = 0, \quad \eta = .375$

x/c \ a°	0	6	12	15	18	24	27	30	33	36
90	+.014	-.049	+.007	+.028	+.028	+.042	+.042	+.049	+.014	-.071
80	-.014	-.084	0	+.035	+.042	+.071	+.084	+.098	+.084	+.035
70	-.035	-.091	+.014	+.042	+.063	+.105	+.126	+.148	+.155	+.127
60	-.070	-.098	+.007	+.042	+.078	+.141	+.169	+.198	+.218	+.212
50	-.125	-.105	+.014	+.056	+.098	+.190	+.232	+.268	+.296	+.310
40	-.148	-.105	+.028	+.084	+.141	+.246	+.289	+.345	+.381	+.395
30	-.176	-.091	+.071	+.134	+.204	+.338	+.388	+.438	+.480	+.500
25	-.190	-.070	+.091	+.169	+.240	+.380	+.437	+.494	+.529	+.550
20	-.204	-.056	+.127	+.213	+.282	+.430	+.486	+.536	+.578	+.592
15	-.197	-.035	+.176	+.260	+.345	+.486	+.529	+.579	+.620	+.641
10	-.197	+.028	+.240	+.334	+.408	+.543	+.591	+.635	+.649	+.670
7.5	-.169	+.084	+.310	+.395	+.458	+.571	+.606	+.641	+.649	+.676
5	-.162	+.141	+.360	+.430	+.480	+.536	+.543	+.557	+.557	+.606
2.5	-.141	+.204	+.388	+.409	+.388	+.275	+.204	+.218	+.226	+.360
0	+.388	+.105	-1.042	-1.900	-2.55	-4.33	-4.30	-2.861	-1.960	-.860

TABLE 15

UPPER SURFACE PRESSURE COEFFICIENTS

$C_\mu = 0, \quad \eta = .250$

x/c \ α°	0	6	12	15	18	24	27	30	33	36
90	-.007	0	-.014	-.035	-.056	-.070	-.120	-.226	-.606	-.565
80	-.021	-.028	-.049	-.077	-.113	-.141	-.169	-.359	-.734	-.593
70	-.056	-.077	-.113	-.148	-.197	-.254	-.310	-.507	-.831	-.607
60	-.098	-.127	-.176	-.220	-.275	-.366	-.437	-.676	-.916	-.621
50	-.141	-.176	-.240	-.296	-.359	-.508	-.578	-.874	-1.000	-.635
40	-.155	-.233	-.324	-.388	-.459	-.676	-.760	-1.170	-1.058	-.649
30	-.183	-.296	-.409	-.500	-.585	-.874	-.986	-1.521	-1.100	-.656
25	-.183	-.310	-.452	-.550	-.649	-.965	-1.150	-1.676	-1.114	-.656
20	-.197	-.352	-.522	-.627	-.754	-1.070	-1.396	-1.890	-1.130	-.656
15	-.183	-.359	-.564	-.698	-.846	-1.200	-1.747	-2.085	-1.144	-.673
10	-.183	-.452	-.705	-.880	-1.070	-1.438	-2.539	-2.325	-1.151	-.673
7.5	-.169	-.479	-.775	-.980	-1.220	-1.640	-3.100	-2.450	-1.158	-.673
5	-.155	-.543	-.895	-1.170	-1.500	-2.037	-3.790	-2.450	-1.158	-.673
2.5	-.105	-.620	-1.228	-1.600	-2.085	-2.878	-4.47	-2.465	-1.158	-.673
0	+.437	+.007	-1.170	-2.05	-3.120	-5.87	-6.380	-2.980	-1.158	-.673

TABLE 16

LOWER SURFACE PRESSURE COEFFICIENTS

$C_\mu = 0, \quad \eta = .250$

%c \ a^o	0	6	12	15	18	24	27	30	33	36
90	-.007	-.007	+.014	+.035	+.049	-.076	+.077	+.063	+.049	-.070
80	-.021	-.028	+.014	+.049	+.070	+.120	+.127	+.134	+.120	+.070
70	-.056	-.042	+.021	+.049	+.084	+.141	+.162	+.190	+.197	+.183
60	-.098	-.049	+.021	+.063	+.105	+.183	+.219	+.244	+.275	+.282
50	-.141	-.063	+.028	+.084	+.148	+.233	+.275	+.317	+.352	+.366
40	-.155	-.077	+.042	+.091	+.176	+.289	+.338	+.388	+.437	+.451
30	-.183	-.063	+.077	+.148	+.226	+.360	+.423	+.473	+.530	+.544
25	-.183	-.049	+.091	+.183	+.268	+.402	+.473	+.531	+.585	+.592
20	-.197	-.035	+.141	+.226	+.310	+.459	+.531	+.585	+.641	+.648
15	-.183	+.007	+.197	+.282	+.367	+.524	+.592	+.643	+.684	+.698
10	-.183	+.042	+.261	+.346	+.437	+.571	+.629	+.677	+.720	+.734
7.5	-.169	+.091	+.310	+.395	+.473	+.578	+.615	+.656	+.698	+.720
5	-.155	+.148	+.366	+.444	+.508	+.557	+.557	+.585	+.629	+.684
2.5	-.105	+.226	+.423	+.465	+.486	+.388	+.310	+.592	+.395	+.522
0	+.437	+.120	-.945	-1.731	-2.765	-5.40	-7.22	-7.08	-2.79	-.360

TABLE 17

UPPER SURFACE PRESSURE COEFFICIENTS

$C_\mu = 0, \quad \eta = .125$

x/c \ α°	0	6	12	15	18	24	27	30	33	36
90	-.014	-.021	-.028	-.049	-.056	-.077	-.120	-.226	-.620	-.635
80	-.042	-.070	-.091	-.120	-.134	-.183	-.266	-.359	-.719	-.662
70	-.091	-.127	-.162	-.205	-.233	-.303	-.401	-.535	-.874	-.676
60	-.105	-.155	-.212	-.261	-.296	-.395	-.521	-.690	-.959	-.683
50	-.141	-.212	-.275	-.331	-.381	-.500	-.650	-.846	-1.015	-.683
40	-.162	-.275	-.360	-.430	-.507	-.649	-.818	-1.030	-1.085	-.690
30	-.176	-.296	-.409	-.486	-.578	-.768	-.910	-1.141	-1.141	-.690
25	-.169	-.296	-.437	-.529	-.635	-.853	-.986	-1.227	-1.184	-.690
20	-.169	-.324	-.479	-.578	-.690	-.951	-1.141	-1.382	-1.240	-.697
15	-.148	-.324	-.507	-.606	-.761	-1.042	-1.347	-1.438	-1.269	-.704
10	-.141	-.381	-.592	-.734	-.888	-1.212	-1.628	-2.03	-1.340	-.718
7.5	-.134	-.395	-.649	-.810	-.993	-1.369	-1.675	-2.44	-1.381	-.718
5	-.155	-.465	-.860	-1.064	-1.290	-1.728	-1.980	-3.03	-1.425	-.723
2.5	-.070	-.493	-1.240	-1.262	-1.550	-2.170	-2.53	-3.48	-1.439	-.723
0	+.430	+.091	-.775	-1.472	-2.256	-4.20	-5.40	-6.16	-1.453	-.761

TABLE 18

LOWER SURFACE PRESSURE COEFFICIENTS

$C_\mu = 0, \quad \eta = .125$

x/c \ α°	0	6	12	15	18	24	27	30	33	36
90	-.014	0	+.021	+.042	+.049	+.084	+.105	+.105	+.091	-.014
80	-.042	-.021	+.007	+.042	+.063	+.127	+.155	+.183	+.183	+.141
70	-.091	-.049	0	+.042	+.070	+.155	+.197	+.233	+.254	+.240
60	-.105	-.056	+.014	+.063	+.098	+.212	+.261	+.303	+.324	+.317
50	-.141	-.063	+.028	+.084	+.141	+.261	+.324	+.374	+.395	+.423
40	-.162	-.056	+.042	+.105	+.162	+.296	+.374	+.430	+.465	+.494
30	-.176	-.042	+.077	+.155	+.233	+.381	+.472	+.522	+.557	+.585
25	-.169	-.028	+.105	+.190	+.268	+.430	+.508	+.571	+.613	+.641
20	-.169	-.014	+.141	+.226	+.310	+.472	+.557	+.627	+.670	+.698
15	-.148	+.021	+.197	+.282	+.367	+.536	+.620	+.684	+.733	+.754
10	-.141	+.070	+.261	+.352	+.437	+.592	+.670	+.747	+.790	+.811
7.5	-.134	+.098	+.303	+.395	+.480	+.614	+.677	+.740	+.790	+.818
5	-.155	+.105	+.324	+.416	+.494	+.592	+.620	+.663	+.719	+.783
2.5	-.070	+.226	+.437	+.494	+.536	+.522	+.479	+.430	+.465	+.663
0	+.430	+.197	-.564	-1.136	-1.919	-3.895	-5.11	-6.51	-7.050	-.985

TABLE 19

UPPER SURFACE PRESSURE COEFFICIENTS

C_μ = .138, η = .921

x/c \ α°	0	1	3	6	12	18	21	24	30	33	36	$37\frac{1}{2}$
90	+.092	+.092	+.092	+.078	+.035	+.014	+.021	-.014	-.106	-.141	-.298	-.426
80	+.078	+.071	+.071	+.064	+.021	-.014	-.078	-.133	-.255	-.310	-.384	-.418
70	+.036	+.035	+.035	+.021	-.014	-.056	-.185	-.362	-.540	-.585	-.625	-.638
60	+.014	+.007	-.007	-.035	-.092	-.127	-.369	-.787	-1.030	-1.064	-1.015	-.986
50	-.170	-.198	-.247	-.334	-.504	-.529	-.974	-1.711	-1.970	-1.860	-1.525	-1.328
40	-.227	-.270	-.352	-.476	-.751	-1.132	-2.072	-2.250	-2.110	-1.902	-1.555	-1.279
30	-.227	-.284	-.360	-.484	-.616	-1.882	-2.281	-2.075	-1.630	-1.420	-1.164	-.880
25	-.440	-.518	-.635	-.781	-.915	-2.350	-2.855	-2.700	-2.110	-1.840	-1.478	-1.179
20	-.575	-.653	-.790	-.910	-1.058	-1.848	-1.945	-2.075	-1.895	-1.705	-1.440	-1.120
15	-.496	-.540	-.585	-.731	-.908	-1.290	-1.350	-1.420	-1.405	-1.275	-1.120	-.972
10	-.263	-.327	-.408	-.518	-.795	-1.220	-1.291	-1.342	-1.350	-1.270	-1.164	-1.080
7.5	-.320	-.355	-.423	-.610	-.930	-1.246	-1.291	-1.335	-1.342	-1.254	-1.115	-1.015
5	-.340	-.405	-.522	-.724	-1.185	-1.445	-1.428	-1.448	-1.461	-1.39	-1.229	-1.080
2.5	-.056	-.049	-.296	-.535	-1.140	-1.72	-1.58	-1.60	-1.530	-1.50	-1.430	-1.540
0	-.313	-.398	-.592	-.900	-1.760	-1.518	-1.455	-1.470	-1.461	-1.382	-1.250	-1.085

TABLE 20

LOWER SURFACE PRESSURE COEFFICIENTS

$C_\mu = .138, \quad \eta = .921$

x/c \ α°	0	1	3	6	12	18	21	24	30	33	36	37½
90	+.092	+1.55	+.057	+.042	+.035	0	+.035	-.035	+.014	-.014	0	-.042
80	+.078	+.45	+.042	+.014	0	-.028	+.071	-.014	-.042	-.057	-.071	-.099
70	+.036	+.25	+.021	-.021	-.035	-.092	-.035	-.092	-.113	-.105	-.121	-.127
60	+.014	+.15	+.021	-.014	-.035	-.085	-.063	-.156	-.226	-.254	-.262	-.255
50	-.170	-.90	-.085	-.085	-.050	-.035	-.028	-.057	-.057	-.057	-.043	-.042
40	-.227	-1.35	-.128	-.092	-.028	+.007	-.071	+.021	+.049	+.071	+.085	+.092
30	-.227	-1.05	-.064	-.021	+.064	+.099	+.120	+.128	+.128	+.128	+.198	+.218
25	-.440	-2.35	-.206	-.121	-.021	+.028	+.071	+.099	+.155	+.183	+.198	+.211
20	-.575	-3.15	-.263	-.135	-.085	-.014	+.042	+.078	+.134	+.176	+.198	+.211
15	-.496	-2.55	-.177	-.071	0	+.071	+.113	+.149	+.211	+.246	+.270	+.289
10	-.263	-1.60	-.099	-.021	+.085	+.135	+.176	+.213	+.254	+.275	+.291	+.303
7.5	-.320	-1.90	-.106	-.028	+.085	+.121	+.148	+.178	+.211	+.226	+.234	+.240
5	-.340	-1.90	-.128	-.021	+.106	+.128	+.162	+.170	+.164	+.148	+.142	+.141
2.5	-.056	-.014	+.077	+.183	+.261	+.233	-.226	-.212	+.141	+.106	+.098	+.120
0	-.313	-1.75	-.078	-.014	-.007	+.220	+.211	+.178	+.105	+.049	+.021	+.141

TABLE 21

UPPER SURFACE PRESSURE COEFFICIENTS

$C_\mu = .138, \quad \eta = .875$

x/c \ α°	0	1	3	6	12	18	21	24	30	33	36	37½
90	+.078	+.077	+.078	+.071	+.043	+.028	0	-.042	-.176	-.270	-.402	-.480
80	+.057	+.049	+.042	+.042	0	-.071	-.056	-.127	-.338	-.455	-.522	-.515
70	+.028	+.021	+.007	0	-.057	-.049	-.121	-.247	-.592	-.738	-.740	-.705
60	-.056	-.063	-.078	-.113	-.213	-.219	-.289	-.591	-1.115	-1.250	-1.115	-1.021
50	-.121	-.134	-.162	-.226	-.383	-.247	-.289	-.740	-1.340	-1.450	-1.276	-1.114
40	-.206	-.232	-.275	-.366	-.554	-.275	-.924	-1.521	-1.685	-1.620	-1.375	-1.114
30	-.312	-.345	-.416	-.521	-.674	-1.700	-2.43	-2.340	-1.975	-1.740	-1.446	-1.120
25	-.355	-.402	-.486	-.585	-.736	-2.060	-2.73	-2.460	-1.968	-1.720	-1.440	-1.120
20	-.376	-.415	-.507	-.592	-.758	-1.950	-2.15	-2.110	-1.750	-1.590	-1.375	-1.114
15	-.348	-.388	-.473	-.550	-.758	-1.670	-1.665	-1.630	-1.580	-1.500	-1.320	-1.108
10	-.333	-.374	-.466	-.621	-.894	-1.630	-1.685	-1.685	-1.610	-1.520	-1.328	-1.100
7.5	-.305	-.360	-.466	-.621	-.965	-1.620	-1.692	-1.700	-1.621	-1.535	-1.340	-1.114
5	-.291	-.366	-.501	-.720	-1.200	-1.680	-1.740	-1.74	-1.635	-1.535	-1.320	-1.108
2.5	-.234	-.331	-.529	-.916	-1.570	-1.705	-1.761	-1.740	-1.615	-1.528	-1.328	-1.114
0	+.320	+.251	+.042	-.528	-2.516	-2.070	-1.881	-1.760	-1.600	-1.520	-1.320	-1.114

TABLE 22

LOWER SURFACE PRESSURE COEFFICIENTS

C_μ = .138, η = .875

$\%c \backslash a^o$	0	1	3	6	12	18	21	24	30	33	36	$37\frac{1}{2}$
90	+.078	+.042	+.057	+.049	+.049	+.210	+.021	+.042	+.042	+.028	0	-.035
80	+.057	+.028	+.035	+.042	+.035	+.014	+.014	+.028	+.035	+.028	+.014	-.007
70	+.028	+.021	+.021	+.035	+.007	0	+.007	0	+.014	+.014	0	-.014
60	-.056	-.049	-.028	-.021	-.007	-.007	0	-.028	-.007	0	0	-.007
50	-.121	-.134	-.085	-.049	-.014	+.014	+.028	+.028	+.056	+.071	+.084	+.077
40	-.206	-.162	-.113	-.071	-.007	+.035	+.064	+.078	+.127	+.155	+.169	+.176
30	-.312	-.211	-.156	-.098	-.007	+.056	+.085	+.121	+.190	+.226	+.254	+.254
25	-.355	-.226	-.163	-.091	+.007	+.064	+.071	+.071	+.141	+.176	+.190	+.190
20	-.376	-.240	-.170	-.091	+.021	+.099	+.156	+.199	+.282	+.317	+.346	+.353
15	-.348	-.233	-.156	-.063	+.063	+.156	+.199	+.248	+.338	+.367	+.395	+.401
10	-.333	-.233	-.142	-.035	+.119	+.213	+.256	+.298	+.374	+.395	+.416	+.416
7.5	-.305	-.240	-.064	0	+.169	+.284	+.326	+.362	+.360	+.423	+.437	+.430
5	-.291	-.176	+.042	+.084	+.268	+.348	+.369	+.398	+.409	+.395	+.388	+.395
2.5	-.234	-.099	+.184	+.219	+.359	+.340	+.312	+.284	+.218	+.162	+.127	+.121
0	+.320	+.352	+.284	-.049	-1.460	-2.36	-2.17	-2.03	-1.720	-1.592	-1.510	-1.401

TABLE 23

UPPER SURFACE PRESSURE COEFFICIENTS

$C_\mu = .138, \quad \eta = .812$

x/c \ α°	0	1	3	6	12	18	21	24	30	33	36	37½
90	+.078	+.063	+.063	+.063	+.049	+.014	-.014	-.042	-.247	-.388	-.578	-.557
80	+.042	+.021	+.021	+.021	0	-.035	-.084	-.127	-.424	-.600	-.712	-.655
70	+.007	-.007	-.021	-.042	-.071	-.084	-.120	-.212	-.661	-.851	-.874	-.840
60	-.063	-.078	-.106	-.148	-.218	-.183	-.148	-.360	-1.000	-1.177	-1.092	-1.010
50	-.106	-.127	-.162	-.218	-.317	-.162	-.084	-.451	-1.170	-1.331	-1.209	-1.108
40	-.212	-.246	-.296	-.374	-.472	-.289	-.733	-1.381	-1.705	-1.595	-1.346	-1.120
30	-.275	-.332	-.360	-.458	-.556	-.712	-2.10	-2.30	-1.975	-1.700	-1.418	-1.150
25	-.184	-.246	-.275	-.360	-.486	-1.278	-2.37	-2.51	-1.931	-1.655	-1.390	-1.161
20	-.303	-.360	-.416	-.486	-.641	-1.966	-2.27	-2.32	-1.820	-1.600	-1.375	-1.161
15	-.296	-.346	-.416	-.515	-.698	-2.095	-1.90	-2.10	-1.720	-1.572	-1.360	-1.161
10	-.275	-.346	-.444	-.571	-.851	-2.150	-1.775	-1.960	-1.761	-1.615	-1.390	-1.161
7.5	-.246	-.318	-.430	-.585	-.936	-2.150	-1.790	-1.930	-1.790	-1.628	-1.40	-1.178
5	-.226	-.318	-.458	-.648	-1.145	-2.120	-1.811	-1.960	-1.820	-1.628	-1.418	-1.178
2.5	-.155	-.275	-.479	-.951	-1.375	-2.135	-1.775	-1.720	-1.790	-1.620	-1.430	-1.200
0	-.332	+.268	+.071	-.416	-2.095	-2.32	-2.03	-2.015	-1.779	-1.609	-1.418	-1.190

TABLE 24

LOWER SURFACE PRESSURE COEFFICIENTS

C_μ = .138, η = .812

x/c \ α^o	0	1	3	6	12	18	21	24	30	33	36	$37\frac{1}{2}$
90	+.078	+.063	+.056	+.056	+.056	+.042	+.028	+.042	+.021	+.021	-.014	-.035
80	+.042	+.021	+.028	+.028	+.028	+.028	+.014	+.021	+.014	+.021	+.014	0
70	+.007	-.007	+.014	+.014	+.014	+.028	+.021	+.021	+.014	+.028	+.028	+.028
60	-.063	-.071	-.028	-.028	0	+.028	+.035	+.021	+.042	+.056	+.071	+.078
50	-.106	-.113	-.084	-.049	0	+.042	+.056	+.071	+.090	+.127	+.155	+.162
40	-.212	-.190	-.113	-.071	0	+.063	+.084	+.106	+.155	+.190	+.226	+.240
30	-.275	-.240	-.141	-.084	+.007	+.099	+.135	+.162	+.247	+.282	+.324	+.338
25	-.184	-.268	-.148	-.084	+.021	+.120	+.155	+.197	+.290	+.331	+.366	+.381
20	-.303	-.261	-.148	-.071	+.056	+.162	+.205	+.247	+.332	+.374	+.416	+.423
15	-.296	-.247	-.134	-.042	+.106	+.240	+.282	+.325	+.416	+.444	+.386	+.500
10	-.275	-.226	-.099	+.021	+.190	+.324	+.366	+.402	+.486	+.501	+.522	+.529
7.5	-.246	-.218	-.091	+.049	+.240	+.366	+.402	+.430	+.472	+.494	+.507	+.515
5	-.226	-.162	-.014	+.127	+.324	+.423	+.437	+.430	+.459	+.444	+.437	+.437
2.5	-.155	-.071	-.099	-.251	+.395	+.381	+.352	+.296	+.233	+.325	+.162	+.155
0	-.332	+.352	+.296	-.021	-1.42	-3.035	-2.60	-2.38	-1.98	-1.78	-1.589	-1.494

TABLE 25

UPPER SURFACE STATIC PRESSURE COEFFICIENTS

C_μ = .138, η = .750

x/c \ α°	0	1	3	6	12	18	21	24	30	33	36	37½
90	+.063	+.063	+.049	+.049	+.007	+.014	+.007	+.028	-.228	-.436	-.634	-.591
80	+.007	+.014	0	-.014	-.063	-.042	-.007	-.113	-.394	-.634	-.768	-.705
70	-.021	-.014	-.035	-.056	-.135	-.071	-.084	-.127	-.564	-.810	-.894	-.852
60	-.084	-.084	-.095	-.154	-.261	-.113	-.091	-.198	-.845	-1.070	-1.035	-.852
50	-.134	-.143	-.190	-.240	-.353	-.148	-.078	-.310	-1.150	-1.302	-1.212	-1.13
40	-.226	-.218	-.247	-.324	-.424	-.275	-.282	-.832	-1.660	-1.612	-1.345	-1.179
30	-.275	-.290	-.331	-.416	-.522	-.889	-1.636	-2.080	-2.12	-1.830	-1.46	-1.220
25	-.282	-.296	-.360	-.437	-.564	-1.200	-2.175	-2.490	-2.125	-1.820	-1.465	-1.230
20	-.282	-.296	-.381	-.459	-.621	-1.640	-2.50	-2.765	-2.080	-1.775	-1.465	-1.234
15	-.275	-.296	-.388	-.487	-.712	-1.930	-2.385	-2.60	-1.940	-1.731	-1.45	-1.230
10	-.261	-.303	-.416	-.558	-.881	-2.095	-2.215	-2.315	-1.950	-1.750	-1.465	-1.234
7.5	-.233	-.282	-.409	-.550	-.971	-2.045	-2.13	-2.20	-2.00	-1.782	-1.492	-1.250
5	-.226	-.296	-.451	-.649	-1.170	-2.14	-2.13	-2.225	-2.038	-1.790	-1.492	-1.250
2.5	-.191	-.268	-.487	-.939	-1.454	-2.20	-2.06	-2.165	-2.015	-1.782	-1.500	-1.250
0	+.339	+.296	+.916	-.445	-2.284	-2.55	-2.38	-2.145	-1.973	-1.760	-1.492	-1.234

TABLE 26

LOWER SURFACE STATIC PRESSURE COEFFICIENTS

C_μ = .138, η = .750

y/c \ $\alpha°$	0	1	3	6	12	18	21	24	30	33	36	$37\frac{1}{2}$
90	+.063	+.063	+.056	+.049	+.042	+.042	+.028	+.035	+.035	+.014	-.021	-.049
80	+.007	+.021	+.021	+.021	+.014	+.028	+.021	+.021	+.035	+.035	+.021	+.014
70	-.021	+.007	+.021	-.007	+.021	+.042	+.042	+.049	+.071	+.063	+.071	+.071
60	-.084	-.042	-.042	-.035	+.007	+.042	+.042	+.063	+.098	+.105	+.120	+.127
50	-.134	-.120	-.098	-.071	-.007	+.049	+.063	+.084	+.135	+.162	+.176	+.197
40	-.226	-.148	-.113	-.071	+.007	+.078	+.098	+.141	+.212	+.225	+.268	+.296
30	-.275	-.197	-.148	-.091	+.014	+.108	+.148	+.204	+.289	+.317	+.352	+.380
25	-.282	-.204	-.148	-.084	+.035	+.141	+.190	+.232	+.345	+.373	+.408	+.437
20	-.282	-.204	-.141	-.056	+.078	+.197	+.240	+.303	+.395	+.430	+.465	+.494
15	-.275	-.204	-.127	-.028	+.007	+.268	+.331	+.380	+.479	+.500	+.528	+.550
10	-.261	-.176	-.084	+.035	+.225	+.366	+.409	+.458	+.528	+.543	+.556	+.570
7.5	-.233	-.162	-.072	+.056	+.254	+.408	+.444	+.486	+.521	+.528	+.528	+.550
5	-.226	-.134	-.007	+.141	+.345	+.444	+.465	+.480	+.479	+.465	+.458	+.465
2.5	-.191	-.056	+.091	+.253	+.395	+.352	+.338	+.296	+.183	+.134	+.106	+.113
0	+.339	+.359	+.296	-.035	-1.451	-3.115	-2.26	-2.25	-2.16	-1.965	-1.74	-1.620

TABLE 27

UPPER SURFACE PRESSURE COEFFICIENTS

$C_\mu = .138, \quad \eta = .625$

x/c \ α°	0	1	3	6	12	18	21	24	30	33	36	37½
90	+.028	+.035	+.021	+.021	-.014	-.035	+.007	-.028	-.162	-.381	-.663	-.663
80	-.035	-.035	-.049	-.056	-.085	-.105	-.063	-.098	-.310	-.578	-.845	-.866
70	-.063	-.070	-.098	-.120	-.155	-.176	-.091	-.127	-.402	-.733	-.959	-.980
60	-.113	-.113	-.148	-.176	-.226	-.240	-.105	-.162	-.529	-.930	-1.062	-1.091
50	-.141	-.148	-.197	-.226	-.275	-.310	-.148	-.183	-.804	-1.240	-1.331	-1.231
40	-.226	-.226	-.268	-.310	-.380	-.458	-.246	-.352	-1.510	-1.810	-1.522	-1.290
30	-.226	-.226	-.268	-.331	-.437	-.571	-.507	-.86	-2.100	-2.03	-1.580	-1.298
25	-.183	-.162	-.296	-.287	-.465	-.599	-.922	-1.635	-2.470	-2.17	-1.650	-1.320
20	-.246	-.261	-.338	-.395	-.578	-.860	-1.840	-2.455	-2.565	-2.128	-1.608	-1.302
15	-.240	-.268	-.366	-.479	-.711	-1.150	-2.715	-3.170	-2.665	-2.128	-1.635	-1.320
10	-.254	-.289	-.409	-.591	-.915	-1.615	-3.265	-3.41	-2.665	-2.128	-1.650	-1.320
7.5	-.240	-.289	-.423	-.599	-1.007	-1.90	-2.955	-3.03	-2.58	-2.128	-1.664	-1.326
5	-.289	-.346	-.494	-.698	-1.410	-2.29	-2.90	-3.03	-2.665	-2.160	-1.692	-1.326
2.5	-.169	-.254	-.451	-.733	-1.445	-2.53	-2.74	-3.062	-2.58	-2.14	-1.708	-1.326
0	+.296	-.226	-.042	-.620	-3.080	-3.34	-2.90	-2.91	-2.51	-2.16	-1.715	-1.326

TABLE 28

LOWER SURFACE PRESSURE COEFFICIENTS

C_μ = .138, η = .625

%c \ α°	0	1	3	6	12	18	21	24	30	33	36	37½
90	+.028	-.014	+.028	+.028	+.028	+.035	+.028	+.042	+.028	+.021	-.007	-.028
80	-.035	-.085	-.035	-.028	-.021	0	-.007	+.014	+.035	+.049	+.042	+.035
70	-.063	-.113	-.056	-.042	-.014	+.014	+.021	+.042	+.077	+.091	+.105	+.105
60	-.113	-.141	-.085	-.056	-.007	+.042	+.056	+.085	+.135	+.155	+.183	+.183
50	-.141	-.148	-.113	-.070	-.014	+.063	+.085	+.127	+.184	+.212	+.247	+.255
40	-.226	-.218	-.141	-.098	0	+.085	+.127	+.170	+.254	+.289	+.324	+.352
30	-.226	-.211	-.141	-.070	+.042	+.148	+.197	+.261	+.352	+.388	+.437	+.451
25	-.183	-.218	-.141	-.056	+.070	+.197	+.247	+.317	+.416	+.458	+.486	+.486
20	-.246	-.211	-.127	-.028	+.113	+.240	+.310	+.381	+.479	+.515	+.550	+.564
15	-.240	-.211	-.121	-.021	+.162	+.310	+.380	+.437	+.536	+.564	+.600	+.614
10	-.254	-.204	-.098	+.028	+.240	+.380	+.444	+.494	+.564	+.585	+.607	+.614
7.5	-.240	-.183	-.056	+.071	+.287	+.416	+.472	+.522	+.550	+.557	+.564	+.564
5	-.289	-.211	-.070	+.078	+.301	+.394	+.437	+.444	+.416	+.395	+.388	+.388
2.5	-.169	-.085	+.070	+.233	+.380	+.317	+.317	+.254	+.098	+.049	+.042	+.035
0	+.296	+.360	+.331	+.049	-1.324	-3.610	-2.65	-2.901	+2.836	-2.51	-2.10	-1.85

TABLE 29

UPPER SURFACE PRESSURE COEFFICIENTS

C_μ = .138, η = .500

y/c \ α°	0	1	3	6	12	18	21	24	30	33	36	37½
90	+.014	+.007	0	0	+.071	-.070	-.021	-.035	-.113	-.303	-.606	-.733
80	-.021	-.028	-.035	-.042	-.046	-.120	-.063	-.846	-.162	-.360	-.705	-.916
70	-.084	-.091	-.105	-.120	-.134	-.226	-.127	-.155	-.268	-.522	-.874	-1.100
60	-.105	-.120	-.141	-.169	-.197	-.310	-.205	-.211	-.388	-.754	-1.114	-1.212
50	-.169	-.155	-.190	-.218	-.275	-.422	-.289	-.275	-.578	-1.120	-1.41	-1.310
40	-.190	-.204	-.215	-.268	-.338	-.528	-.388	-.360	-.895	-1.164	-1.640	-1.354
30	-.211	-.226	-.253	-.324	-.437	-.661	-.529	-.496	-1.729	-2.310	-1.832	-1.381
25	-.226	-.245	-.303	-.352	-.500	-.740	-.585	-.557	-2.265	-2.545	-1.890	-1.390
20	-.226	-.253	-.331	-.387	-.570	-.830	-.614	-.816	-2.898	-2.715	-1.920	-1.395
15	-.226	-.253	-.345	-.451	-.682	-.943	-1.080	-2.115	-3.35	-2.740	-1.920	-1.390
10	-.226	-.275	-.387	-.574	-.852	-1.250	-2.98	-4.26	-3.69	-2.740	-1.945	-1.390
7.5	-.211	-.268	-.387	-.521	-.921	-1.365	-3.70	-4.65	-3.76	-2.715	-1.960	-1.390
5	-.219	-.303	-.344	-.705	-1.290	-1.960	-3.83	-4.45	-3.56	-2.732	-1.974	-1.390
2.5	-.176	-.268	-.371	-.830	-1.520	-2.55	-3.63	-3.96	-3.52	-2.750	-1.974	-1.390
0	+.359	-.345	+.035	-.591	-2.78	-6.04	-3.97	-3.85	-3.38	-2.740	-1.974	-1.381

TABLE 30

LOWER SURFACE PRESSURE COEFFICIENTS

$C_\mu = .138, \quad \eta = .500$

x/c \ α°	0	1	3	6	12	18	21	24	30	33	36	37½
90	+.014	-.071	0	0	+.007	+.035	+.014	+.028	+.028	+.035	+.014	+.007
80	-.021	-.098	-.014	-.014	+.014	+.049	+.042	+.063	+.085	+.084	+.084	+.092
70	-.084	-.141	-.071	-.056	-.014	+.035	+.035	+.063	+.105	+.134	+.141	+.162
60	-.105	-.169	-.098	-.071	0	+.056	+.071	+.113	+.170	+.190	+.226	+.240
50	-.169	-.211	-.120	-.085	+.007	+.078	+.113	+.162	+.232	+.268	+.303	+.324
40	-.190	-.226	-.141	-.085	+.014	+.127	+.162	+.226	+.317	+.359	+.395	+.423
30	-.211	-.226	-.141	-.078	+.056	+.190	+.240	+.303	+.416	+.458	+.500	+.515
25	-.226	-.232	-.141	-.078	+.085	+.226	+.282	+.360	+.465	+.515	+.550	+.571
20	-.226	-.226	-.134	-.056	+.127	+.275	+.338	+.416	+.529	+.564	+.606	+.621
15	-.226	-.204	-.112	-.014	+.176	+.346	+.388	+.479	+.578	+.621	+.649	+.664
10	-.226	-.190	-.084	+.035	+.247	+.401	+.465	+.529	+.600	+.621	+.635	+.656
7.5	-.211	-.162	-.049	+.085	+.303	+.444	+.500	+.550	+.585	+.585	+.600	+.613
5	-.219	-.169	-.042	+.113	+.338	+.430	+.465	+.480	+.444	+.430	+.437	+.444
2.5	-.176	-.098	-.049	+.218	+.395	+.346	+.314	+.247	+.049	0	+.007	+.021
0	+.359	+.409	+.353	+.071	-1.312	-3.72	+3.565	-3.86	-3.855	+3.28	-2.565	-2.235

TABLE 31

UPPER SURFACE PRESSURE COEFFICIENTS

$C_\mu = .138, \quad \eta = .375$

x/c \ α°	0	1	3	6	12	18	24	21	30	33	36	37½
90	-.021	-.014	-.021	-.028	-.021	-.077	-.028	-.134	-.105	-.226	-.525	-.775
80	-.042	-.035	-.049	-.070	-.070	-.149	-.098	-.212	-.190	-.296	-.649	-.972
70	-.063	-.063	-.091	-.113	-.127	-.218	-.169	-.278	-.275	-.396	-.816	-1.130
60	-.105	-.105	-.141	-.162	-.197	-.296	-.275	-.367	-.402	-.578	-1.130	-1.243
50	-.169	-.155	-.169	-.204	-.254	-.373	-.381	-.465	-.529	-.790	-1.451	-1.340
40	-.183	-.197	-.204	-.261	-.331	-.472	-.507	-.571	-.690	-1.200	-1.690	-1.398
30	-.197	-.226	-.254	-.303	-.409	-.575	-.634	-.705	-.895	-1.935	-1.930	-1.408
25	-.211	-.233	-.299	-.345	-.486	-.705	-.761	-.818	-1.120	-2.50	-2.060	-1.415
20	-.226	-.247	-.317	-.395	-.564	-.831	-.901	-.974	-1.445	-2.93	-2.10	-1.430
15	-.218	-.247	-.338	-.451	-.661	-1.021	-1.179	-1.243	-2.235	-3.255	-2.14	-1.430
10	-.226	-.261	-.367	-.529	-.839	-1.275	-1.831	-1.591	-4.58	-3.41	-2.155	-1.430
7.5	-.197	-.233	-.352	-.522	-.846	-1.390	-2.51	-1.758	-5.06	-3.34	-2.155	-1.423
5	-.183	-.247	-.388	-.641	-1.042	-1.712	-4.41	-2.27	-5.83	-3.325	-2.170	-1.423
2.5	-.162	-.240	-.423	-.775	-1.340	-2.275	-4.95	-3.13	-5.72	-3.34	-2.177	-1.423
0	+.374	+.331	+.134	-.402	-2.29	-4.95	-5.74	-4.81	-5.54	-3.42	-2.215	-1.423

n.b. Columns 21 and 24 are in reverse order.

TABLE 32

LOWER SURFACE PRESSURE COEFFICIENTS

$C_\mu = .138, \quad \eta = .375$

y/c \ α°	0	1	3	6	12	18	21	24	30	33	36	$37\frac{1}{2}$
90	-.021	-.021	0	-.007	+.007	+.028	+.035	+.042	+.056	+.056	+.042	+.042
80	-.042	-.042	-.014	-.021	+.007	+.049	+.063	+.077	+.113	+.113	+.127	+.127
70	-.063	-.063	-.049	-.042	+.014	+.077	+.098	+.120	+.176	+.191	+.212	+.212
60	-.105	-.126	-.070	-.056	+.014	+.084	+.120	+.155	+.226	+.246	+.282	+.296
50	-.169	-.149	-.091	-.070	+.028	+.113	+.155	+.204	+.296	+.324	+.366	+.387
40	-.183	-.176	-.105	-.070	+.035	+.149	+.204	+.261	+.374	+.409	+.451	+.479
30	-.197	-.190	-.113	-.056	+.070	+.212	+.275	+.345	+.473	+.508	+.564	+.576
25	-.211	-.197	-.113	-.049	+.098	+.240	+.317	+.388	+.515	+.557	+.606	+.620
20	-.226	-.197	-.113	-.035	+.127	+.282	+.359	+.430	+.564	+.606	+.655	+.662
15	-.218	-.190	-.098	0	+.176	+.338	+.416	+.486	+.606	+.641	+.690	+.698
10	-.226	-.176	-.077	+.035	+.240	+.402	+.472	+.536	+.628	+.655	+.684	+.691
7.5	-.197	-.141	-.028	+.098	+.310	+.451	+.507	+.564	+.606	+.627	+.648	+.662
5	-.183	-.113	0	+.149	+.360	+.458	+.486	+.514	+.620	+.466	+.479	+.493
2.5	-.162	-.077	+.056	+.212	+.381	+.468	+.296	+.218	-.042	-.098	-.084	-.028
0	+.374	+.402	+.366	+.098	-.965	-3.16	-3.858	-4.84	-6.00	-5.14	-3.52	-2.76

TABLE 33

UPPER SURFACE PRESSURE COEFFICIENTS

$C_\mu = .138, \quad \eta = .250$

s/c \ a°	0	1	3	6	12	18	21	24	30	33	36	37½
90	-.021	-.021	-.042	-.035	-.056	-.063	-.063	-.077	-.120	-.169	-.310	-.748
80	-.042	-.042	-.070	-.070	-.098	-.120	-.127	-.148	-.197	-.268	-.451	-.930
70	-.077	-.084	-.113	-.120	-.162	-.204	-.219	-.247	-.317	-.409	-.606	-1.085
60	-.120	-.113	-.148	-.162	-.219	-.282	-.303	-.345	-.438	-.550	-.860	-1.200
50	-.148	-.176	-.183	-.212	-.289	-.374	-.409	-.458	-.586	-.719	-1.185	-1.328
40	-.176	-.190	-.226	-.268	-.367	-.486	-.543	-.613	-.818	-.916	-1.592	-1.382
30	-.190	-.218	-.275	-.317	-.452	-.599	-.720	-.840	-1.130	-1.228	-1.975	-1.425
25	-.197	-.225	-.289	-.338	-.486	-.670	-.818	-1.010	-1.348	-1.468	-2.119	-1.439
20	-.197	-.232	-.303	-.374	-.557	-.755	-.930	-1.235	-1.670	-1.975	-2.29	-1.453
15	-.183	-.218	-.317	-.367	-.592	-.854	-1.050	-1.390	-2.052	-2.85	-2.40	-1.453
10	-.183	-.232	-.338	-.466	-.740	-1.064	-1.276	-1.600	-2.296	-3.862	-2.50	-1.453
7.5	-.162	-.218	-.324	-.500	-.811	-1.191	-1.440	-1.778	-2.46	-4.73	-2.54	-1.453
5	-.148	-.211	-.345	-.571	-.938	-1.425	-1.720	-2.098	-2.70	-5.26	-2.54	-1.453
2.5	-.105	-.183	-.359	-.655	-1.141	-1.770	-2.20	-2.718	-3.40	-6.09	-2.555	-1.453
0	+.438	+.416	+.310	-.014	-1.228	-3.20	-4.58	-6.18	-9.75	-8.49	-2.64	-1.453

TABLE 34

LOWER SURFACE PRESSURE COEFFICIENTS

$C_\mu = .138, \quad \eta = .250$

x/c \ α°	0	1	3	6	12	18	21	24	30	33	36	$37\frac{1}{2}$
90	-.021	-.028	-.007	-.014	0	+.035	+.049	+.056	+.098	+.070	+.098	+.056
80	-.042	-.042	-.028	-.028	+.014	+.063	+.084	+.105	+.162	+.155	+.197	+.155
70	-.077	-.084	-.070	-.049	+.014	+.084	+.105	+.134	+.212	+.226	+.268	+.254
60	-.120	-.127	-.091	-.063	+.021	+.113	+.141	+.176	+.275	+.310	+.352	+.338
50	-.148	-.148	-.105	-.070	+.035	+.148	+.183	+.233	+.352	+.395	+.437	+.437
40	-.176	-.169	-.127	-.070	+.049	+.176	+.226	+.275	+.409	+.465	+.522	+.522
30	-.190	-.183	-.127	-.063	+.070	+.226	+.282	+.359	+.494	+.564	+.620	+.613
25	-.197	-.183	-.120	-.056	+.098	+.260	+.324	+.401	+.550	+.613	+.676	+.662
20	-.197	-.176	-.113	-.035	+.134	+.303	+.366	+.444	+.599	+.662	+.705	+.705
15	-.183	-.155	-.084	+.007	+.196	+.359	+.430	+.494	+.648	+.705	+.740	+.747
10	-.183	-.148	-.070	+.042	+.255	+.416	+.487	+.550	+.662	+.712	+.740	+.747
7.5	-.162	-.120	-.028	+.084	+.310	+.458	+.507	+.557	+.606	+.634	+.676	+.683
5	-.148	-.084	+.014	+.155	+.374	+.501	+.528	+.557	+.500	+.479	+.522	+.550
2.5	-.105	-.035	+.084	+.226	+.430	+.479	+.437	+.529	+.141	+.028	+.098	+.169
0	+.438	+.437	+.380	+.113	-.986	-2.815	-4.07	-5.62	-9.20	-10.66	-6.79	-3.95

TABLE 35

UPPER SURFACE PRESSURE COEFFICIENTS

C_μ = .138, η = .125

x/c \ α°	0	1	3	6	12	18	21	24	30	33	36	$37\frac{1}{2}$
90	-.042	-.042	-.042	-.056	-.063	-.063	-.084	-.098	-.141	-.183	-.380	-.945
80	-.084	-.056	-.091	-.113	-.134	-.155	-.183	-.211	-.282	-.324	-.536	-1.086
70	-.141	-.141	-.148	-.169	-.212	-.254	-.297	-.331	-.437	-.500	-.732	-1.227
60	-.155	-.155	-.169	-.197	-.261	-.310	-.366	-.416	-.564	-.649	-.915	-1.31
50	-.176	-.183	-.197	-.247	-.317	-.395	-.465	-.529	-.705	-.839	-1.130	-1.395
40	-.190	-.212	-.240	-.303	-.395	-.514	-.599	-.676	-.881	-1.112	-1.465	-1.436
30	-.212	-.219	-.261	-.331	-.444	-.585	-.705	-.781	-.965	-1.248	-1.732	-1.465
25	-.204	-.212	-.268	-.331	-.465	-.634	-.771	-.881	-1.00	-1.310	-1.873	-1.480
20	-.197	-.212	-.268	-.345	-.507	-.690	-.831	-.986	-1.028	-1.352	-2.158	-1.492
15	-.169	-.197	-.261	-.345	-.528	-.746	-.902	-1.100	-1.214	-1.338	-2.455	-1.509
10	-.162	-.197	-.274	-.402	-.620	-.887	-1.058	-1.269	-1.896	-2.100	-2.845	-1.538
7.5	-.155	-.190	-.274	-.416	-.676	-.993	-1.200	-1.401	-2.200	-2.860	-2.96	-1.550
5	-.169	-.226	-.334	-.486	-.902	-1.290	-1.530	-1.756	-2.410	-3.181	-3.38	-1.564
2.5	-.084	-.155	-.282	-.521	-1.041	-1.550	-1.896	-2.22	-2.920	-3.34	-3.521	-1.578
0	+.409	+.395	+.310	+.063	-.816	-2.261	-3.241	-4.325	-6.84	-8.40	-4.52	-1.661

TABLE 36

LOWER SURFACE PRESSURE COEFFICIENTS

$C_\mu = .138, \quad \eta = .125$

%c \ α°	0	1	3	6	12	18	21	24	30	33	36	$37\frac{1}{2}$
90	-.042	-.042	-.028	-.021	0	+.049	+.070	+.084	+.127	+.113	+.127	+.098
80	-.084	-.077	-.063	-.042	0	+.070	+.098	+.127	+.197	+.211	+.240	+.219
70	-.141	-.127	-.098	-.070	0	+.077	+.120	+.162	+.255	+.282	+.317	+.310
60	-.155	-.134	-.098	-.070	+.014	+.113	+.162	+.219	+.324	+.352	+.394	+.394
50	-.176	-.162	-.120	-.070	+.028	+.141	+.197	+.268	+.387	+.423	+.465	+.465
40	-.190	-.183	-.134	-.070	+.035	+.169	+.233	+.303	+.437	+.493	+.550	+.536
30	-.212	-.183	-.127	-.056	+.077	+.226	+.296	+.380	+.529	+.578	+.634	+.634
25	-.204	-.176	-.120	-.042	+.113	+.268	+.345	+.430	+.578	+.634	+.676	+.683
20	-.197	-.169	-.098	-.021	+.148	+.303	+.387	+.479	+.620	+.683	+.733	+.733
15	-.169	-.141	-.070	+.014	+.197	+.373	+.451	+.536	+.676	+.733	+.790	+.790
10	-.162	-.127	-.049	+.056	+.255	+.437	+.507	+.592	+.719	+.761	+.818	+.832
7.5	-.155	-.105	-.021	+.091	+.296	+.479	+.550	+.620	+.719	+.740	+.783	+.804
5	-.169	-.120	-.028	+.098	+.317	+.493	+.550	+.592	+.627	+.620	+.634	+.661
2.5	-.084	-.028	+.084	+.226	+.430	+.529	+.538	+.522	+.394	+.296	+.183	+.226
0	+.409	+.416	+.373	+.183	-.564	-1.904	-2.85	-3.993	-6.68	-8.71	-10.05	-10.20

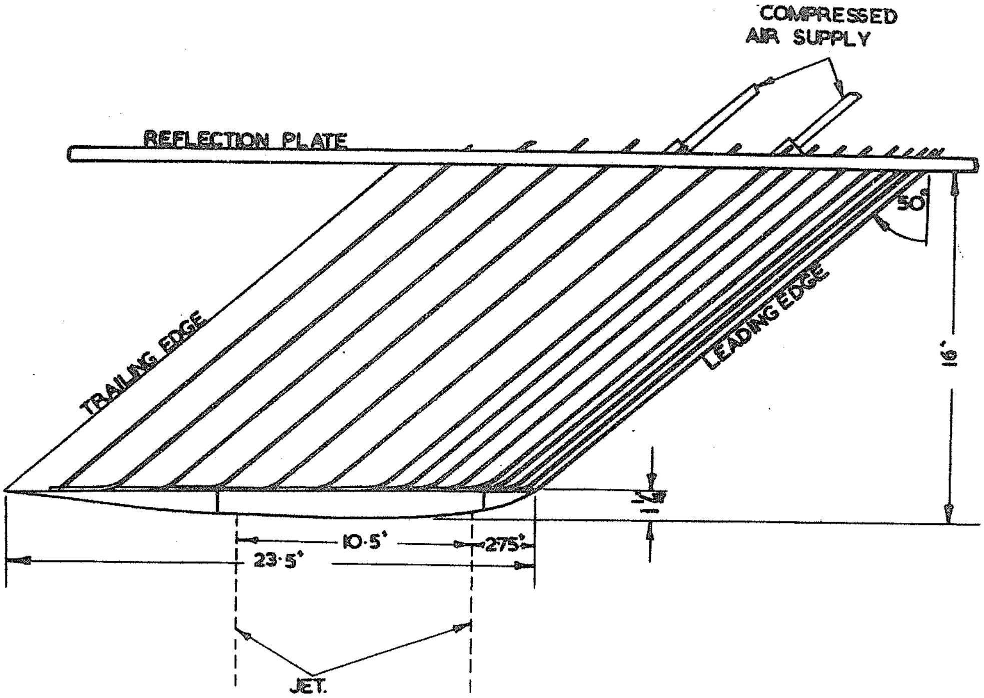

FIG.1. DIAGRAM OF MODEL SHOWING COMPRESSED AIR SUPPLY AND THE LAYOUT OF THE PRESSURE TUBES.

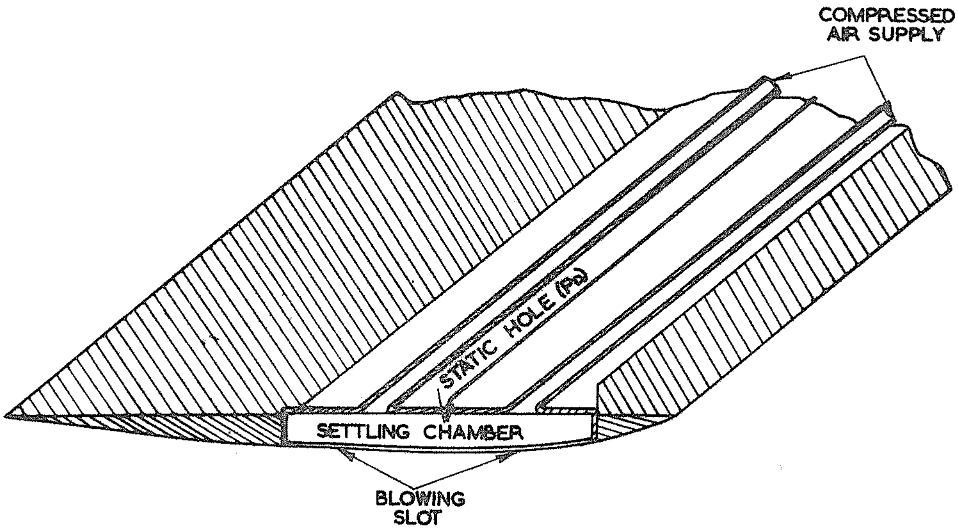

FIG. 2. SECTIONAL DIAGRAM OF WING TIP SHOWING THE ARRAGEMENT OF BLOWING SLOT, COMPRESSED AIR SUPPLY, AND STATIC HOLE.

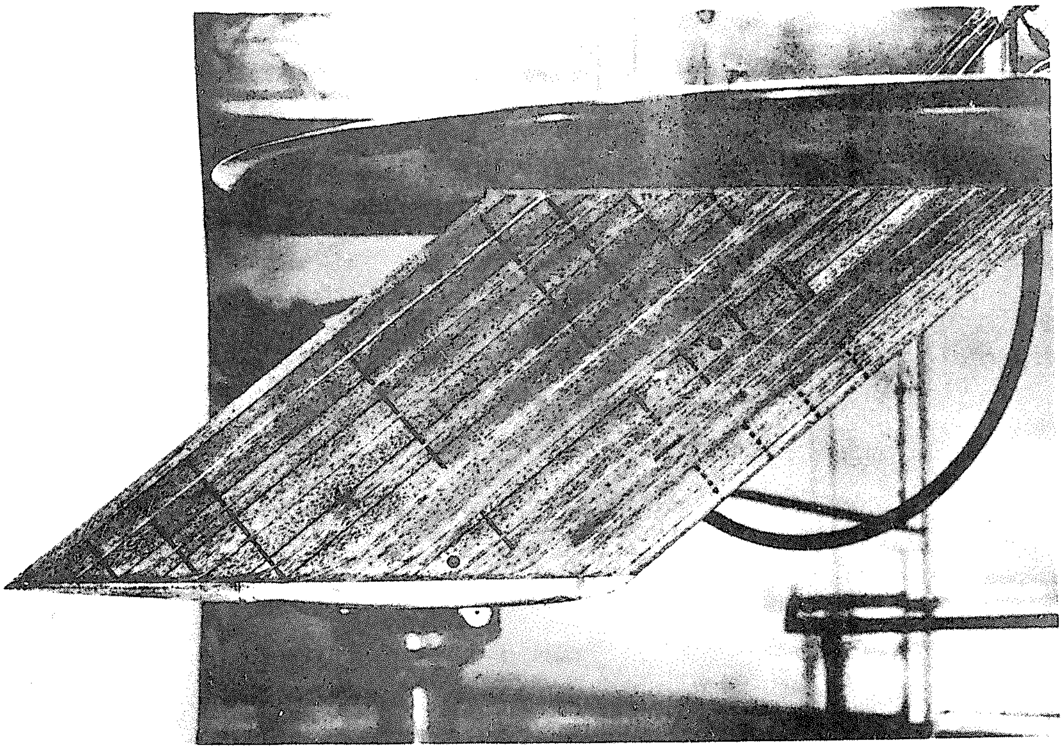

FIG. 3. VIEW OF WING SURFACE

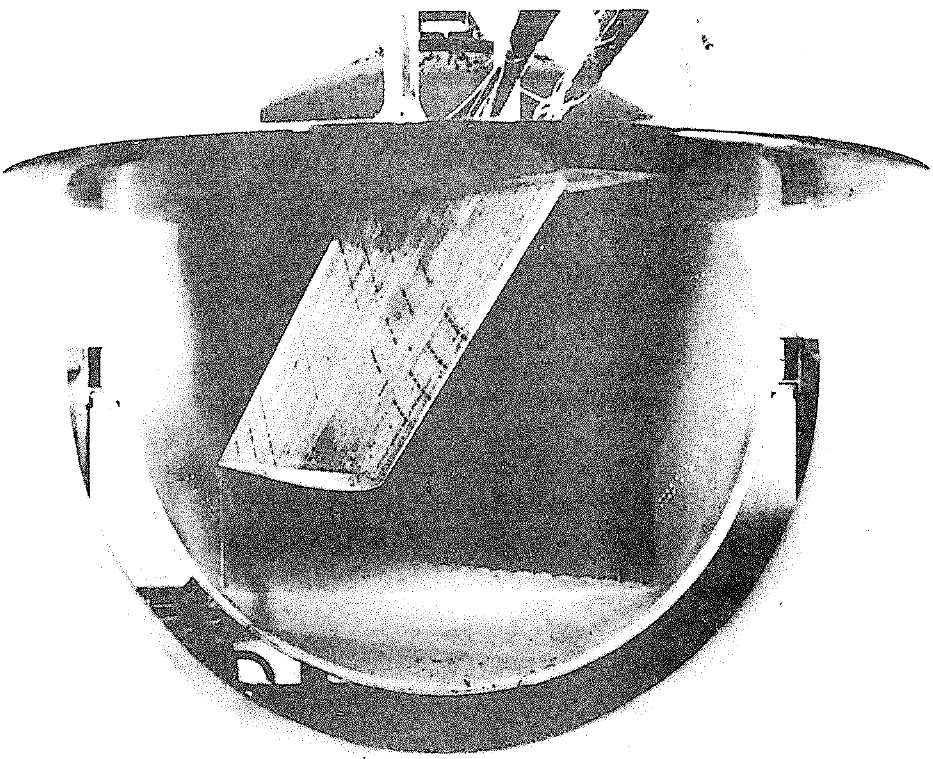

FIG. 4 WING AND ENDPLATE MOUNTED IN TUNNEL WORKING SECTION

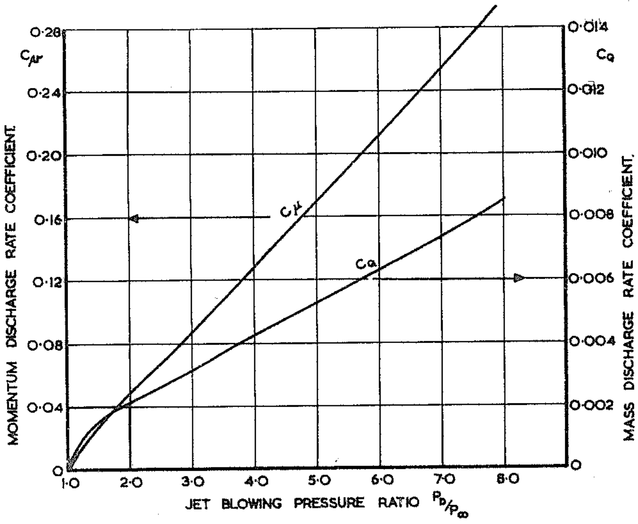

FIG. 5. OPERATING CONDITIONS OF BLOWING AIR SLOT BASED ON APPENDIX I.

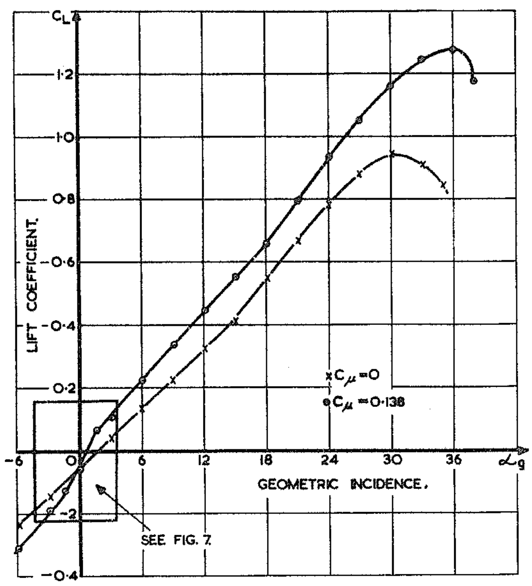

FIG. 6. VARIATION OF C_L WITH INCIDENCE (BALANCE MEASUREMENTS).

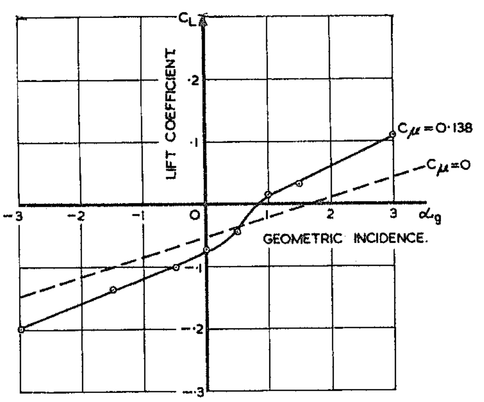

FIG. 7. INVESTIGATION OF C_L IN REGION $\alpha_g = 0$, $C_\mu = \cdot 138$ (BALANCE MEASUREMENTS)

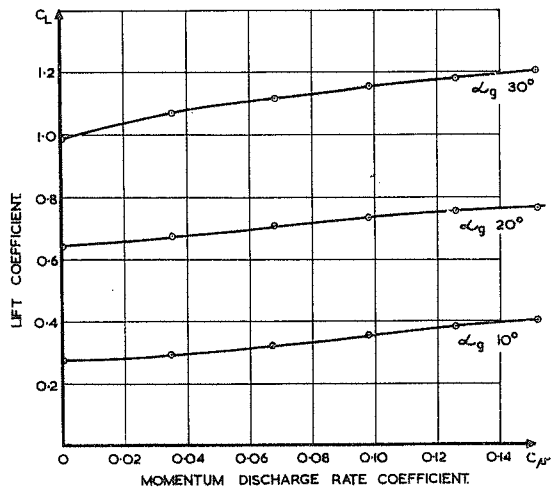

FIG. 8. VARIATION OF C_L WITH C_μ AT CONSTANT α_g (BALANCE MEASUREMENTS)

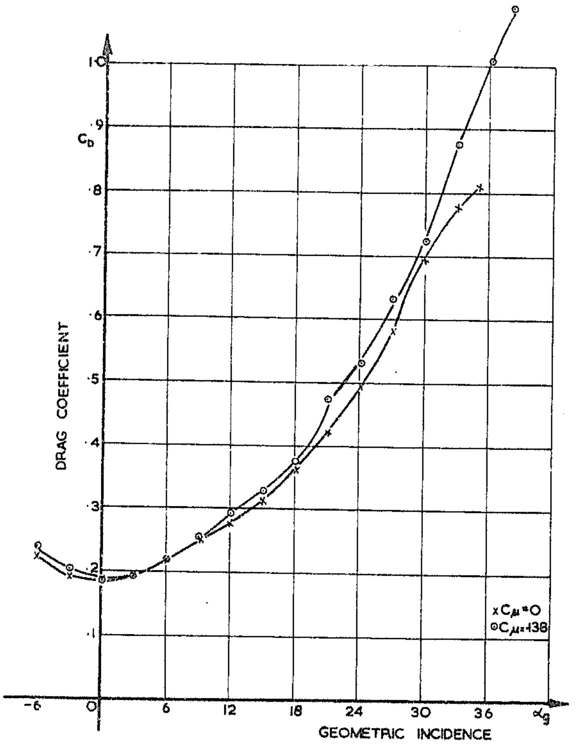

FIG.9. VARIATION OF C_D WITH INCIDENCE (BALANCE MEASUREMENTS).

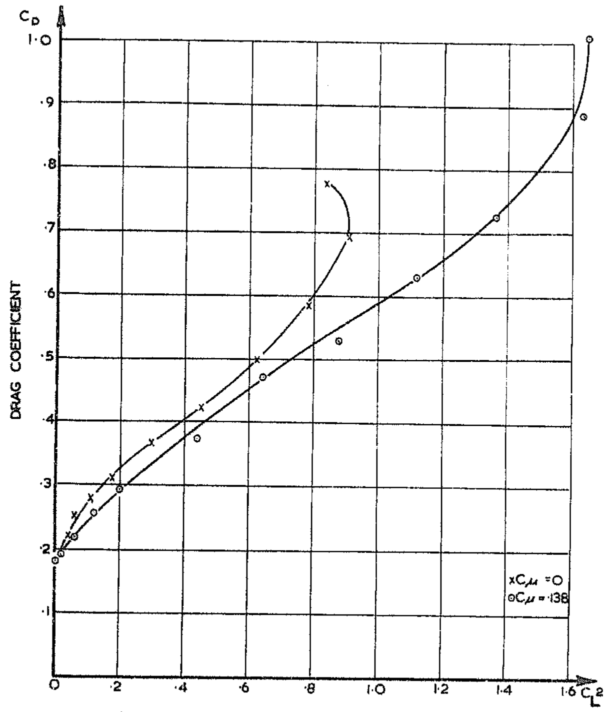

FIG.10. VARIATION OF C_D WITH C_L^2 (BALANCE MEASUREMENTS).

Note: Tare drag coefficient at . $C_L = 0$ is ~ 0.18 approx.

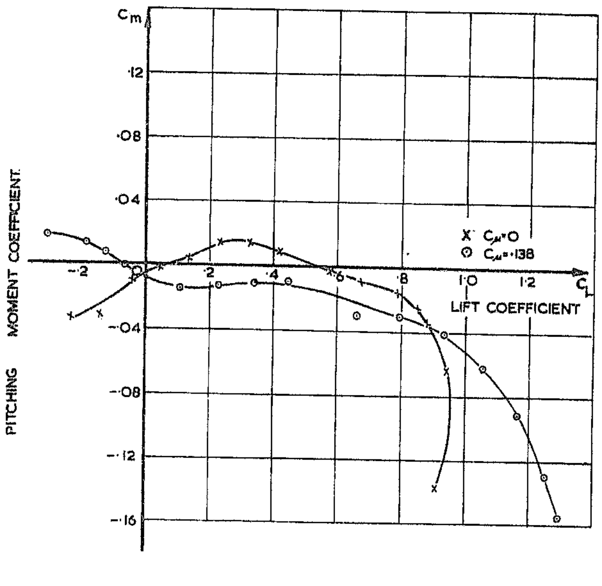

FIG.11. VARIATION OF C_m WITH C_L (BALANCE MEASUREMENTS). MOMENTS TAKEN ABOUT 1/4 CHORD POINT OF M.A.C.

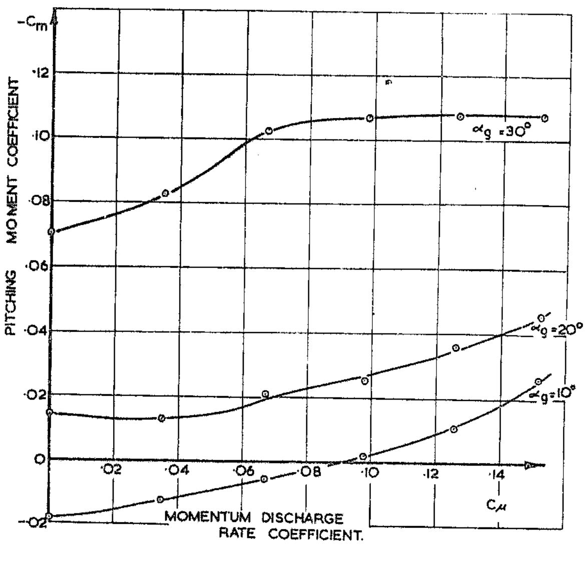

FIG.12. VARIATION OF C_m WITH C_μ FOR CONSTANT α_g. (BALANCE MEASUREMENTS). MOMENTS TAKEN ABOUT 1/4 CHORD POINT OF M.A.C.

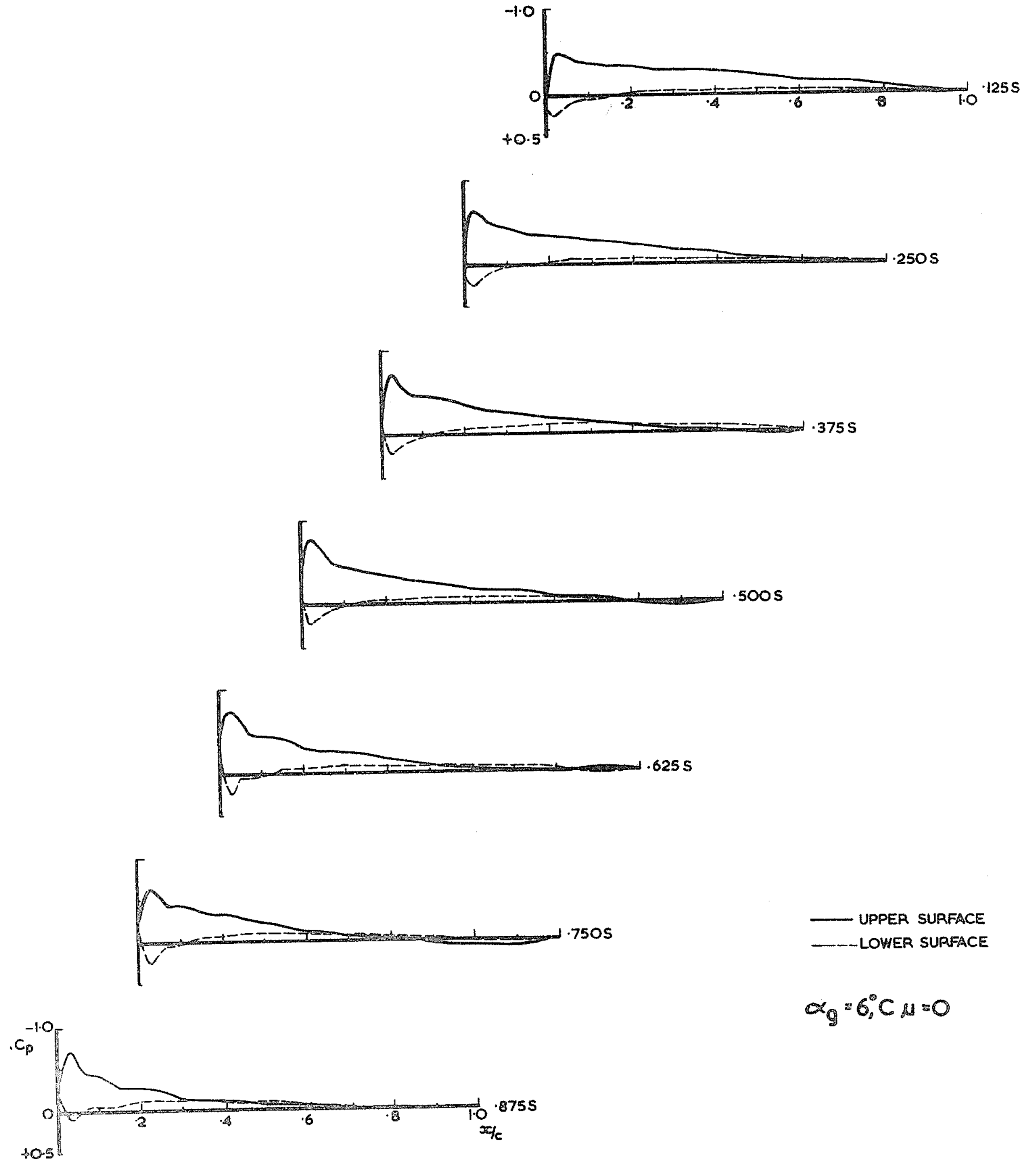

FIG. 13. VARIATION OF PRESSURE COEFFICIENT OVER WING.

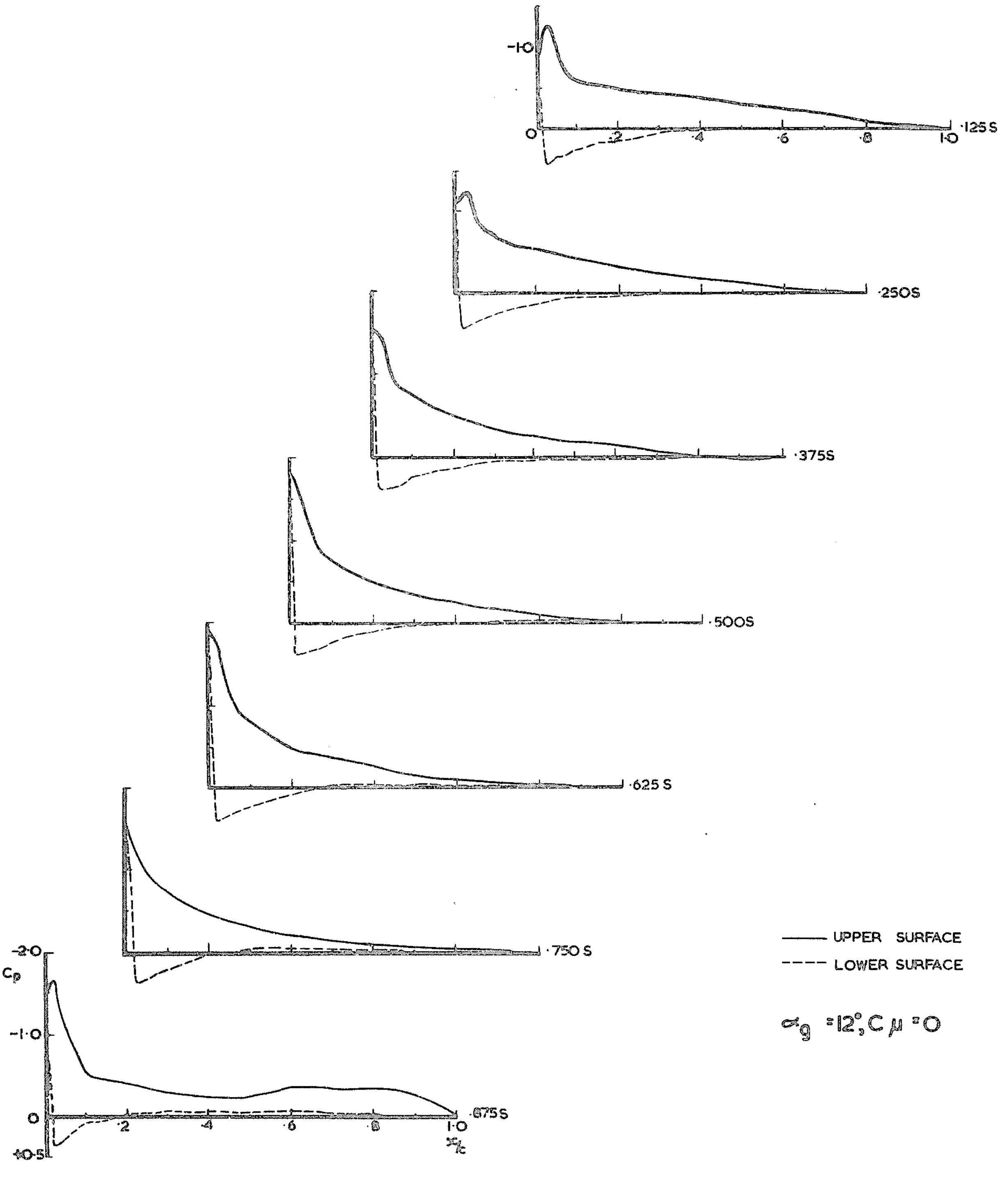

FIG. 14. VARIATION OF PRESSURE COEFFICIENT OVER WING.

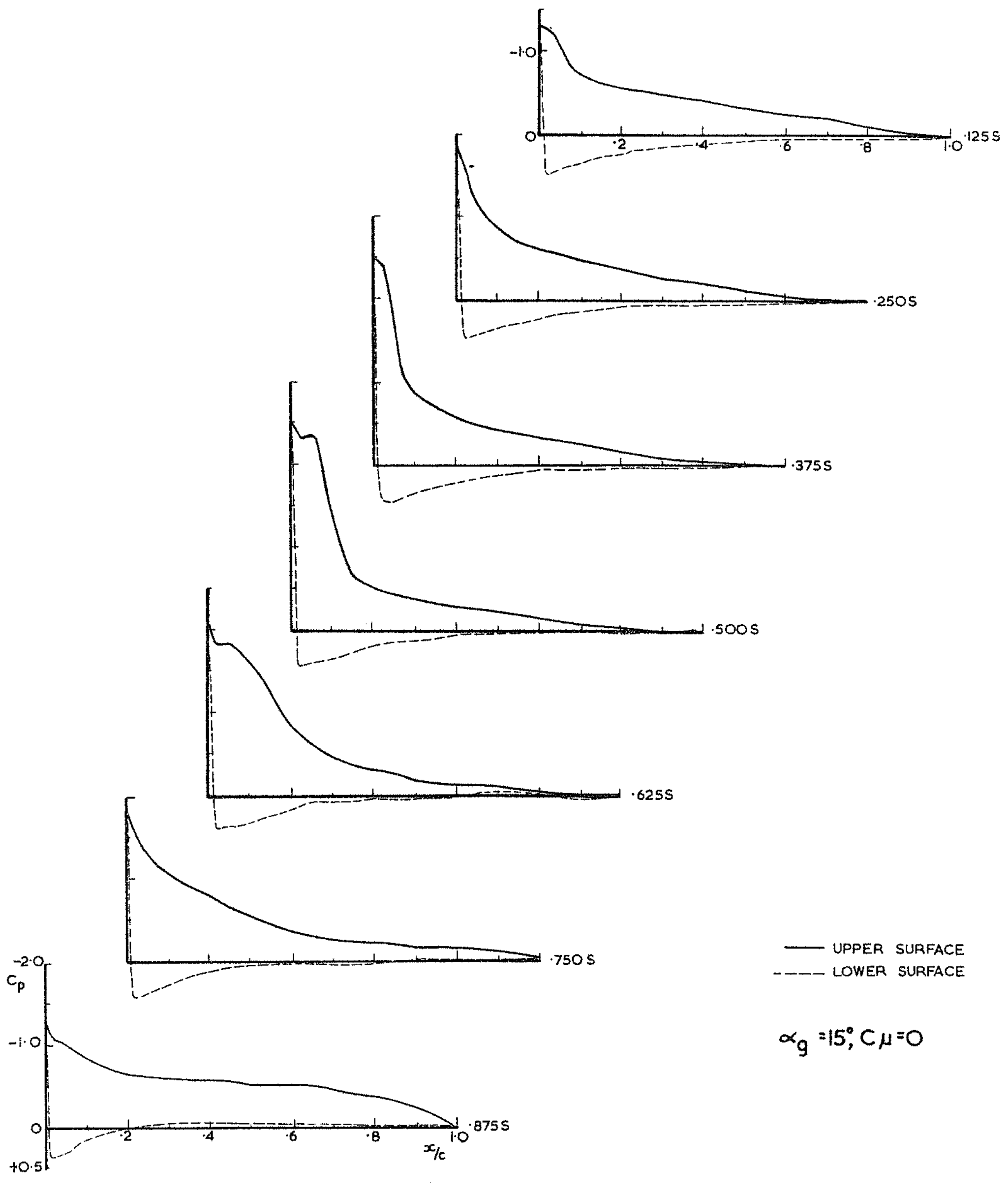

FIG. 15. VARIATION OF PRESSURE COEFFICIENT OVER WING.

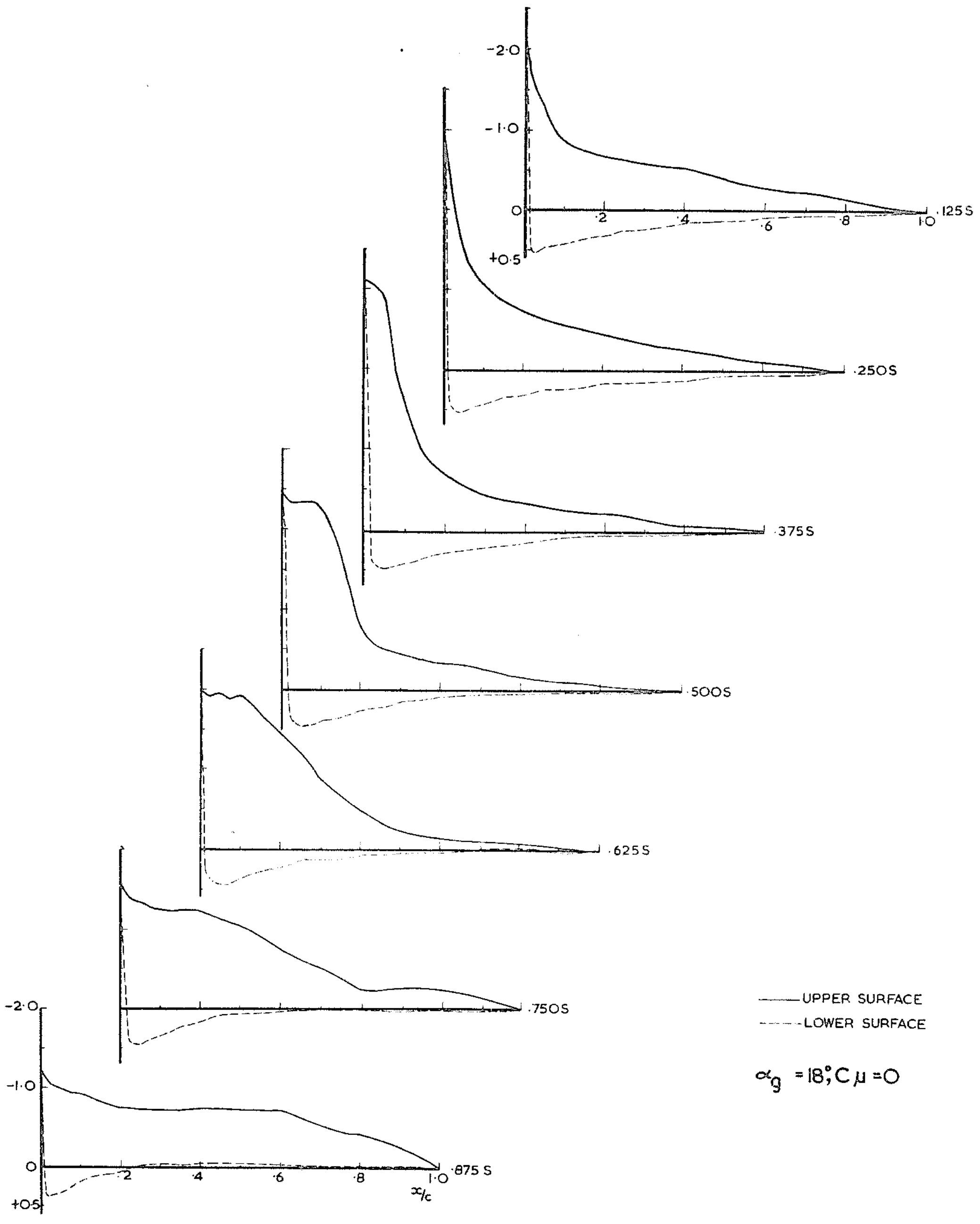

FIG.16. VARIATION OF PRESSURE COEFFICIENT OVER WING.

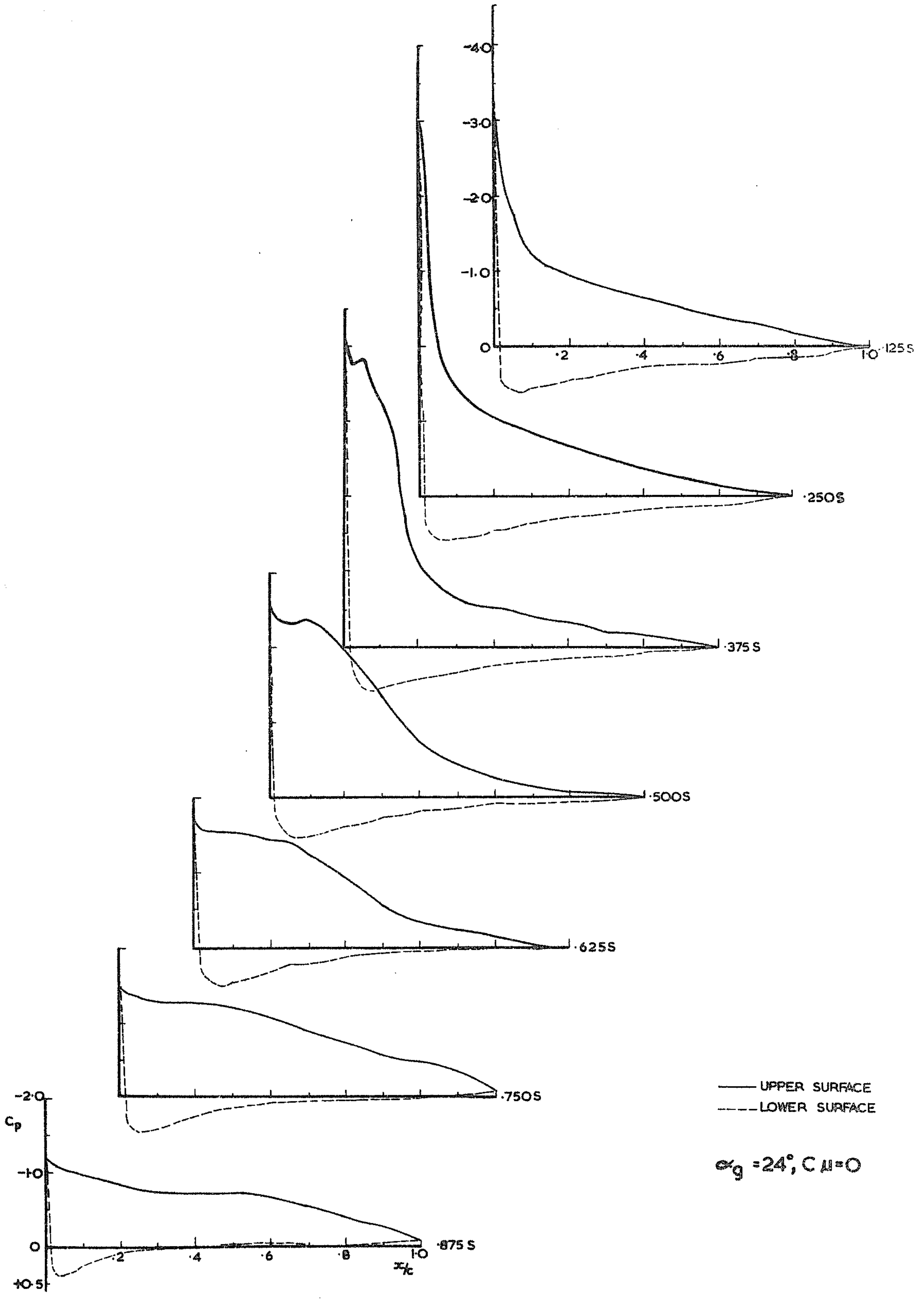

FIG. 17. VARIATION OF PRESSURE COEFFICIENT OVER WING.

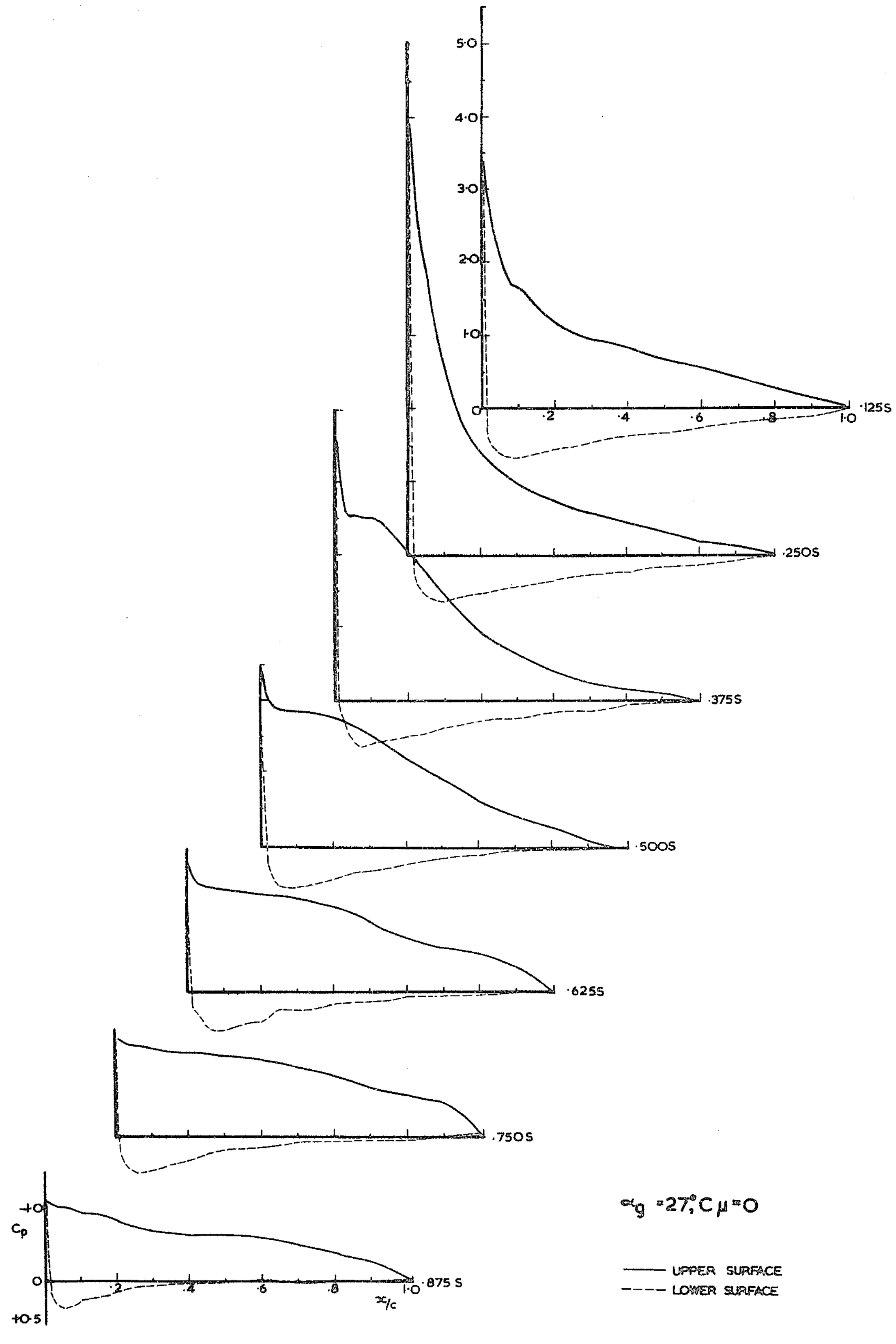

FIG. 18. VARIATION OF PRESSURE COEFFICIENT OVER WING.

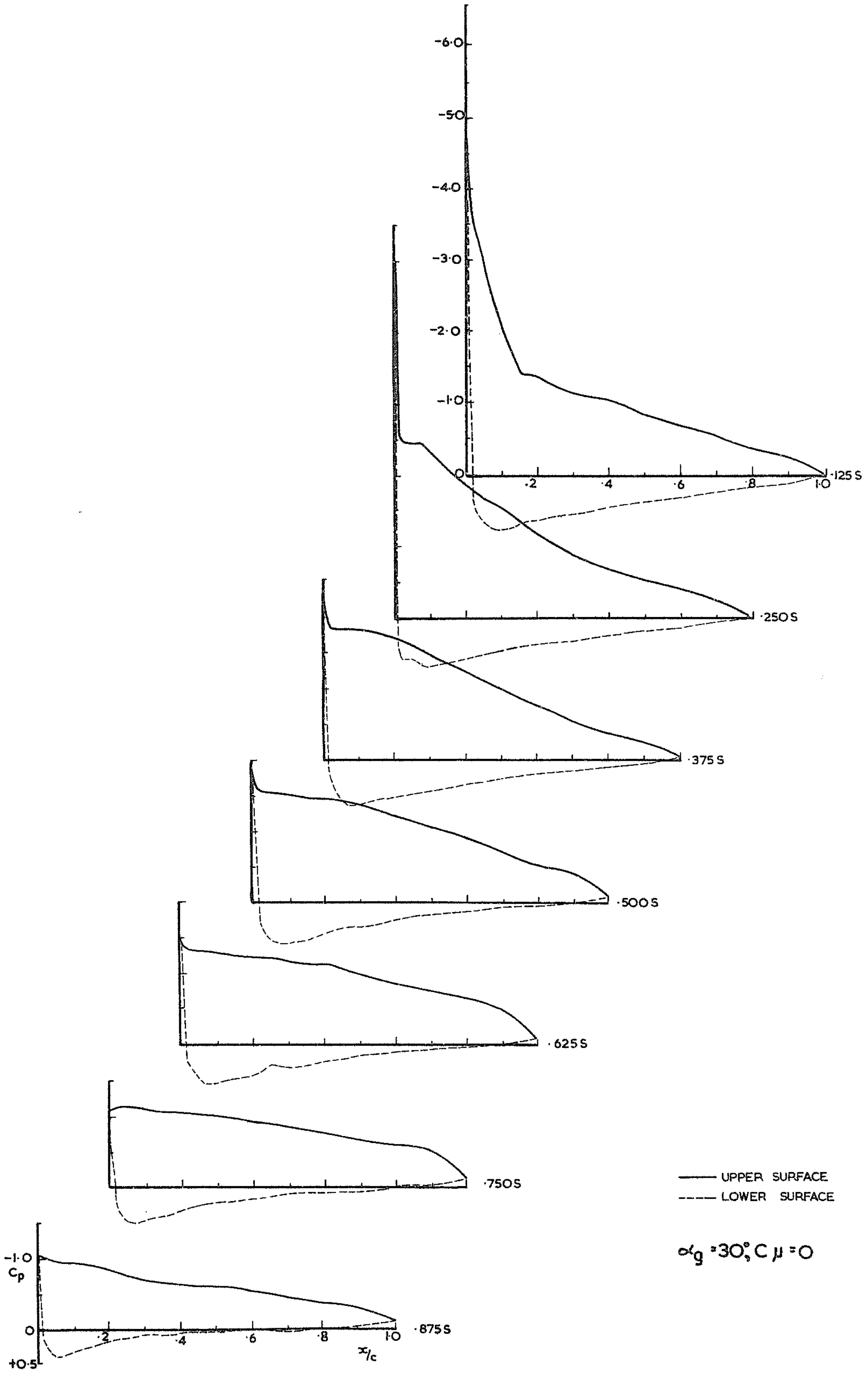

FIG.19. VARIATION OF PRESSURE COEFFICIENT OVER WING.

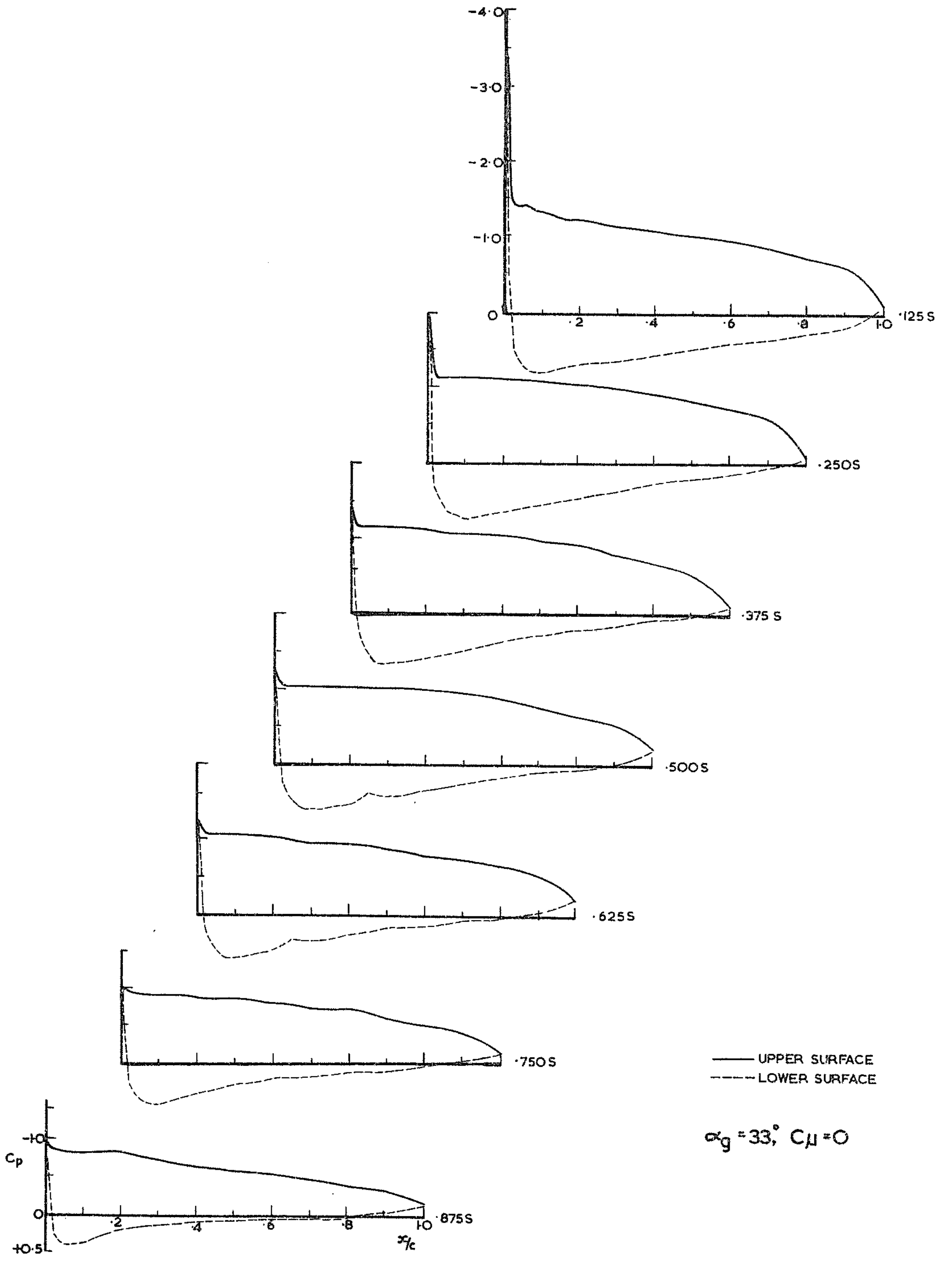

FIG. 20. VARIATION OF PRESSURE COEFFICIENT OVER WING.

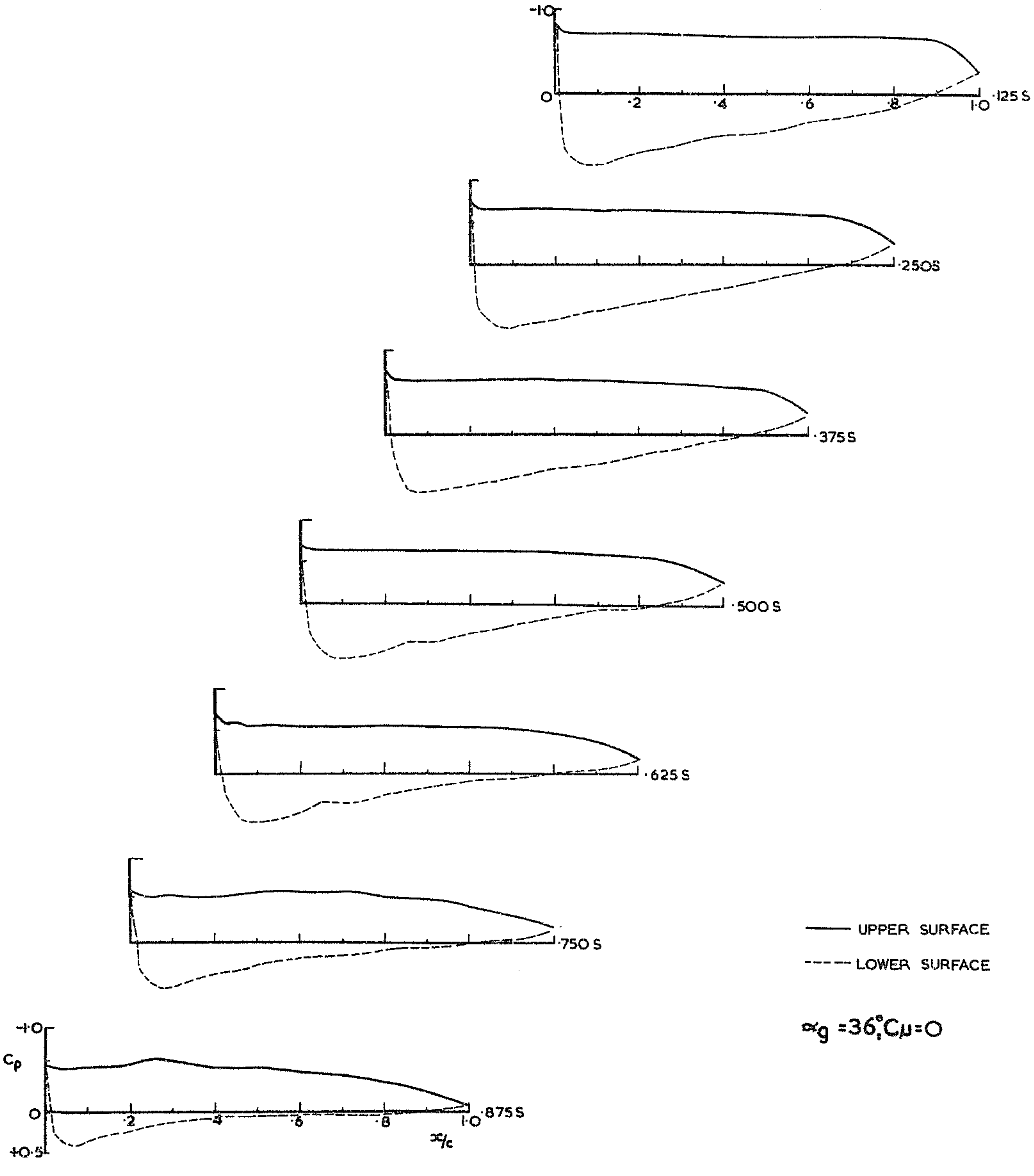

FIG. 21. VARIATION OF PRESSURE COEFFICIENT OVER WING.

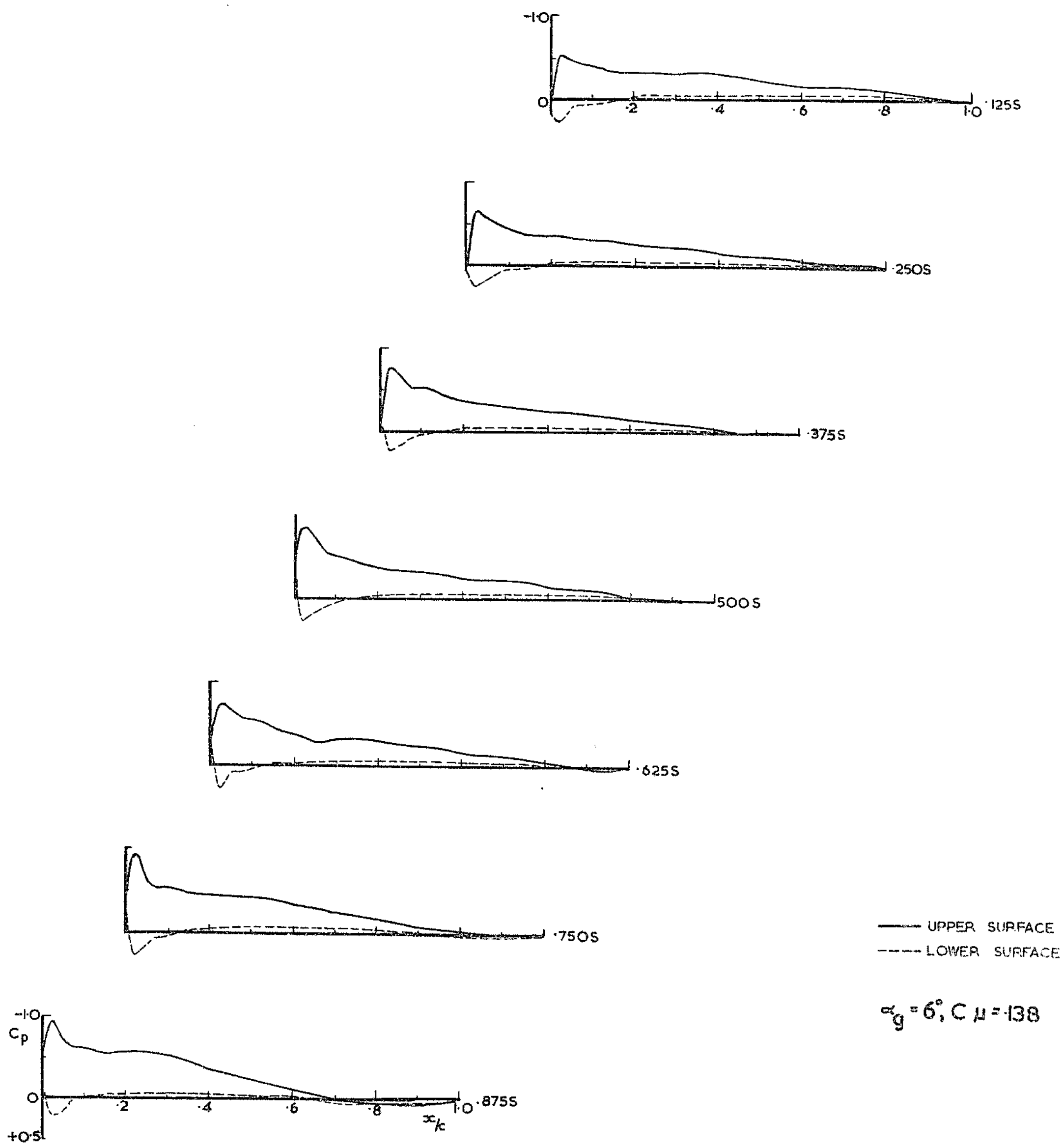

FIG. 22. VARIATION OF PRESSURE COEFFICIENT OVER WING.

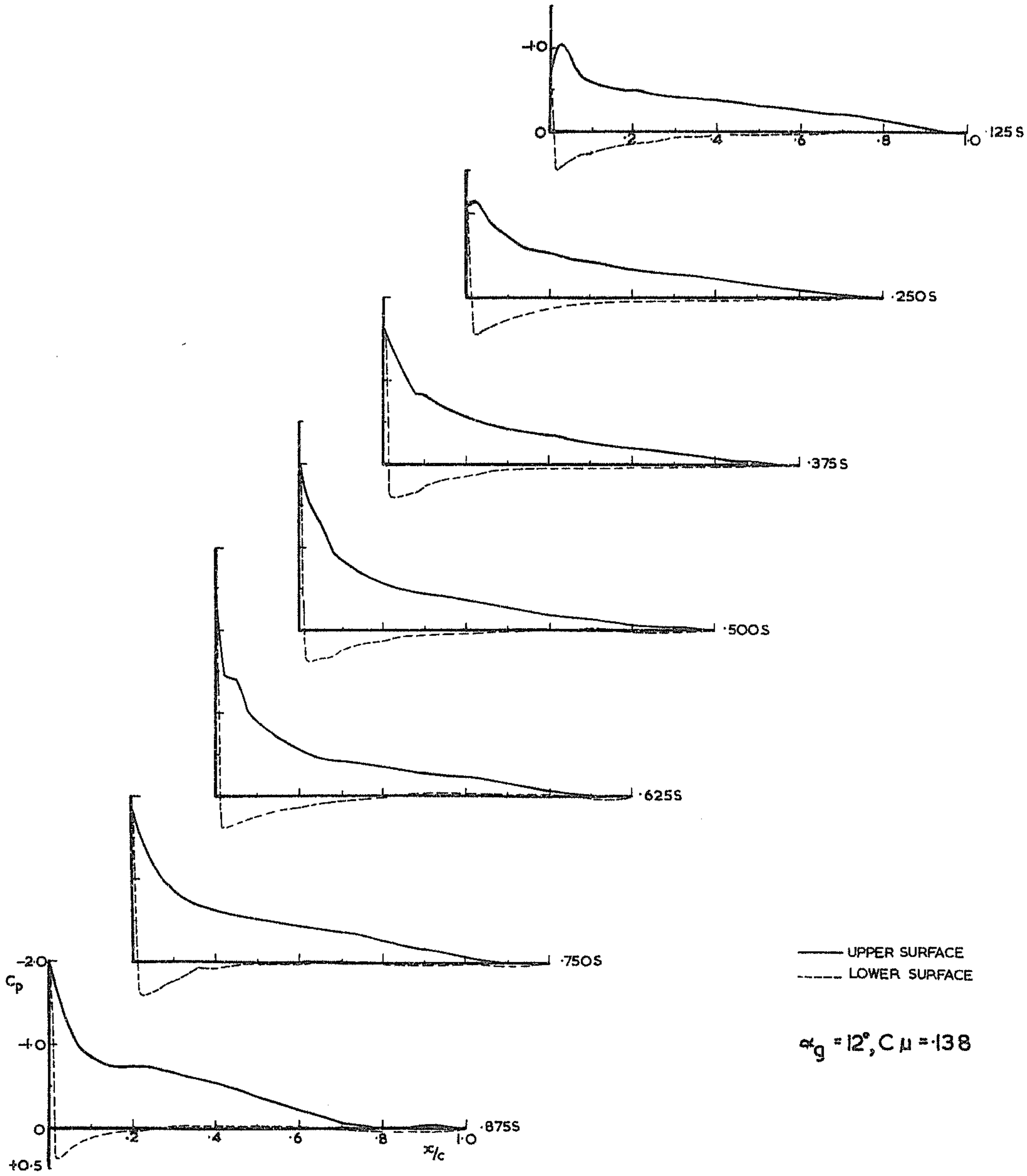

FIG. 23. VARIATION OF PRESSURE COEFFICIENT OVER WING.

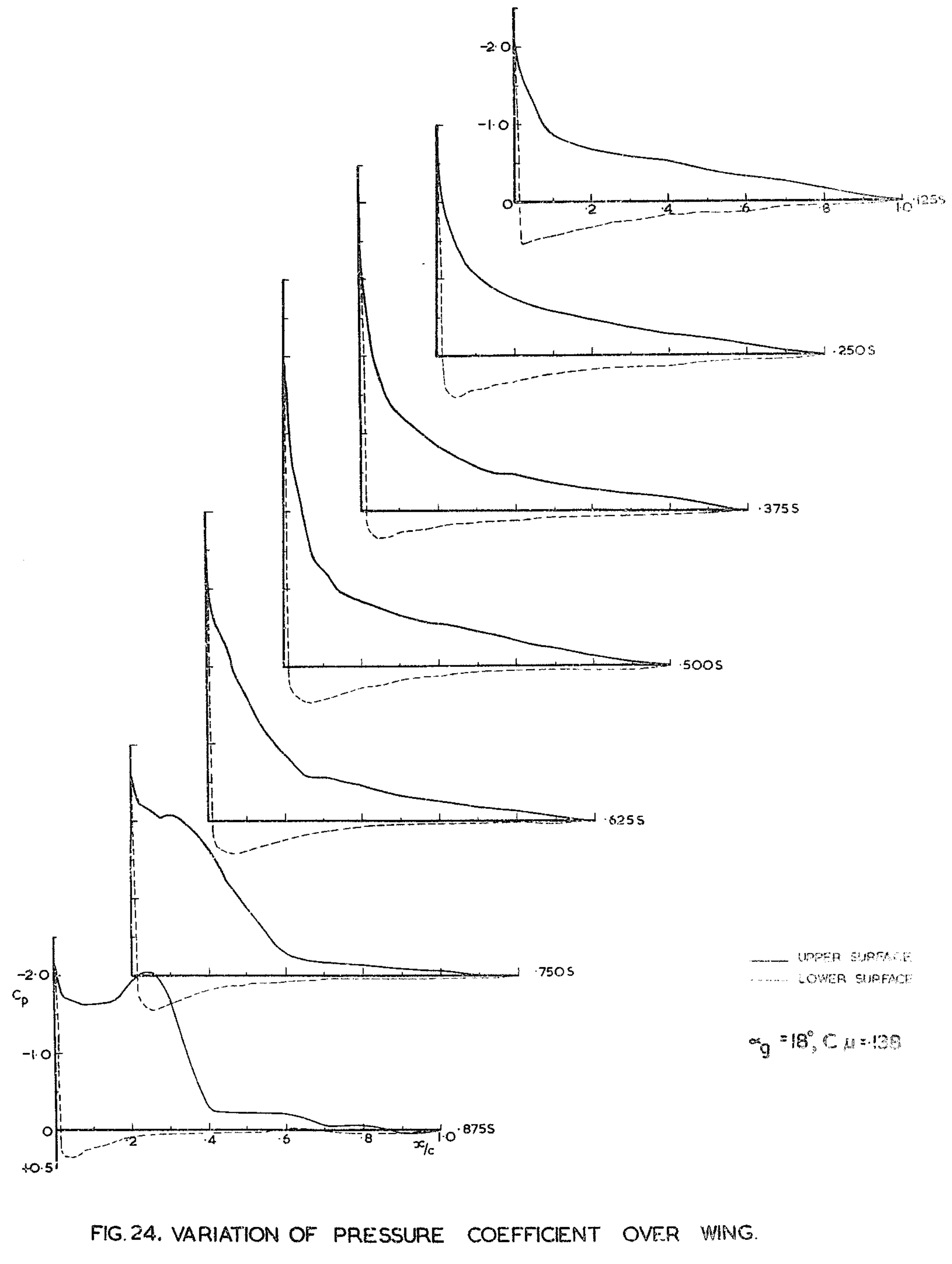

FIG. 24. VARIATION OF PRESSURE COEFFICIENT OVER WING.

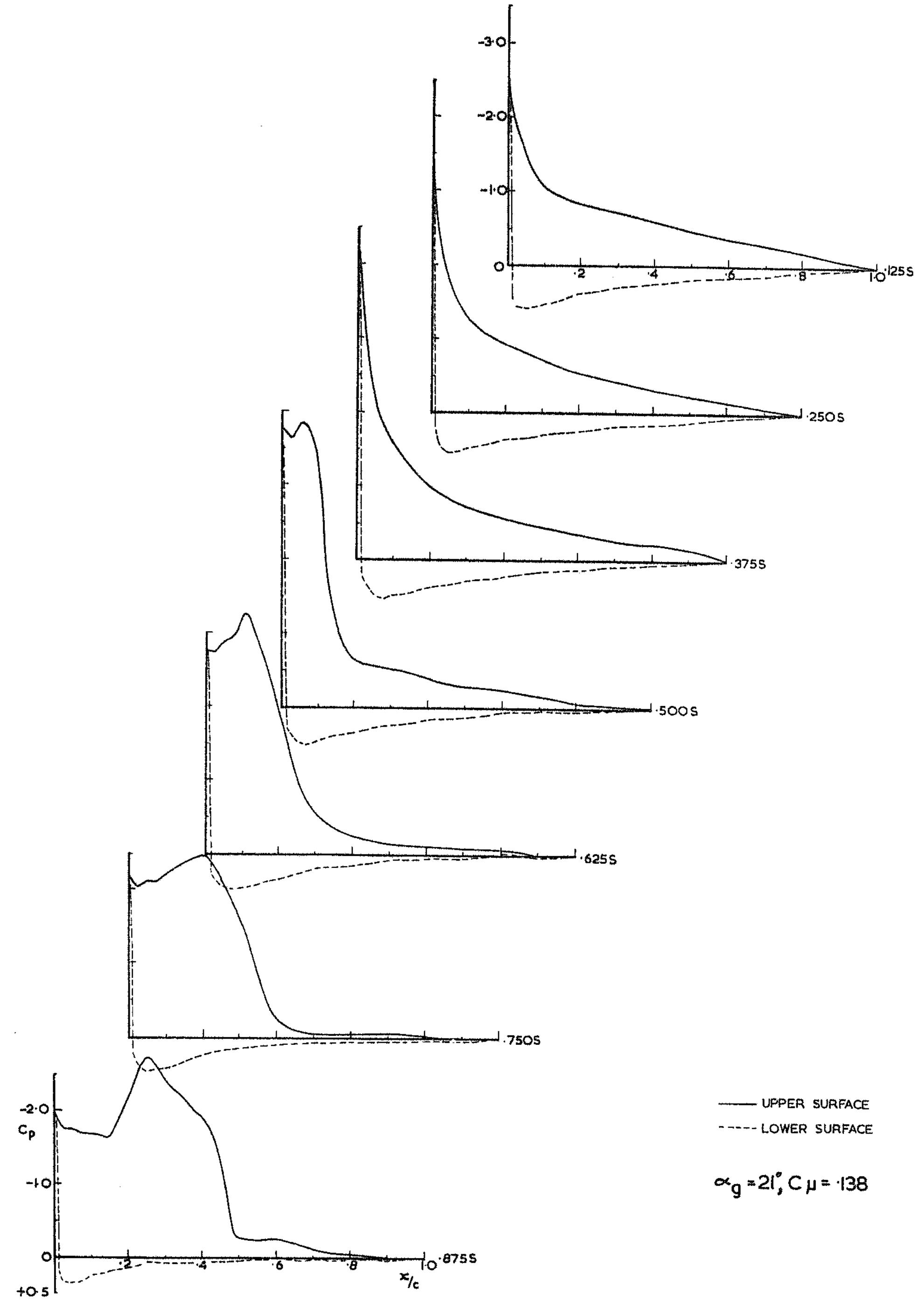

FIG. 25. VARIATION OF PRESSURE COEFFICIENT OVER WING.

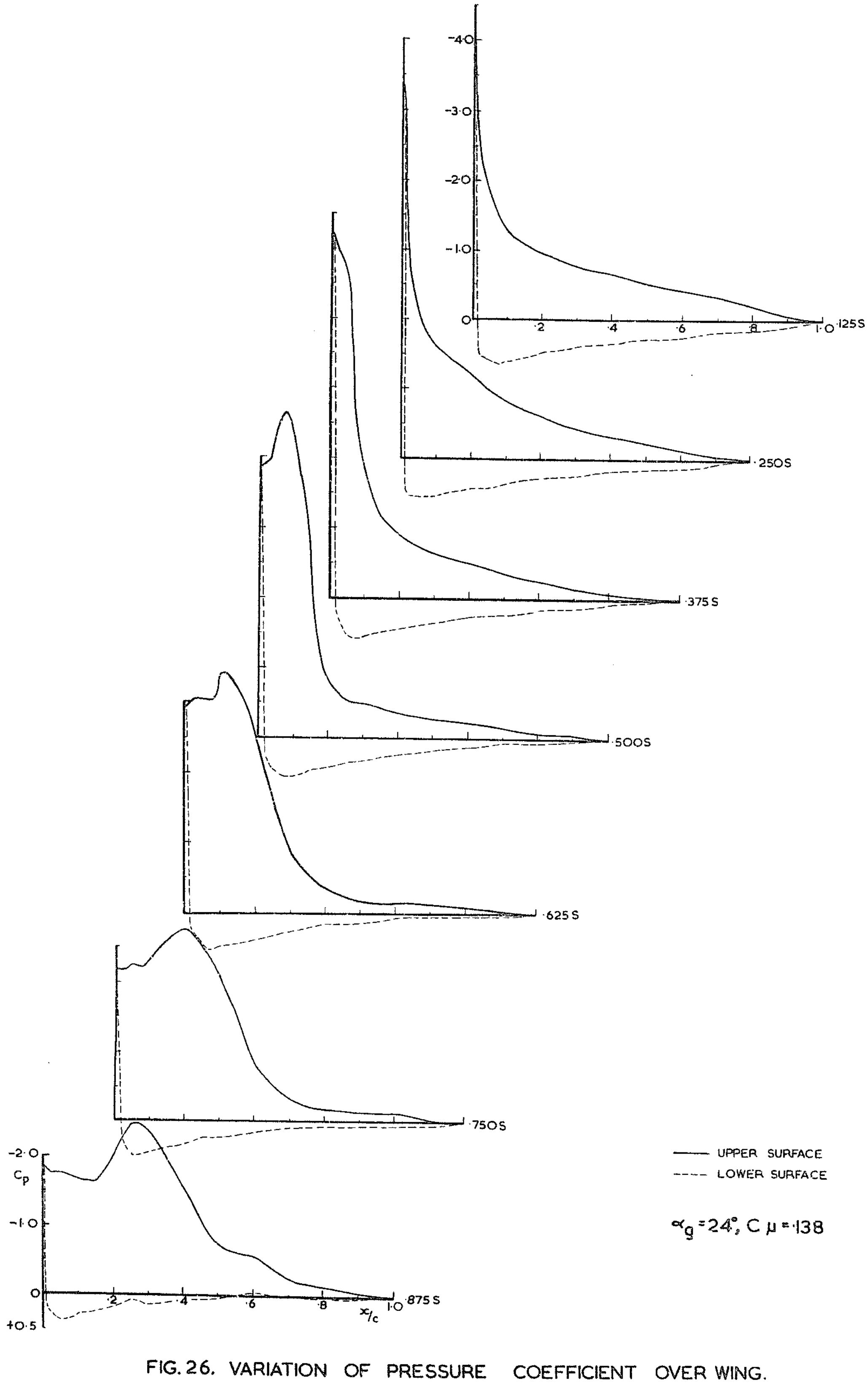

FIG. 26. VARIATION OF PRESSURE COEFFICIENT OVER WING.

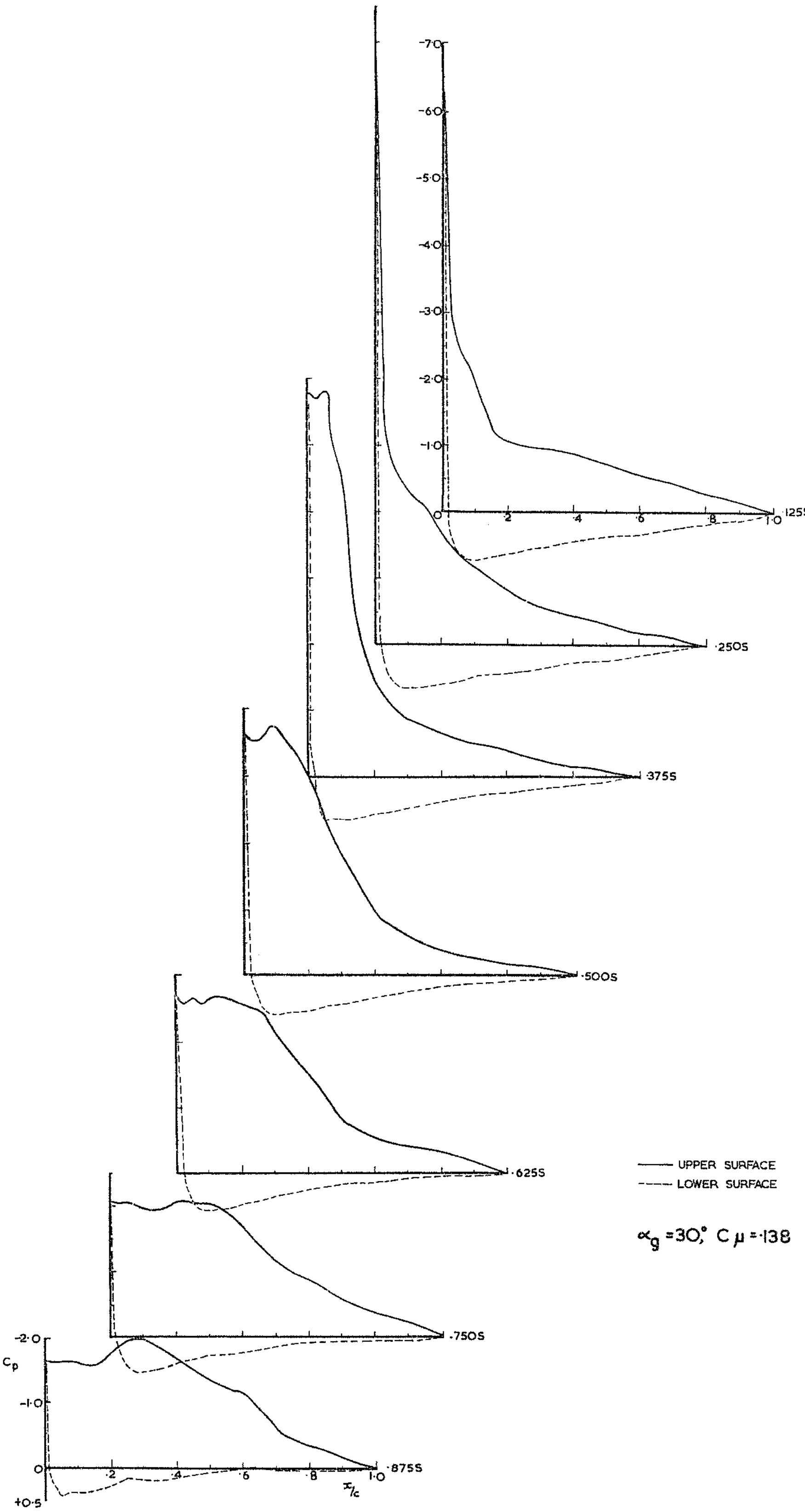

FIG. 27. VARIATION OF PRESSURE COEFFICIENT OVER WING.

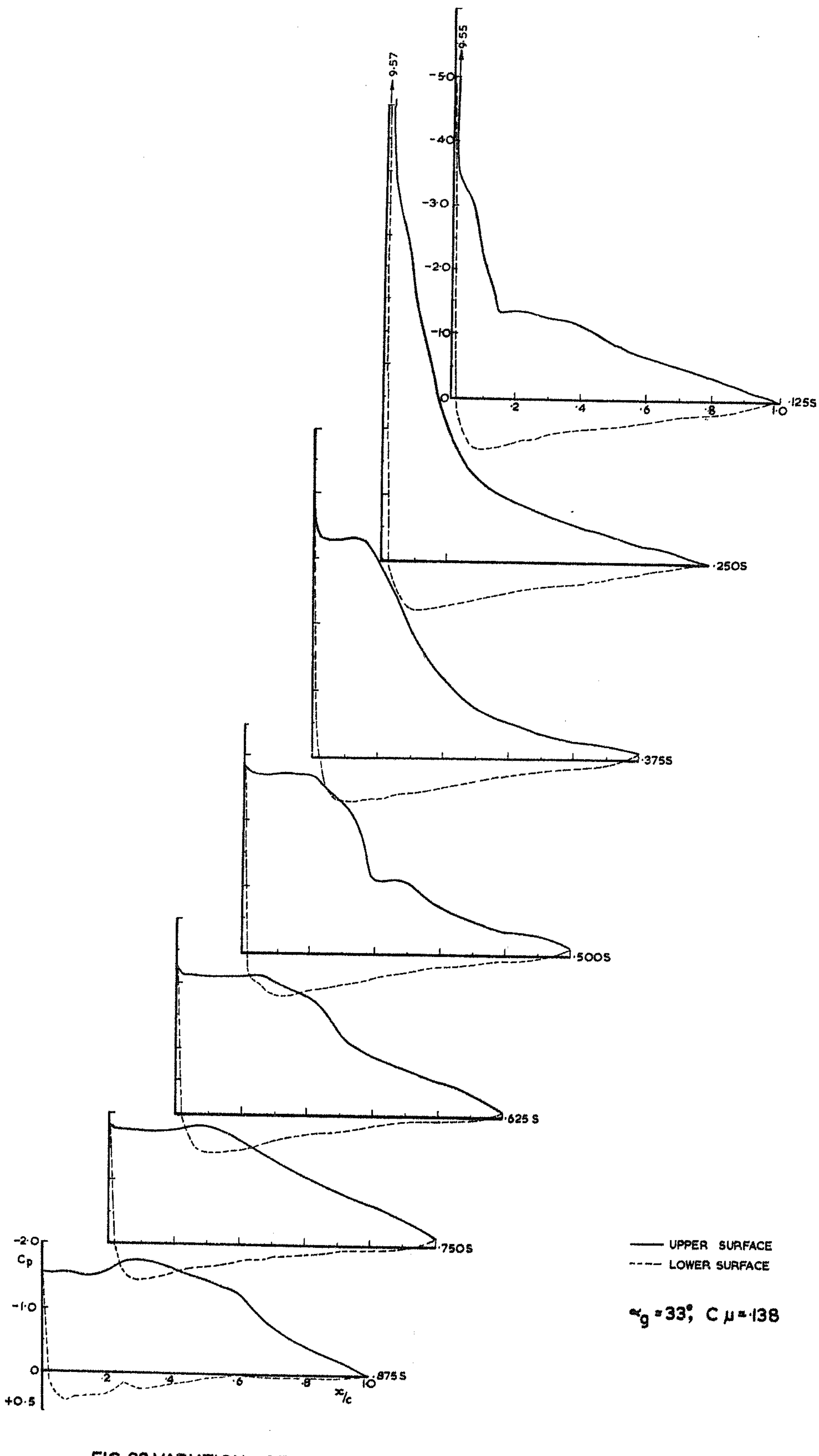

FIG. 28. VARIATION OF PRESSURE DISTRIBUTION OVER WING.

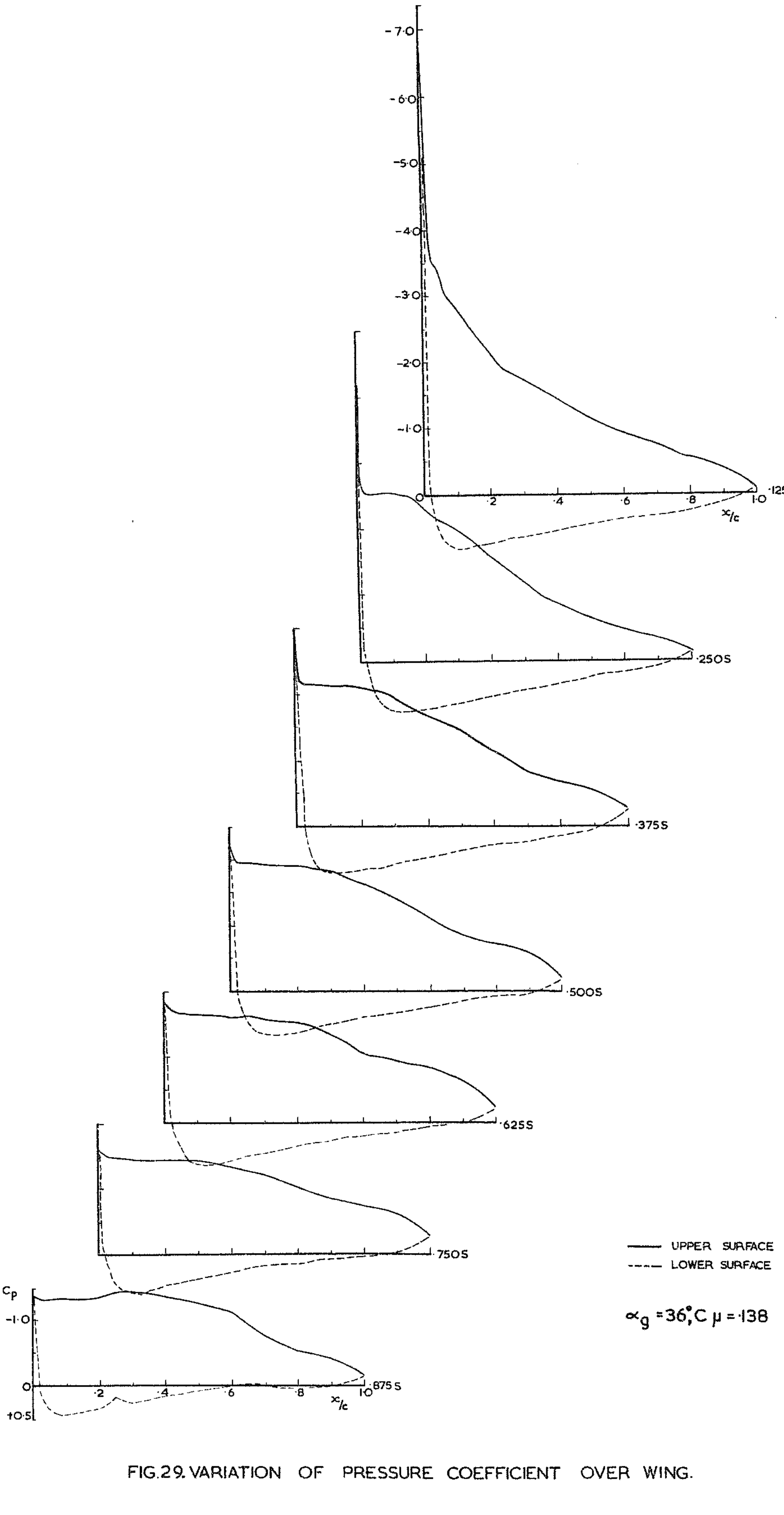

FIG. 29. VARIATION OF PRESSURE COEFFICIENT OVER WING.

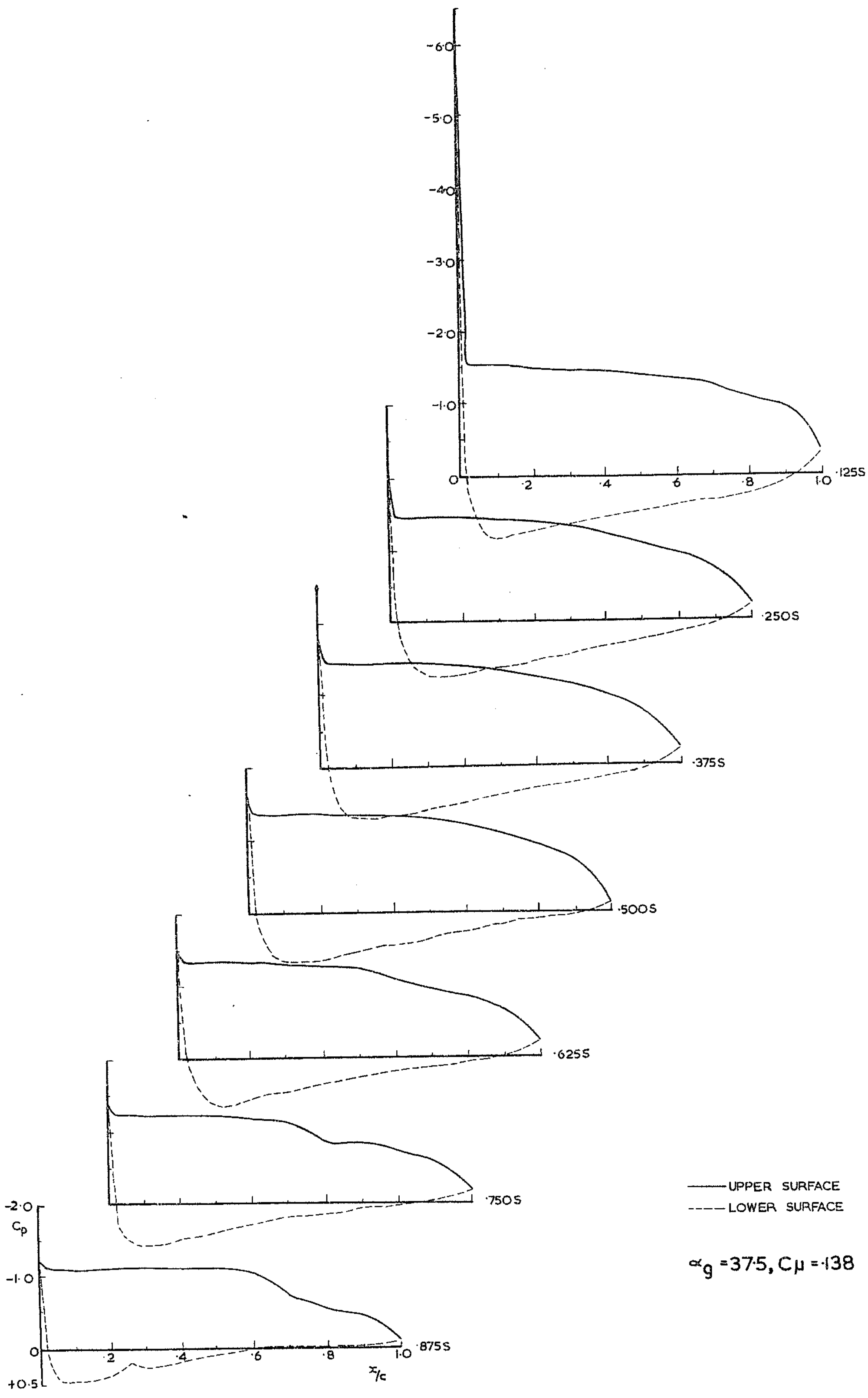

FIG. 30. VARIATION OF PRESSURE COEFFICIENT OVER WING.

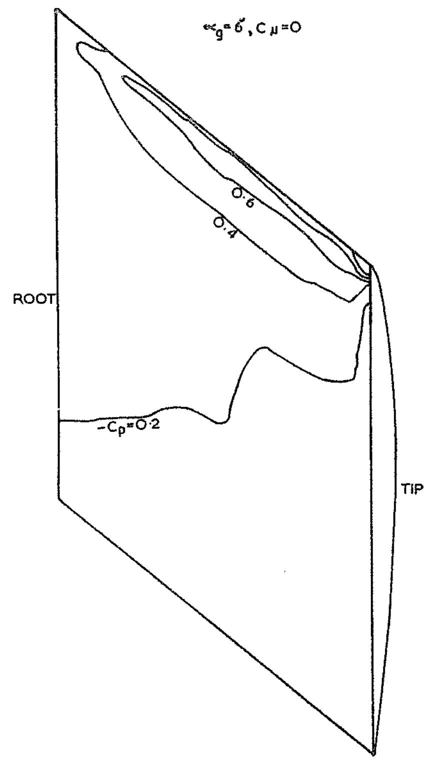

FIG. 31. UPPER SURFACE ISOBAR DIAGRAM.

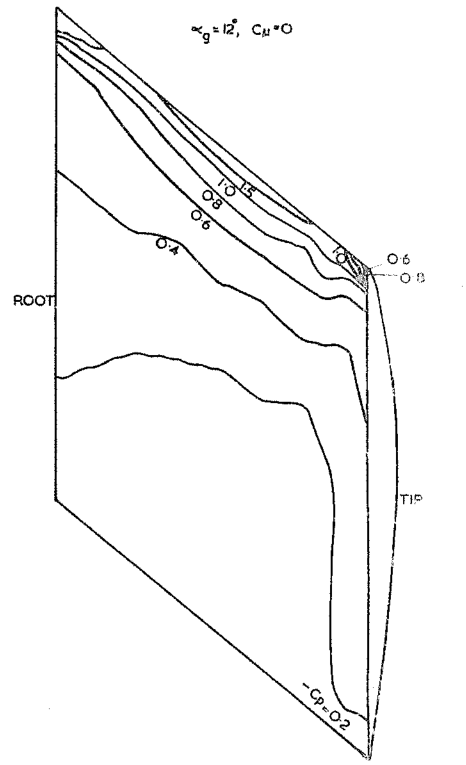

FIG. 32. UPPER SURFACE ISOBAR DIAGRAM.

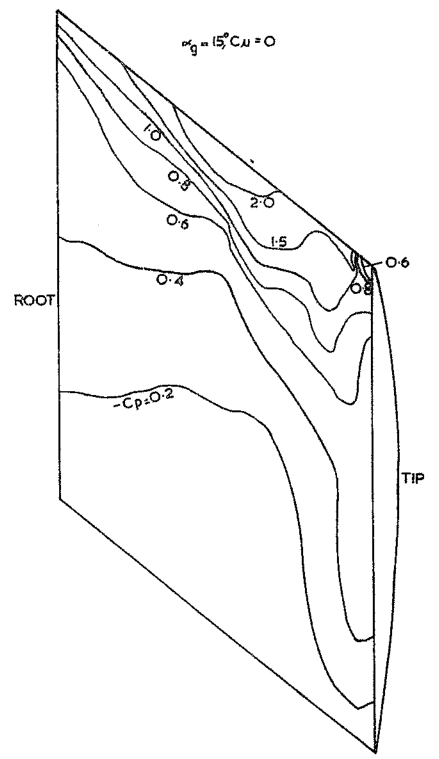

FIG. 33. UPPER SURFACE ISOBAR DIAGRAM.

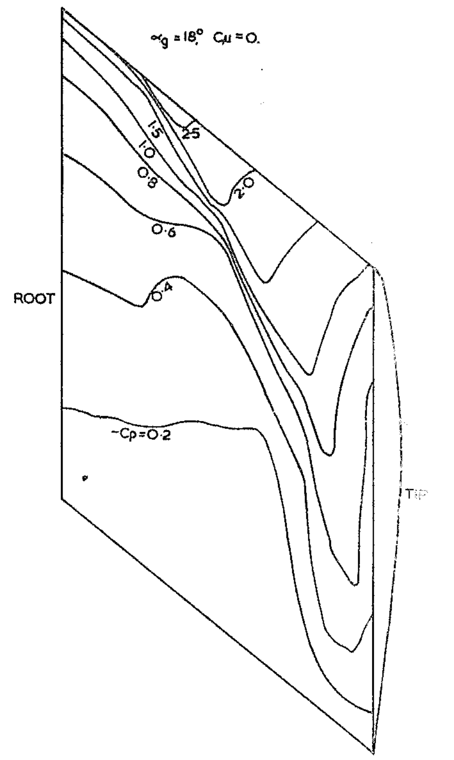

FIG. 34. UPPER SURFACE ISOBAR DIAGRAM.

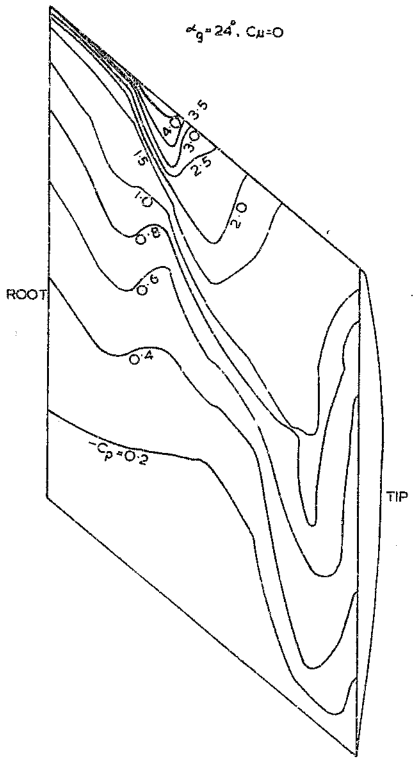

FIG. 35. UPPER SURFACE ISOBAR DIAGRAM

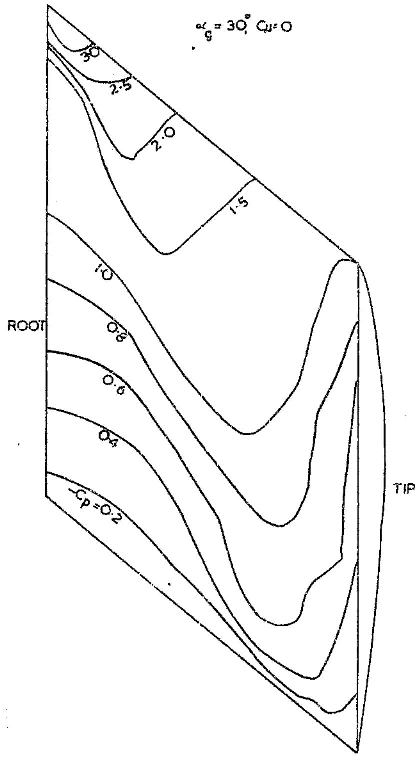

FIG.36. UPPER SURFACE ISOBAR DIAGRAM.

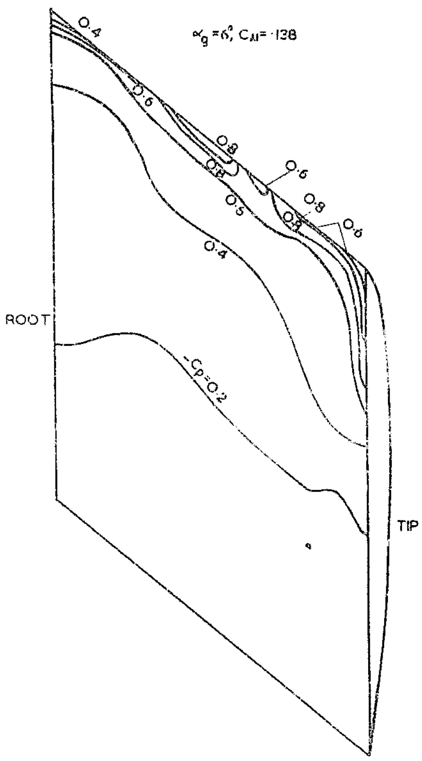

FIG.37. UPPER SURFACE ISOBAR DIAGRAM.

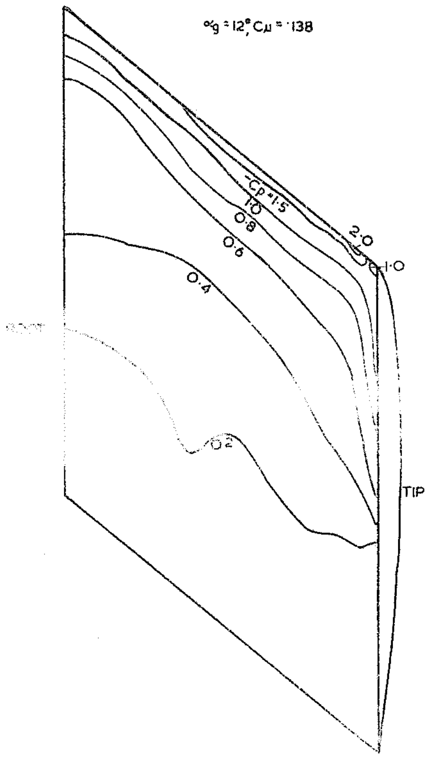

FIG.38. UPPER SURFACE ISOBAR DIAGRAM.

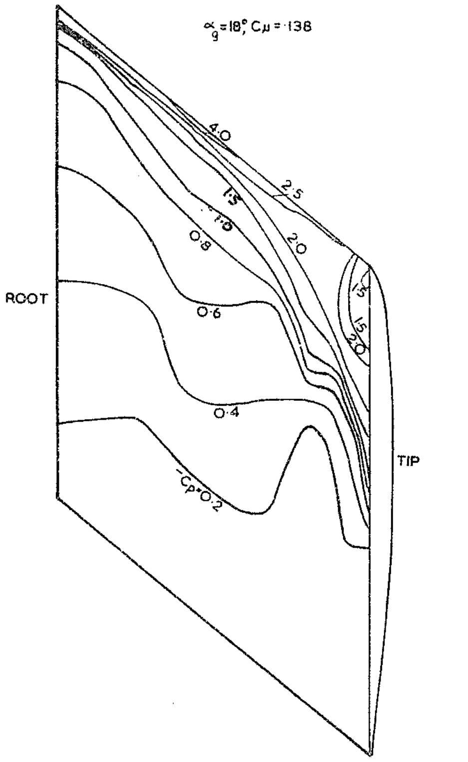

FIG. 39. UPPER SURFACE ISOBAR DIAGRAM.

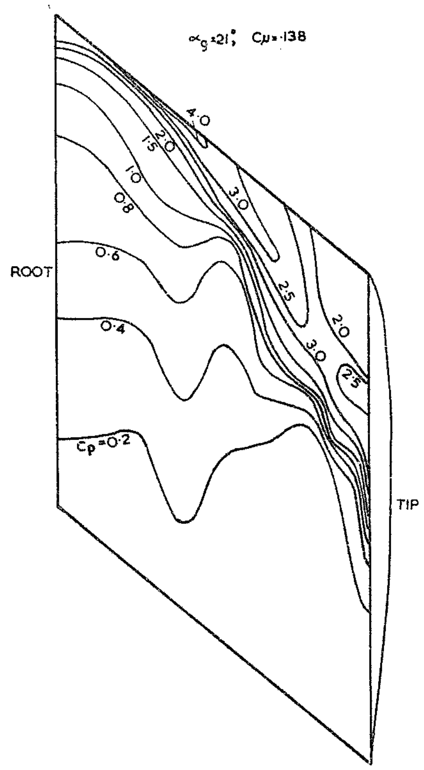

FIG. 40. UPPER SURFACE ISOBAR DIAGRAM.

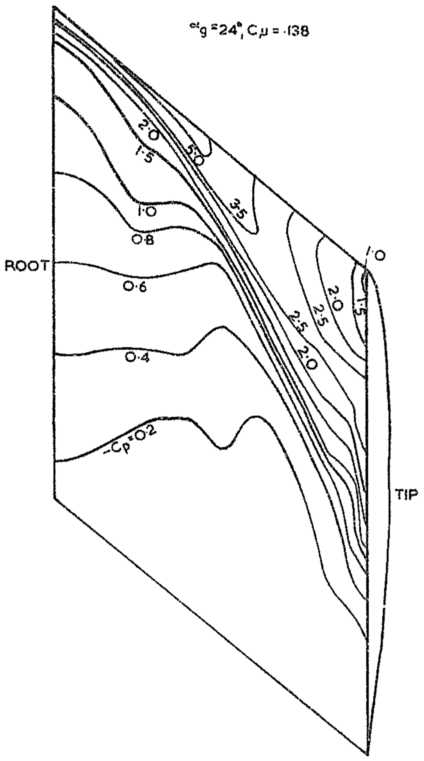

FIG. 41. UPPER SURFACE ISOBAR DIAGRAM.

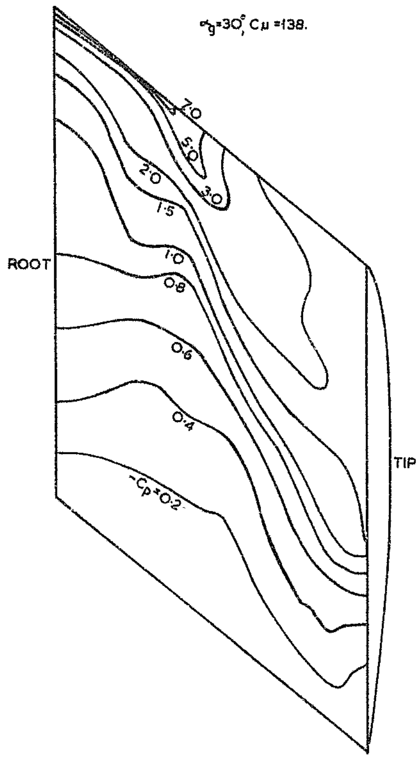

FIG 42. UPPER SURFACE ISOBAR DIAGRAM.

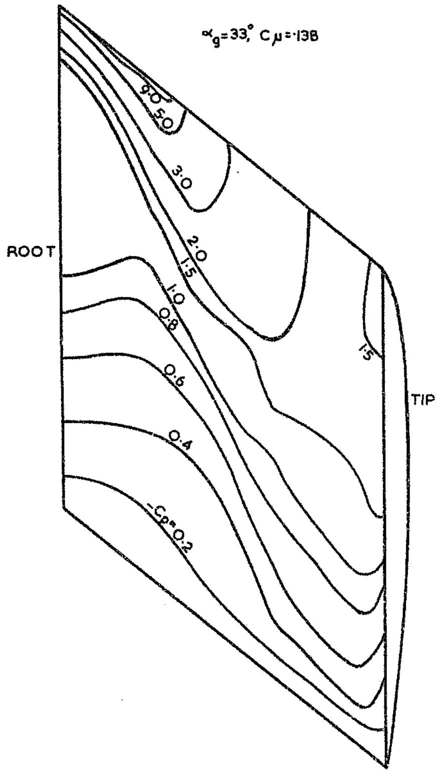

FIG.43. UPPER SURFACE ISOBAR DIAGRAM.

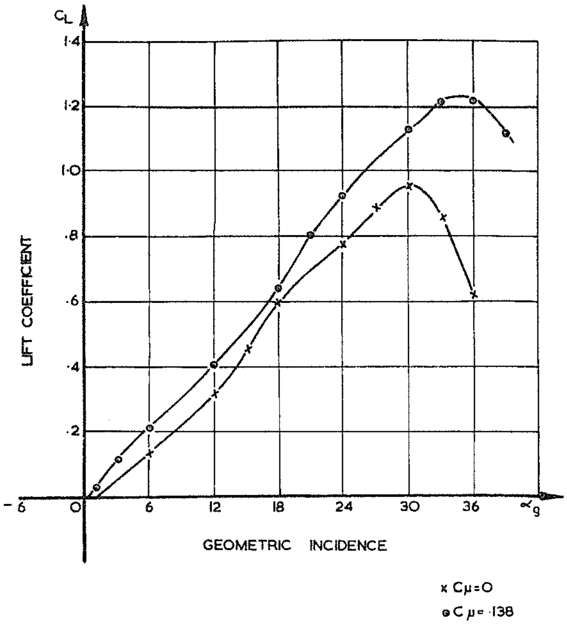

FIG. 44. VARIATION OF LIFT COEFFICIENT WITH INCIDENCE (PRESSURE DISTRIBUTIONS).

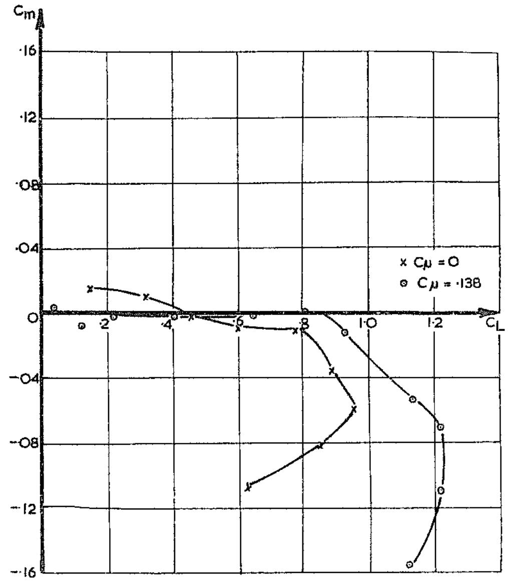

FIG. 45. VARIATION OF C_m WITH C_L (PRESSURE DISTRIBUTIONS).

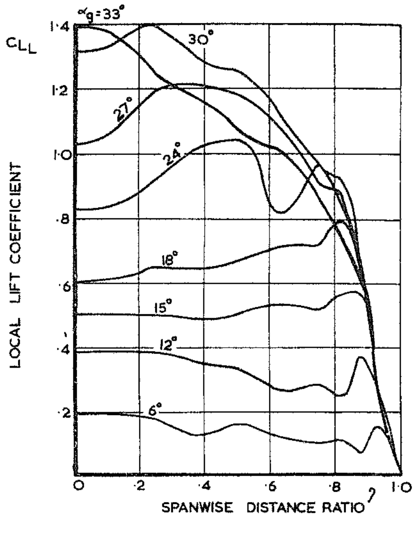

FIG. 46. SPANWISE DISTRIBUTION OF LIFT.

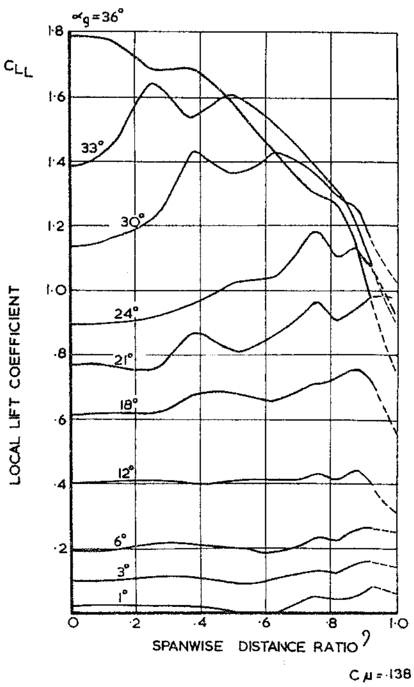

FIG. 47. SPANWISE DISTRIBUTION OF LIFT.

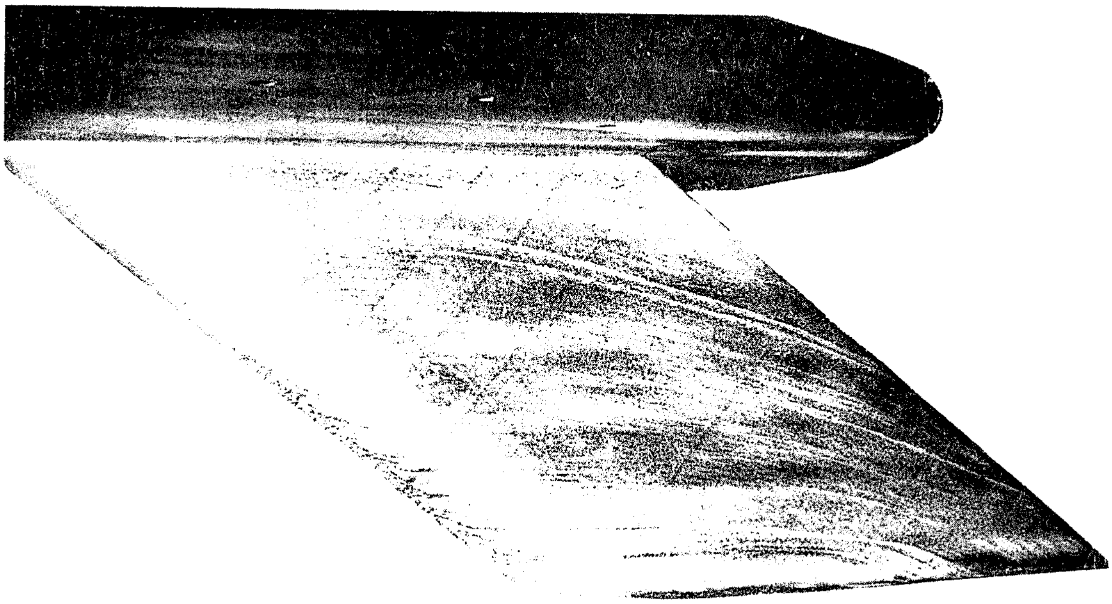

FIG. 48. **LIQUID FILM PATTERN** $\alpha_g = 6°$, $C_\mu = 0$ **(upper surface)**

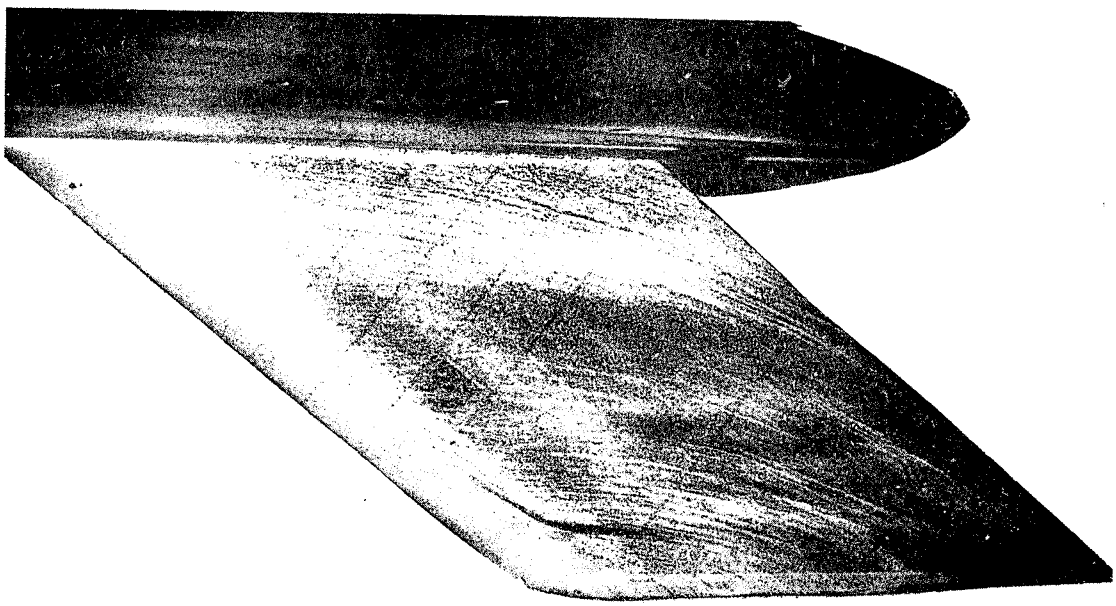

FIG. 49. LIQUID FILM PATTERN $\alpha_g = 6°$, $C_\mu = .138$ (upper surface)

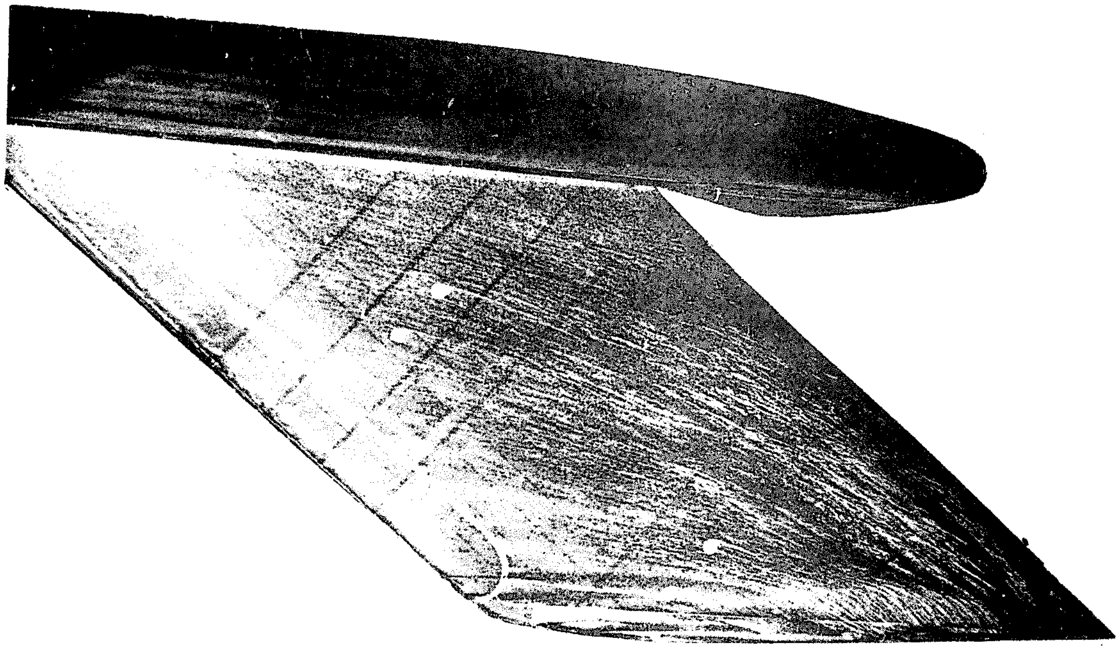

FIG. 50. LIQUID FILM PATTERN $\alpha_g = 12°$, $C_\mu = 0$ (upper surface)

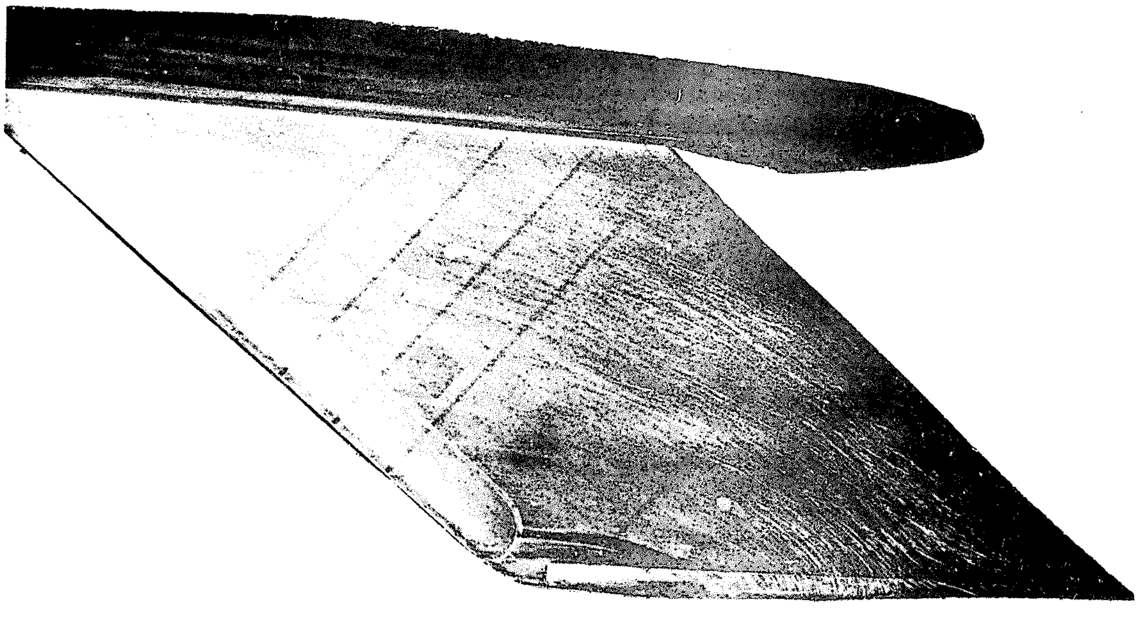

FIG. 51. LIQUID FILM PATTERN $\alpha_g = 12°$, $C_\mu = .138$ (upper surface)

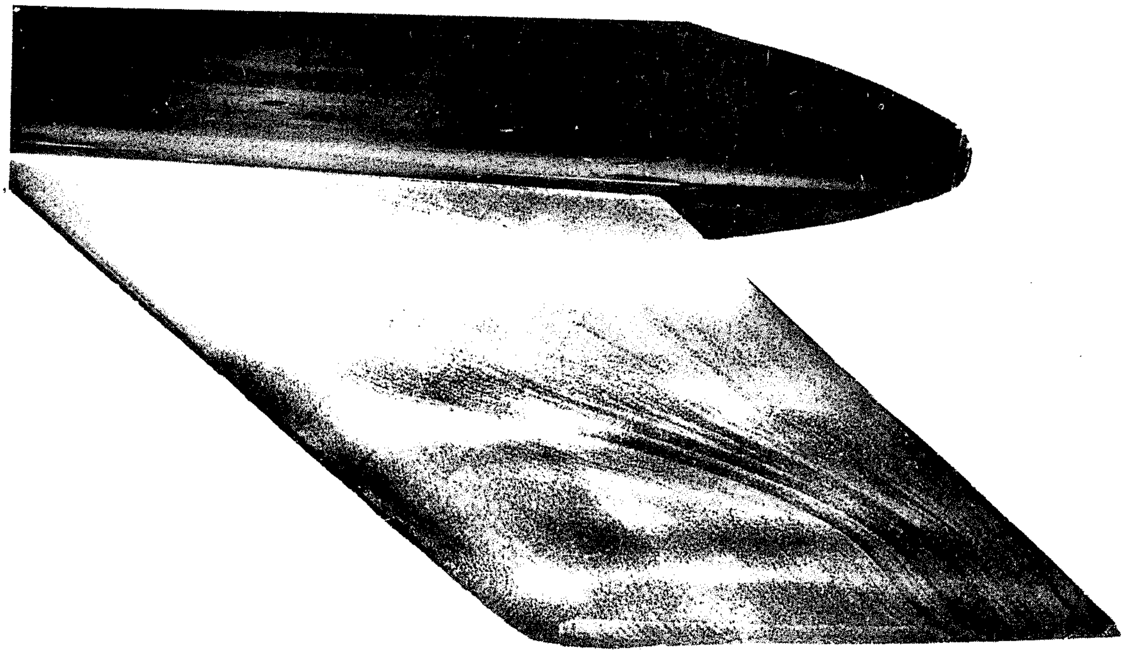

FIG 52 LIQUID FILM PATTERN $\alpha_g = 18°$, $C\mu = 0$ (upper surface)

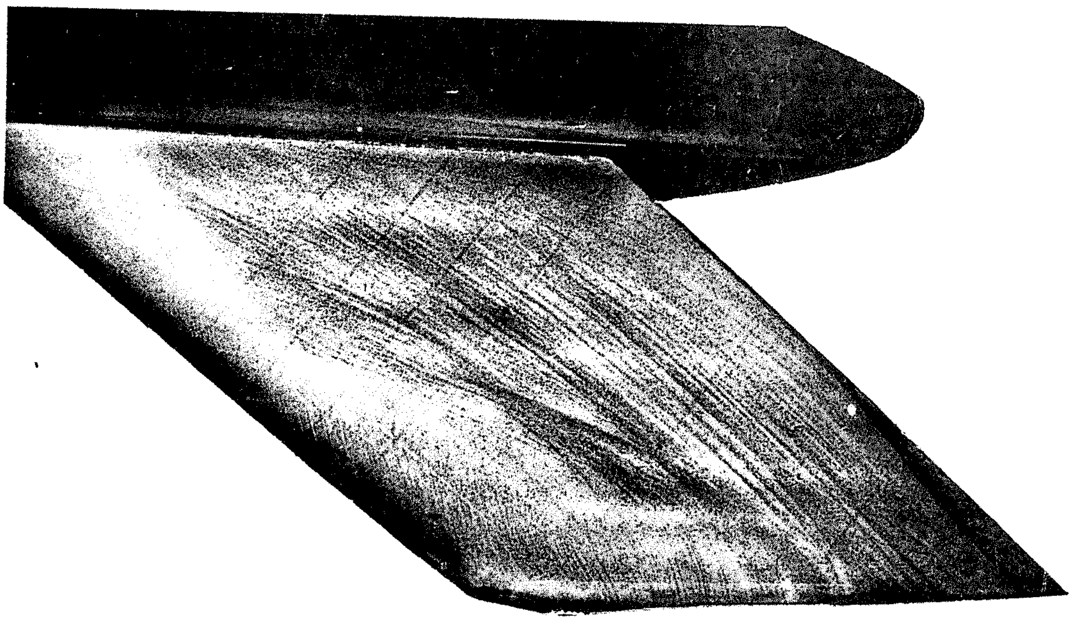

FIG. 53. LIQUID FILM PATTERN $\alpha_g = 18°$, $C_\mu = .138$ (upper surface)

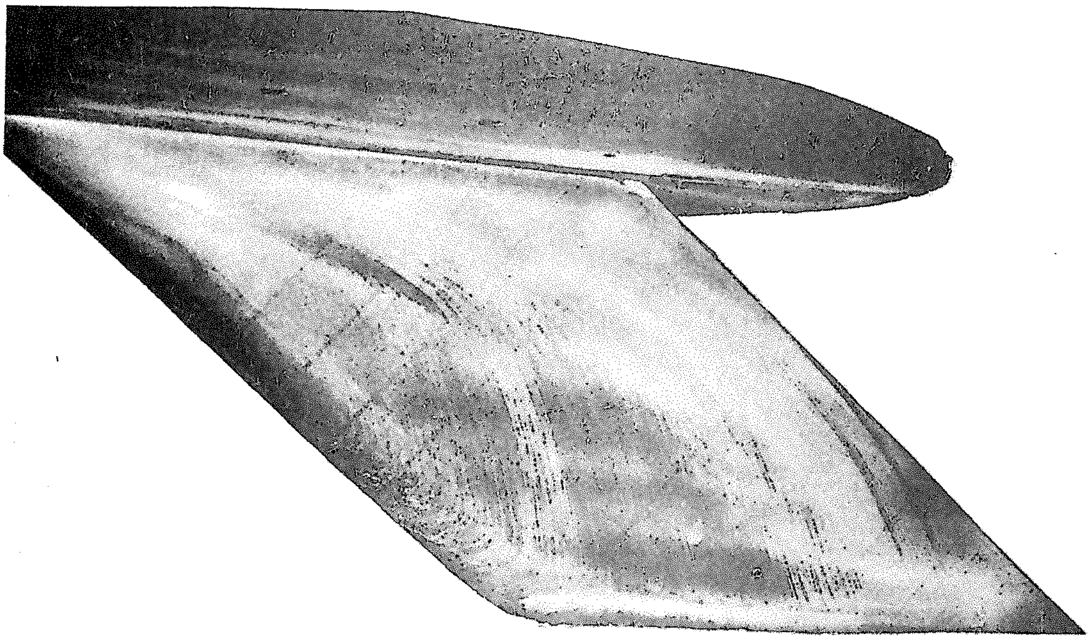

FIG. 56 LIQUID FILM PATTERN $\alpha_g = 30°, C_\mu = 0$ (upper surface)

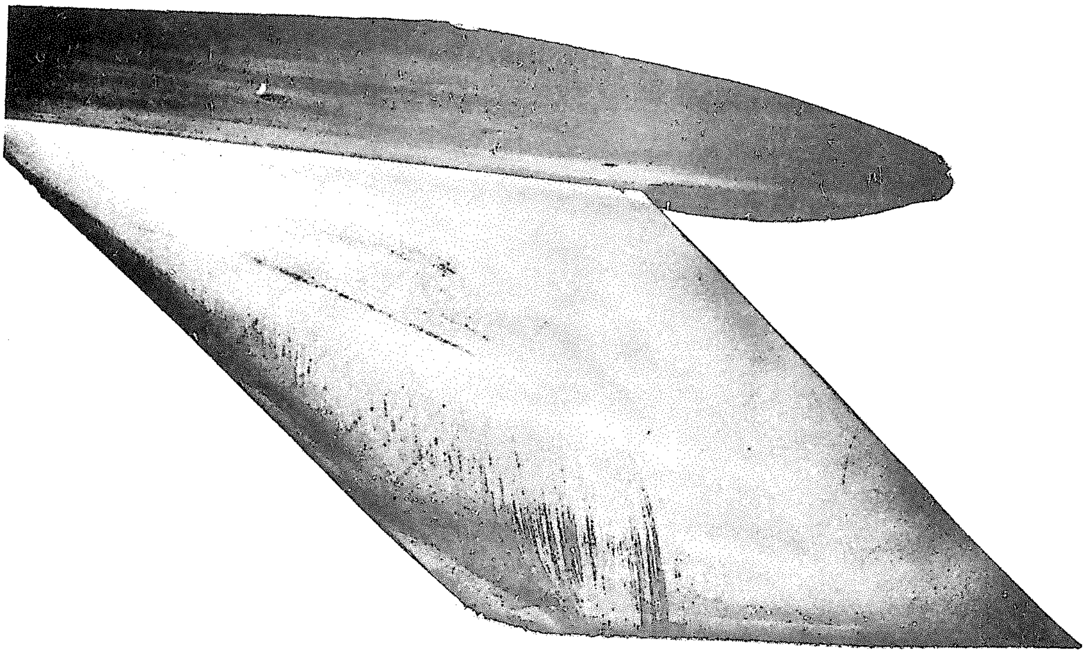

FIG. 57 LIQUID FILM PATTERN $\alpha_g = 30°, C_\mu = .138$ (upper surface)

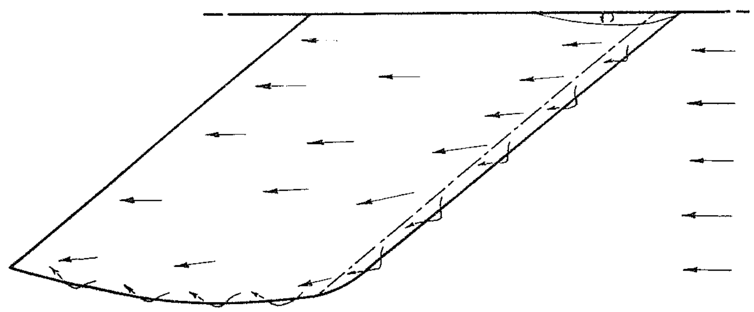

FIG. 58. FLOW DIRECTIONS (CONE-TECHNIQUE)
$\alpha_g = 12^\circ$, $C_\mu = 0$. LOWER SURFACE.

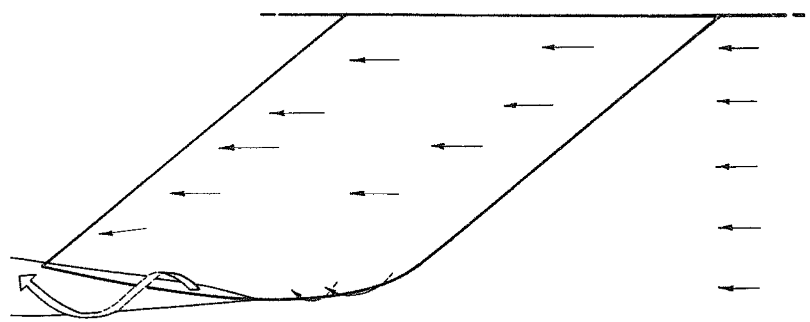

FIG. 59. FLOW DIRECTIONS (CONE-TECHNIQUE)
$\alpha_g = 12^\circ$, $C_\mu = 0$. UPPER SURFACE.

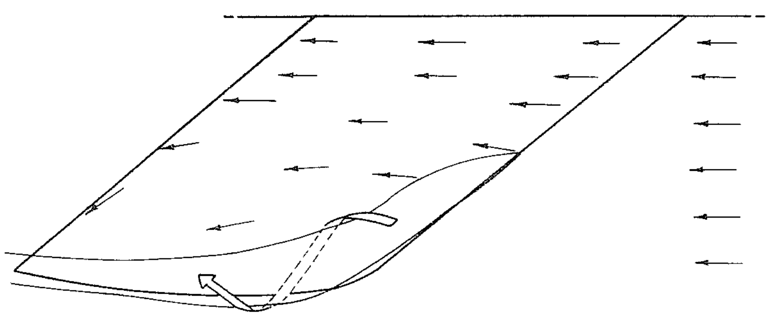

FIG. 60. FLOW DIRECTIONS (CONE-TECHNIQUE)
$\alpha_g = 18^\circ$, $C_\mu = 0$. UPPER SURFACE.

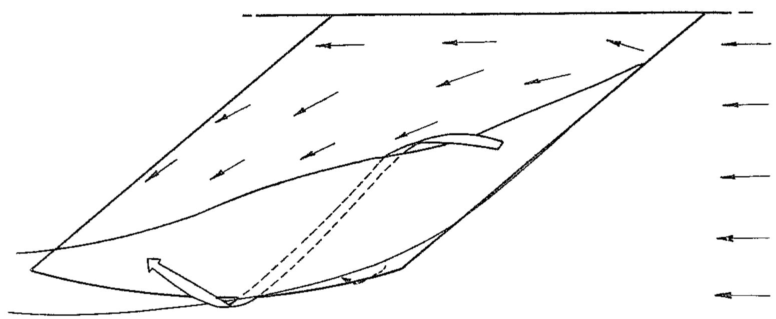

FIG. 61. FLOW DIRECTIONS (CONE-TECHNIQUE)
$\alpha_g = 30^\circ$, $C_\mu = 0$, UPPER SURFACE.

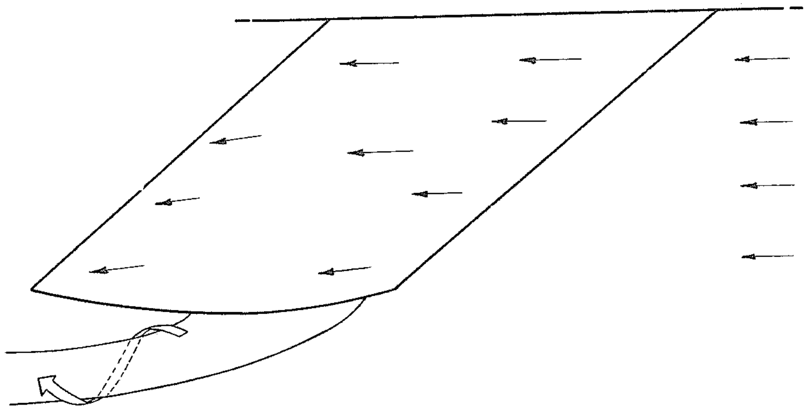

FIG. 62. FLOW DIRECTIONS (CONE TECHNIQUE)
$\alpha_g = 12°$ $C\mu = \cdot138$ UPPER SURFACE.

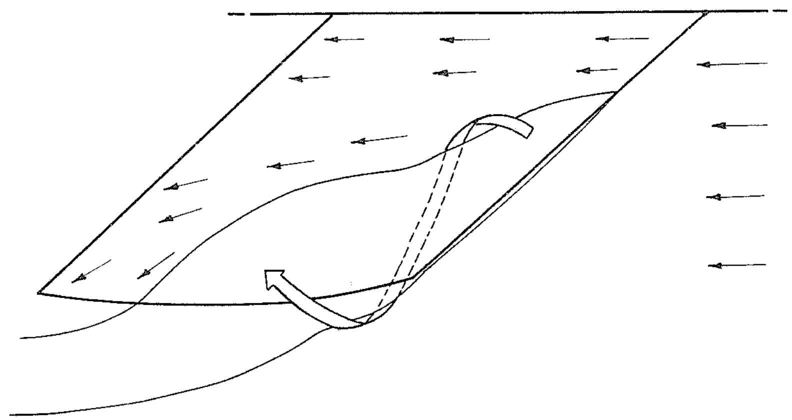

FIG. 63. FLOW DIRECTIONS (CONE TECHNIQUE)
$\alpha_g = 21°$, $C\mu = \cdot138$, UPPER SURFACE.

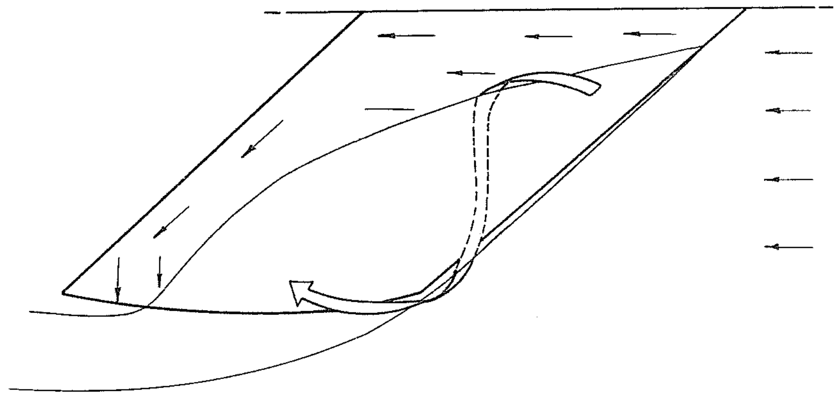

FIG, 64. FLOW DIRECTIONS (CONE TECHNIQUE)
$\alpha_g = 36°$ $C\mu = \cdot138$. UPPER SURFACE.